POLITECNICO DI TORINO

Master's Degree in Electronic Engineering

Master's Degree Thesis

Impedance Database Generation for the Automated Design of Metasurface Antennas

Supervisor and Tutor

Prof. Giuseppe VECCHI

Dott. Marcello ZUCCHI

Candidate matr. 277936

Francesco LATTANZIO

October 2023

Abstract

Metasurface antennas are thin, two-dimensional metamaterial layers that allow or inhibit the propagation of electromagnetic waves in desired directions in free space or on the antenna surface. In literature, they have been demonstrated to guide and make surface waves radiate to obtain a specific desired radiation pattern. Their low cost, easy integration, and low losses make them promising candidates for implementing solutions for next-generation receivers and transmitters for high-speed wireless telecommunications, in particular for 5G and beyond 5G standards.

These antennas are planar structures made up of sub-wavelength periodic conductive elements printed on a grounded dielectric substrate. By changing the shape of the individual elements, it is possible to obtain a given current distribution and thereby design a suitable radiation pattern. However, the analysis and design of such structures is particularly challenging because of the multi-scale features that characterize the patterned surface. Electromagnetic behavior is usually described macroscopically by a simplified model with the Impedance Boundary Conditions (IBC). The antenna design is usually done in two separate steps. First, the IBC profile is obtained, and then the individual cell shapes are extracted from a pre-computed database.

In the literature, there are already several numerical methods aimed at automating the design of these IBC profiles, starting from the antenna domain and the constraints on the radiated field. Much work remains to be done in the efficient computation of the database of the individual cells in order to properly cover the desired IBC values. In general, each cell shape is defined by a set of parameters, and it realizes a certain impedance value that changes deeply with the parameter combination.

The main objective of this work is to create a database of different reference cell geometries (e.g., circle, ellipse, etc.) at single or multiple frequencies in such a way that the resulting impedance values are distributed around the desired ones or as uniformly as possible in the domain of existence.

The software developed in this thesis is able to take a generic user-defined cell geometry and its parametrization, evaluate the impedance value from the scattered fields obtained from simulations, and automatically choose the sampling of the parameter values in order to minimize the distance between the desired impedance points.

The algorithm works by partitioning the domain of interest into boxes from a coarse database of impedance points, evaluated from uniform samples of the parameters. New parameter points are obtained through local interpolant inversion of the points already present. These points are then simulated with an external software module

that is able to evaluate the scattering matrix of the metasurface, from which it is possible to extract the new impedance points. The database is updated iteratively in this way. After exploring all boxes, it is possible to iterate through these steps again in order to refine the database if needed by imposing constraints, such as the minimum number of impedance points needed. It is also possible to give specific impedance points to the algorithm in order to refine the search close to these points. Numerical results highlight an improvement in terms of lower average distances between the desired points and the database points with respect to older solutions. As a consequence, it is possible to realize more accurately the wanted IBCs on the surface, leading to lower discrepancies in the radiation pattern.

Acknowledgements

Table of Contents

List of Figures

Acronyms

MTS
  Metasurface

PSSM
  Periodic Surface Spatial-Spectral Modeler

IBC
  Impedance Boundary Condition

GSTC
  Generalized Sheet Transition Conditions

MoM
  Method of Moments

EIFE
  Electrical Integral Formulation Equation

FSS
  Frequency Selective Surfaces

SRE
  Smart Radio Environment

MIMO
  Multiple Input Multiple Output

PCA
  Principal Component Analysis

Chapter 1

Introduction

Metasurface antennas are one of the most promising technologies for the physical layer of new communication systems based on innovative radio standards (i.e., 6G) due to their low cost, easy integration, and low losses.

MTS antennas are typically made up of thousands of elements, or unit cells, that texture the surface and realize specific Impedance Boundary Conditions (IBCs).

The typical design process involves the design of these IBCs on the antenna surface, according to some radiation mask constraints, making necessary the generation of an impedance database at the working frequency.

This database contains all the realizable impedance values according to the shape geometry of the unit cell and the sampled parameters for that geometry.

The goal of this thesis work is to propose a method to properly sample the space of the parameters X in order to generate impedance databases that have some features. The most important of them is to generate impedance points $Z(X)$ as close as possible to some desired points $Z_{desired}$, which are the outcome of the typical design process for a MTS antenna. Methods for "smart" sampling have not yet been extensively explored in the literature and represent a real challenge due to the generality of the problem. Indeed, the latter refers to the inversion of an unknown multivariate numerical output $Z(X)$ that may have no solutions. It is necessary to find a converging method for database generation that have to generate as many impedance points as possible near the desired ones.

This thesis work is organized into 5 chapters:

- Chapter 1: Introduction

- Chapter 2: Background information

- Chapter 3: Impedance Database Generation Algorithms

- Chapter 4: Numerical results

- Chapter 5: Conclusions

1.1   Metasurface Overview

In this section, it is given a brief overview of the main fields of applications of metasurfaces and some useful theory elements to understand this topic that has been extensively explored in literature [1][2][3][4]. Generally speaking, those kinds of 2D and electrically thin structures are properly engineered in order to shape arbitrary surface waves or incident wave reflections to achieve some purpose. Typically, antenna applications involve reshaping radiation energy in space.

The MTSs are usually constituted, in microwave and beyond range, by a regular and periodic texture of metallic elements of sub-wavelength size printed on a grounded dielectric substrate, as shown in Figure 1.1 and 1.2. In order to have effective leaky wave radiation, typical antenna sizes are in the order of tens of wavelengths, as shown in Figure 1.5.
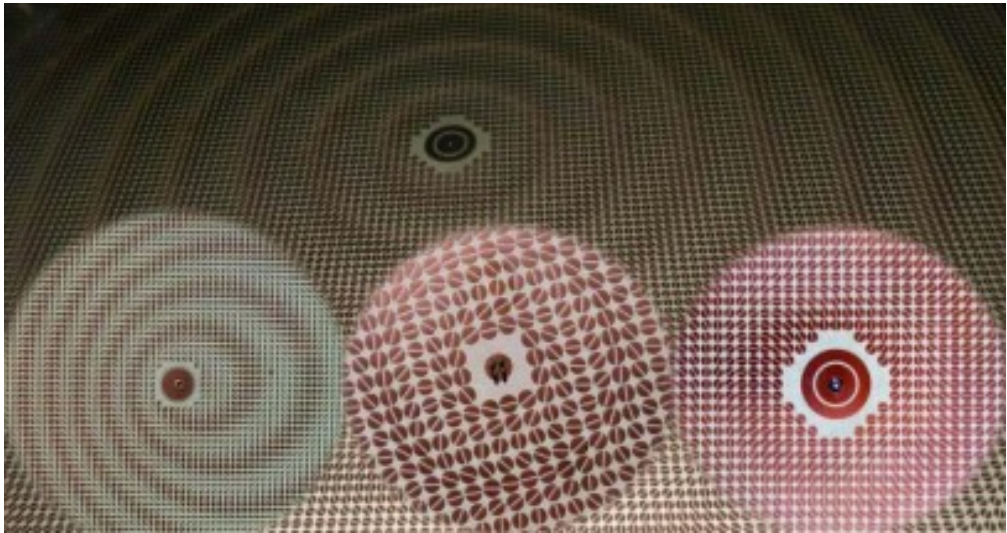
Figure 1.1: Metasurface antennas - circular structure [5]

Printed elements that texture the MTS antenna are used to realize an effective capacitance or inductance on the antenna surface; each element is coupled with the nearest one, as shown in Figure 1.3. In our case study, only the metallic elements are considered on the substrate without any vias.

This capacitance can be spatially modulated by locally changing the size and orientation of the texture elements. This allows for a deformation of the excited surface wavefront, which experiences distributed reflections due to the spatial modulation of the local wavevector (or refractive index). In other words, it is like
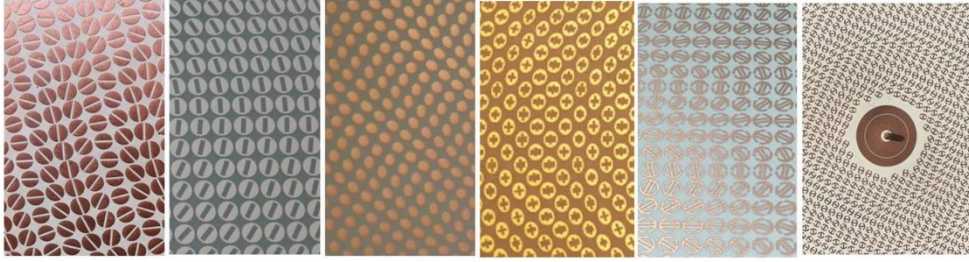
Figure 1.2: Metasurface antennas - typical unit cell elements (left) and feeding (right) [2]
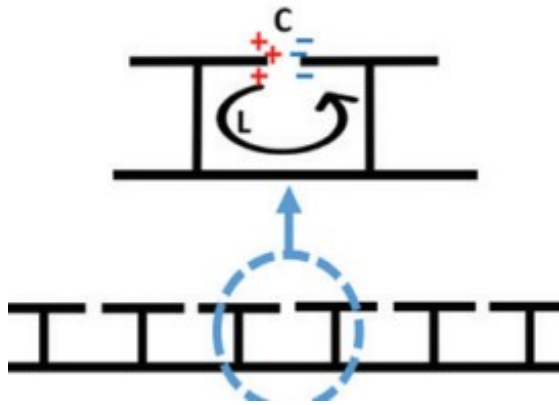
Figure 1.3: MTS realizing an effective surface capacitance and inductance by cell elements coupling and vias with ground plane [1]

the surface locally changes the transmission or reflection angle with the adjacent texture element of the surface wave, resulting in a possible reshape of the aperture field or equivalent electric current on the surface, as shown in Figure 1.4.

This wavenumber modulation can also enable leaky wave radiation, which is the phenomenon of our interest for a transmitting or receiving device. Because of the subwavelength texturing of the structure, theoretical analysis of transmission, reflection, or absorption properties can be performed using Generalized Sheet Transition Conditions (GSTC) or Impedance Boundary Conditions (IBCs); see Chapter 2. Due to the latter, it is very common to address those structures with "impedance surfaces". IBCs are used for EM characterization of the surfaces, allowing the use of equivalent lumped transmission line models and making them suitable for several numerical implementations aimed at solving the EM problem of the structure [7][8][6][9][5].

The nature of the structure is intrinsically multi-scale, as shown in Figure 1.5, which makes the MTS structures extremely computationally expansive for a classic
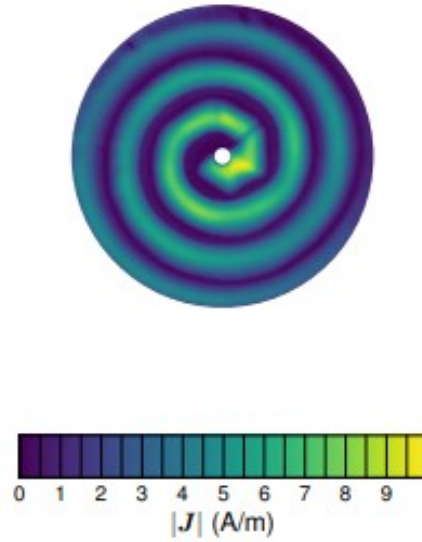
Figure 1.4: Current distribution implementing a pencil beam, circular polarized radiation pattern [6]

full-wave solver. In this need, new models and numerical methods (i.e., IBC-EIFE [7]) for the analysis of such EM structures are required to speed up analysis and optimization.
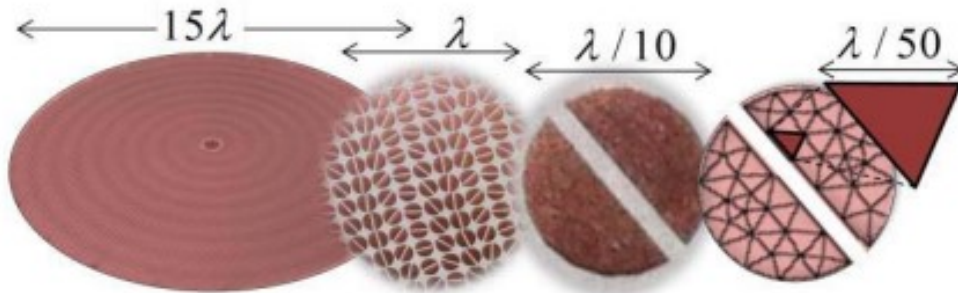
Figure 1.5: MTS structure with coffee bean unit cell; Lef to right - antenna, textured elements, unit cell element and mesh of the unit cell element [5]

Future research topics will focus on the development of active re-configurable impedance surfaces [10][11][12][4] as enabling technology for the next 6G radio standard and new massive MIMO techniques or beamforming, allowing flexible

high directive beam scanning for base stations with the minimum profile, maximum efficiency, and higher transmission performances.

A classification of MTS antennas can be made according to some well-known application fields:

1. **Metasurface absorbers**:
   Absorbers are often realized with bulky, lossy materials or multiple-layer structures, resulting in a high profile. Modern systems require compact design, and low-profile absorbers are preferred. MTSs exhibit mechanical properties such as low profile, light weight, and low cost, and they are very appropriate to be installed on vehicles, buildings, etc. as microwave absorbers to protect sensitive electronic devices from external wave interferences. Further applications extend to photodetectors and solar cells, scattering control, anechoic chambers, and microbolometers.
   New MTS structures have been studied recently with the aim of increasing the allowable incidence angle and making them polarization insensitive, together with enhanced bandwidth [13][14]. Switchable absorption and tunable resonant frequency features are also possible with active reconfigurable metasurface absorbers.

2. **Metasurface Waveguides**:
   Whenever the wave vector along the surface is greater than the free space wave vector, the surface supports the wave propagating along the surface, and it is also bound to it (planar waveguide). Then, it is possible to convert an incoming incident wave into a surface wave without reflections or transmission. This is very similar to what happens to light entering an optical fiber, where the wave is confined into the core by total internal reflection due to the refractive index discontinuity. On the contrary, some applications require the wave to propagate over a smoothly varying refractive index, allowing a "bending" on the surface, truly creating paths where the surface wave is confined; this is the MTS case. According to this principle, it is also possible to build several conventional optical or microwave devices, such as the magic-T structures.

3. **Cloaking and Lenses**:
   A challenging electromagnetic topic that has been extensively studied in the literature is the development of an "invisibility cloak", a metamaterial screen that works wideband and with all the polarizations. The surface reactance of the MTS screens can be used to compensate for the object's reactance, placed at some distance from the screen, in order to create waves with destructive interference to cancel out the scattering with the object. This impedance matching happens at a fixed frequency, but using varactors (active MTSs), it is possible to tune the reactance to obtain a higher bandwidth [15].

Non-uniform impedance surfaces can also be used to manufacture low-profile lenses since it is possible to realize negative refractive index materials with almost total transmission in free space, making them almost perfect lenses with low profile and weight.

Other electromagnetic functionalities of MTSs are engineered beam refraction and/or reflection, spectrum filtering, and encoding for secure communication. In antenna applications, MTS are used to improve bandwidth and enhance antenna gain through advanced radiation pattern molding, beam splitting and steering, multi-beam scanning, and polarization manipulation. They can also be used as superstrates for high-gain low-profile antennas and to bend leaky waves in high-gain planar antennas.

1.2   Metasurface History and Applications

Antenna systems for many applications need large gain and low latency to satisfy communications link requirements, together with proper polarization of the radiation pattern. Nowadays, massive data rates are required in many systems in order to satisfy the huge number of multimedia information requests. Fifth-generation standard radio (5G) is currently issued due to the fact that data-intensive applications are available on the market for users and the actual transmission speed starts to be inadequate for managing such digital traffic [4]. The need for new communication techniques, especially at the physical layer, is necessary to cope with this problem.
The concept of Smart Radio Environment (SRE) has recently emerged as a new paradigm for modern wireless telecommunication, where the propagation environment needs to be controlled and programmed jointly with the transmitter and receiver. The next incoming radio standard (6G) needs to have an electrically programmable physical layer that is low profile, low consumption, low latency, and high efficiency [16] in order to enable the use of some novel communication techniques (MIMO, beamforming, spatial multiplexing, etc.) together with high flexibility in reconfiguration. Radio software, ideally, will dynamically change the physical layer features and not only the modulation format of the transmission or input power.
The use of very large planar arrays is already exploited in many antenna systems due to their capability of creating narrow beamwidth, high gain, and dynamically beamforming. However, the feeding systems are usually complex and hardly minimize feeding losses and phase errors. Leaky-wave antennas, as MTS, allow the elimination of the feeding networks and then lower losses; they also present higher bandwidth since they are not resonant systems. MTS has a strong impact on antennas and microwave applications. In 2000–2010, MTS were uniform in space

and realized, with some textured elements, an arrangement of periodic printed metallic elements on a grounded substrate. The first generation brought some benefits, such as higher-efficiency planar antennas and enhanced bandwidth. The second generation (2010–2020) MTSs are designed to shape the EM boundary conditions (BCs) of the 2D structure in space to control the field source feed, which could be in-plane or external. This allows, potentially, to shape the incident field in an arbitrary way, allowing for lenses, radomes, and deflector devices beyond antenna applications.

Nowadays, with the improvement of technology, we are facing a transition to the third, where MTSs change BCs in space and time, becoming programmable in the propagation environment. MTS reconfigurability can be achieved by using electronics, time-changing materials, or multiple switchable feed points distributed over the MTS. The possibility of independently controlling the individual elements gave rise to the concept of "programmable MTSs". Reconfigurability makes the MTS amenable to a massive MIMO and capable of readdress beams in nonspecular directions. Therefore, reconfigurable MTSs will become a key enabling technology for the future generation of sensing and communications as the basic constituent of a fully intelligent and cooperative wireless environment. In Figure 1.6 is reported an overview of the evolution through the years in some application fields.
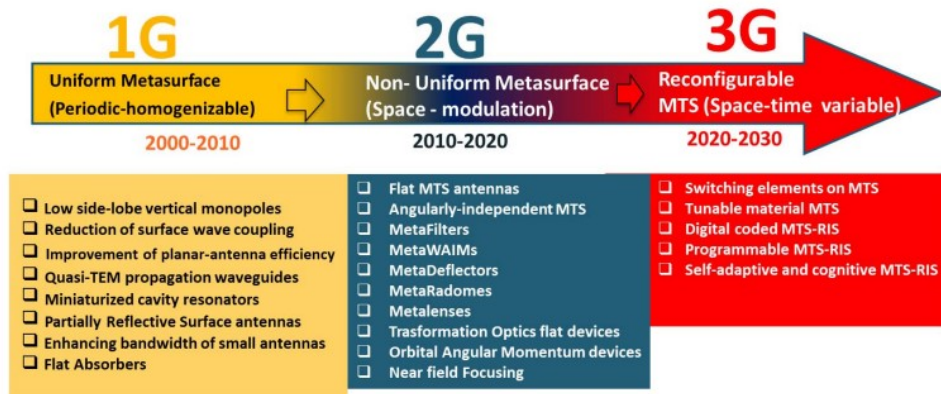
Figure 1.6: Metasurface evolution through years and their applications [4]

MTSs can be used to achieve some unusual reflective or transmission properties of space waves, modify the dispersion properties of surface or guided waves, or operate a conversion between a surface wave (SW) and a space wave (or vice versa).

In Figure 1.7, they are shown the first kind, also called phase gradient surfaces, since they are able to introduce a linear phase difference on the wavevector on the surface and then reshape the output beam with the advantage of maintaining low levels of unwanted reflections or direct transmission; they are also used to guarantee some direct transmission properties, minimizing the losses.

In Figure 1.8, they are reported MTSs that have the same function as the optical lens, and then they are able to focus the incident beam in some direction, allowing them to reshape incoming field energy in space. This is done by modifying the Impedance Boundary Conditions (IBCs) introduced by the MTS properly.

In Figure 1.9 is shown the SW antenna implemented by the MTS that is able to reshape the in-plane monopole feeding wavefront into a curvilinear wavefront leaky wave according to the IBCs imposed on the surfaces, allowing to shape the aperture field, thus molding far-field radiation. Here, the challenge is the effective excitation of the SW (i.e., coaxial cable is good for this purpose but needs some optimization and adjustments), along with the control of the leakage attenuation constant along the SW path. Those MTS antennas are lightweight and low-profile, characterized by low losses and simple, low-cost manufacturing. It is possible reach also higher
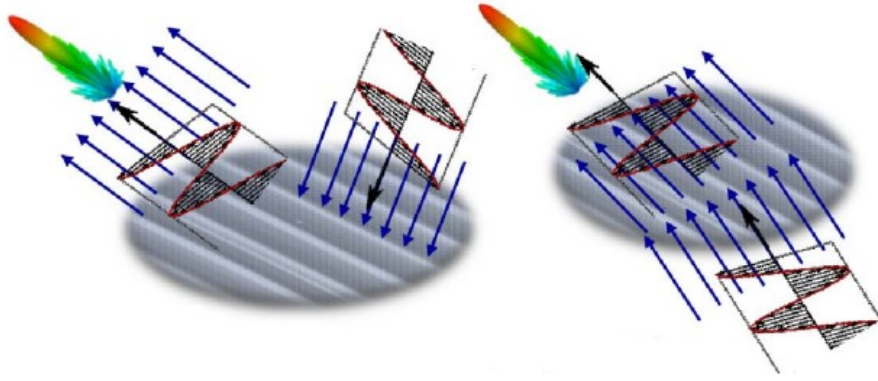
Figure 1.7: Non specular reflective surface (left); Deflector MTS (right) or Metadeflector [4]

bandwidth and high gain compared more bulky solutions, as shown in Figure 1.10. The radiation aperture on SW based MTS antennas can be described according some mathematical models together with Impedance Boundary Conditions (IBCs), under the ideal monopole source feeding hypothesis, as in Equation 1.1.

$$E_s(\rho) = Eoe^{-j\varphi\rho - jk_z z} \tag{1.1}$$

The propagation constant $\varphi = \alpha + j\beta$ of the surface radiation on the antenna determines the surface radiation direction and attenuation, while the normal propagation constant k_z determines if the radiation is coupled to free space. When the latter is purely real, the energy is coupled into free space as radiation since the phase in the normal direction changes. The direction of the radiation can be designed by controlling the value of β, i.e., $\theta = cos(\beta/k_0)$, for open waveguides with air discontinuity [17].
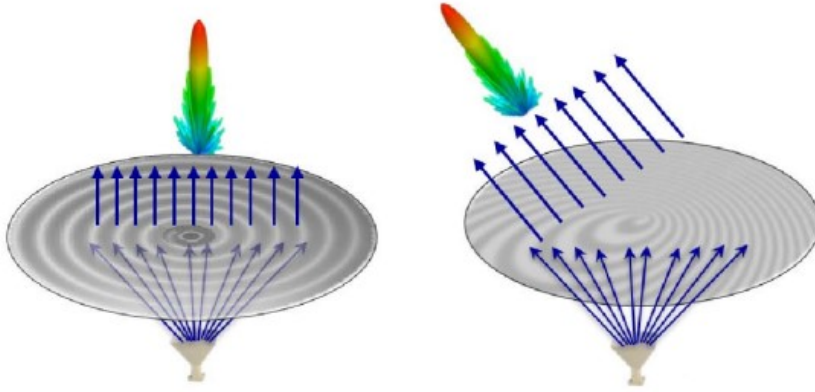
Figure 1.8: MTS lenses; The shaping of the surface IBCs changes the beam focus direction [4]
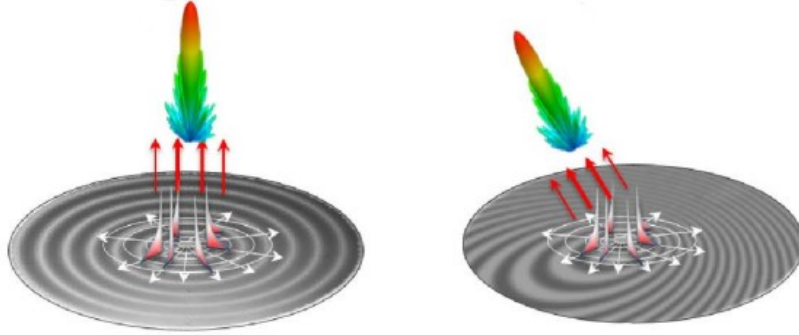
Figure 1.9: MTS antennas based on SW wave control (leaky wave radiation) [4]

The unit cells of the MTS are designed specifically to match the phase delay on the surface with that of the desired beam direction in free space, since each cell redirects the surface wave aperture field differently according to the local k_z value. A modal analysis of the surface structure can also be performed by using the IBCs, reducing the computational burden compared to classical eigenmode solvers [18].
They are also reported some fundamental, well-known results about a planar circular polarized leaky wave MTS antenna with a vertical probe (ideal monopole source) that excites a cylindrical surface wave [19].
The Impedance Boundary Conditions (IBCs) impose a relationship between the average value of the tangent electrical field and the tangent magnetic field at the surface:

$$\vec{E}_t(\rho) = jX_s(\rho)\vec{H}_t \times \hat{z} = jX_s(\rho)\vec{J_{sw}}(\rho) \tag{1.2}$$
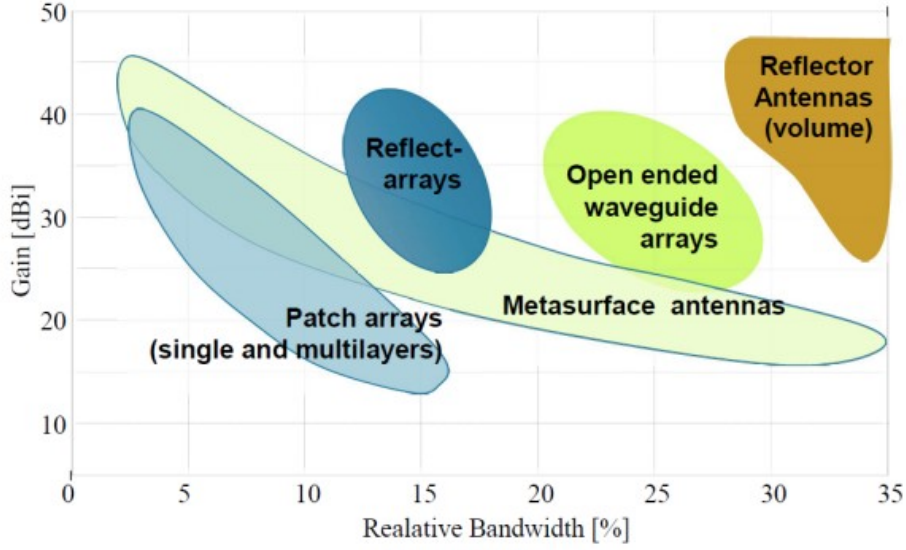
Figure 1.10: MTS antennas achievable Gain vs Bandwidth compared with other solutions [4]

With the $jX_s(\rho)$ being a positive reactance that is imposed on the surface by the MTS textured elements, The aperture field that contributes to the far-field radiation can be approximated as in Equation 1.3 and the surface propagation constant as in Equation 1.4. It is clear that it is possible to shape the aperture field according to the $X_s(\rho)$ IBCs.

$$\vec{E}_t(\rho) = jX_s(\rho)J_{sw} \simeq jX_s(\rho)J_{sw}(\beta_{sw} + \Delta\beta_{sw}, X_s(\rho))\hat{\rho} \tag{1.3}$$

$$\beta_{sw} = k_0\sqrt{1 + \frac{X_0^2}{Z_0^2}} \tag{1.4}$$

The J_{sw} is the TM_0 surface wave mode equivalent current density excited by the ideal monopole, k_0 and Z_0 free space wavevector and impedance. The β_{sw} propagation constant of the surface wave can be extracted by analyzing the $X_s(\rho, \varphi)$ that, in this case, follows a certain kind of modulation (sinusoidal archimedean spiral). The bias term X_o is used to estimate the β_{sw}, while the complex variation $\Delta\beta_{sw}$ is due to the interference of the structure with the incident surface wave itself. The antenna allows good broadside radiation, up to 20 dB of directivity. The surface leaky wave mode does not contribute directly to the far field radiation but dominates the aperture radiation that is used to compute the far field.

Those structures have the advantages of having a low profile and having simple feed structures, allowing them to reach high directivity and avoid beamforming

losses that are typical of large arrays. They also have frequency-dependent beam scanning properties (beam squint), which can be a benefit or drawback, depending on the application. Generally speaking, when we have an equivalent reactance $jX_s(\rho)$ that modulates the surface by means of periodic printed metallic elements of various sizes and orientations, TM modes (respect to the normal to the surface) are supported, described asymptotically by Equation 1.5 [20].

$$E_t(\rho) \sim \hat{k}_t V_0(\rho) e^{-j\phi(\rho)} \tag{1.5}$$

And with characteristic equation given by:

$$k_t \cdot k_t = k_0^2 (1 + \frac{X(\rho)^2}{Z_0^2}) \tag{1.6}$$

The amplitude of the local surface wave $k_t = \nabla_t(\phi(\rho))$ wavector decreases in the center ad increasing at the edges according Eq.1.6; inversely the local phase velocity is greater at the center and lower at the edges, producing this kind of diverging wavefront that is shown in Figure 1.11.
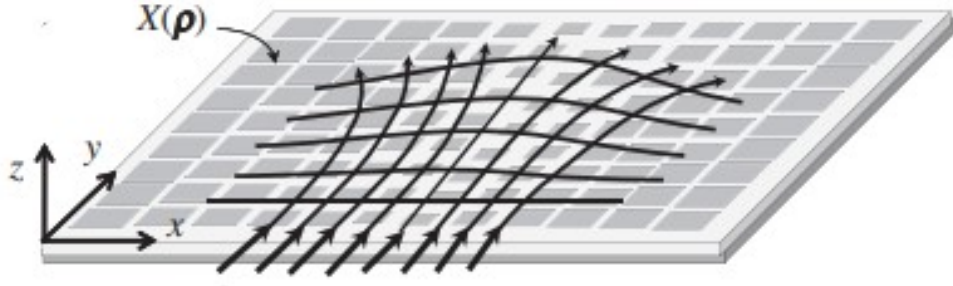
Figure 1.11: SW wavector bending due to local IBCs given by the $X(\rho)$ reactance [20]

A more intuitive explanation for the local variation effect of k_t realized by the MTS can be found in the generalized Snell's Law [3]. Metasurfaces are able to introduce artificial boundary conditions in order to modify the radiation phase and amplitude of an incoming incident wave, obtaining unusual reflecting properties such as the changing of the reflected wave angle (which is no longer equal to the incident angle) and the modified transmission angle in the material; those scattering properties could not be reached with materials that are already present in nature.

$$\begin{cases} n_2 \sin\theta_t - n_1 \sin\theta_i = \frac{\lambda_0}{2\pi}\frac{d\Phi}{dx} \\ n_1 \sin\theta_r - n_1 \sin\theta_i = \frac{\lambda_0}{2\pi}\frac{d\Phi}{dx} \end{cases} \tag{1.7}$$

11
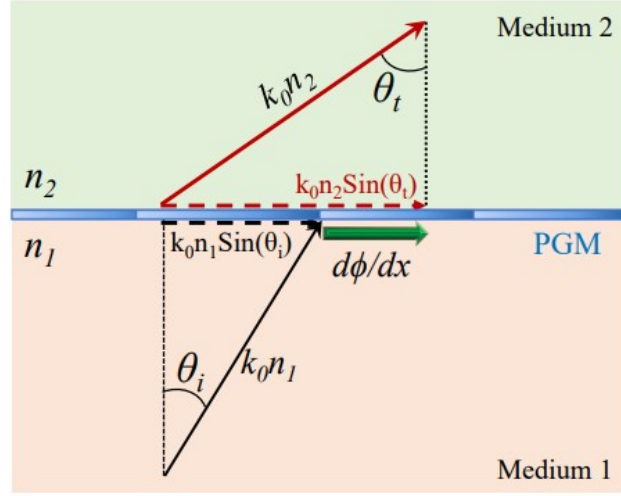
Figure 1.12: Phase gradient MTS (PGM): reflected, transmitted angles are modified according phase gradient introduced artificially by the metasurface [3]

Conventional boundary conditions assume that discontinuity between two surfaces does not change the properties of the impinging EM wave. The constraints imposed by conventional Snell's law include the possibility of decoupling incident, reflected, and refracted angles. Equation 1.7 shows that for a given angle of incidence θ_i, there exists such a value of the phase gradient term $\frac{d\Phi}{dx}$ that results in a parallel wave propagating with $\theta_t = 90\circ$. If $\frac{d\Phi}{dx}$ is increased further, θ_t becomes a complex quantity at which point the refracted waves will vanish and planewaves will be converted to surface waves. Those kinds of surfaces are also referred to as inhomogeneous MTS since the surface waveform changes slowly on the surface due to the changing size and orientation of the textured element.

At last, it is possible to analyze the structure by means of a "local periodicity" assumption, since it is assumed that the structure is made up of a periodic texture. According to the latter, total fields on the surface can be represented as a local periodic Floquet Wave (FW) expansion, which allows us to define them as the sum of orthogonal indexed modes. The average tangential field condition of the surface corresponds directly to the coefficients of the zero-indexed mode of the expansion and are related by the IBCs shown in 1.2; this is a zero-order approximation, of course, but it comes out from that it is a very good model to analyze such complex structures, matching some fundamental theoretical results [7][6][20][21]. The local periodicity assumption also helps the numerical scattering matrix computation of the surface, restricting the analysis only to a single cell element and applying periodicity conditions to the fields. Even if periodic boundary conditions are not perfectly met on a real structure, this method is still very valid for a fast analysis

of the structure compared to a full wave analysis. The IBC model can also be
used to get a faster modal analysis of the structure, since once it is extracted the
impedance tensor components of the MTS structure (see Chapter 3), it is only
needed to plot some fundamental dispersion curves from well-known theoretical
results [18][22][23]. It is useful to understand that the conditions in Equation 1.2
are valid for an opaque surface, where the radiation cannot penetrate inside the
medium, and that the surface impedance takes into account both the sheet and
the grounded dielectric support as well. The design of meta layers must take into
account the contribution of the support where it is physically realized. This can be
done according to the equivalent transmission line model, as shown in Figure 1.13.
Typical values of the dielectric height are much lower than λ. The contribution of
the grounded dielectric can be taken into account using an equivalent transmission
line model for both the TE and TM transverse fields, neglecting Floquet modes
that do not contribute to far-field radiation since they are decaying faster from
above the surface. In this model, it is assumed that the MTS is thin enough to be
electrically thin; in such a way, the impedance is a lumped element and goes in
parallel with the transmission line that represents the grounded dielectric support.
The actual MTS admittance can be evaluated as in Equation 1.8, and it must be
taken into account during the design process since it modifies the total impedance
surface value.

$$\bar{\bar{Y}}_{sheet} = \bar{\bar{Y}}_{in} - \begin{pmatrix} \frac{1}{jZ_0 \tan(k1d)} & 0 \\ 0 & \frac{1}{jZ_0 \tan(k1d)} \end{pmatrix} \tag{1.8}$$

The Equation 1.8 could be very useful since, if we are able to evaluate the total
input admittance $\bar{\bar{Y}}_{in}$ by means of some measurements or simulations, it is possible
to easily de-embedding the contribution of the grounded dielectric support in order
to realize the values needed for the MTS impedance by the radiation constraints.
Once the proper surface reactance or impedance is chosen to obtain some radiation
constraint, a database of unit cell elements is needed that realizes those values
and represents the textured elements of the antenna that are possible to realize.
The continuous ideal profile of the surface is discretized by means of textured
unit cells, introducing a first non-ideality with respect to the theoretical results.
The realizable values of physical printed elements could be very different from the
desired ones, and it is not trivial to find the parameter combination of the cell,
given a specified geometry, that realizes it.
The focus of this thesis work will be to develop an algorithm that could be able to
minimize this kind of error projection of the realizable values with respect to the
desired ones, finding the best parameter combinations needed to physically realize
the cells. Moreover, typical design involves anisotropic structures (implying TE/TM
modes mixing on the surface) that allow a greater degree of freedom for radiation
patterns. However, the surface reactance is a tensor and not a scalar, implying
higher complexity in the point search. It is good to recall that bandwidth and
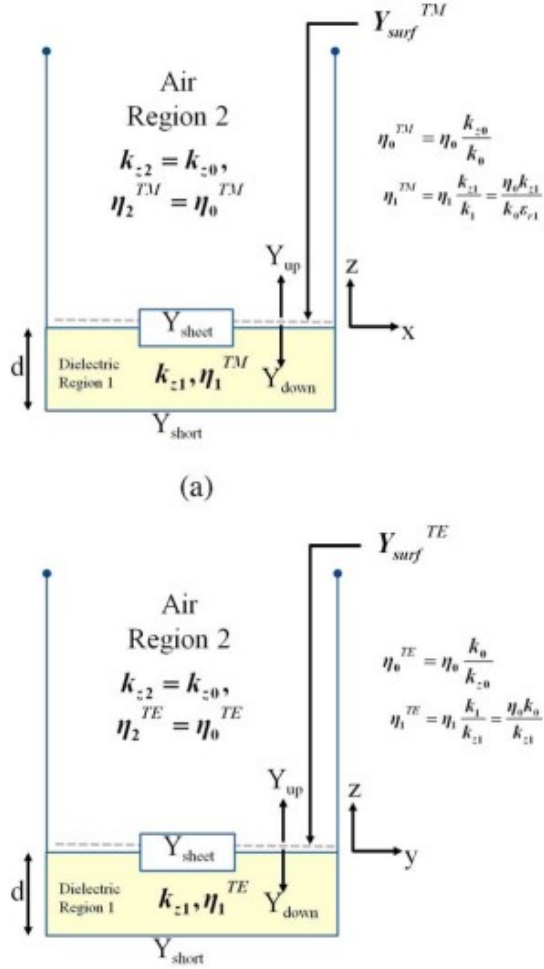
Figure 1.13: Transmission line model for the transverse TM and TE fields: Surface MTS Impedance is in parallel with the grounded dielectric transmission line [24]

sensitivity to manufacturing tolerances are fundamental for antenna realizations since working frequency and manufacturing processes are always subject to certain amounts of tolerance. The choice of the textured element has to be done according to the antenna requirements and user case, as shown in Figure 1.14[5][2].

1.3 MTS Theory Elements

It is given a brief resume of the theory elements and a more rigorous classification that can be found in the literature [25][26], introducing a useful background to better understand such complex electromagnetic problem descriptions. EM problems can

14
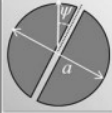
	Coffee Bean	Slotted patch	Grain of Rice	Double anchor	Double π
# parameters	2	3	3	3	3
Anisotropy Control	🙂	😀	😀	😀	😀😀
Range of Xρρ	🙂	😀	🙂	😀😀	😀😀
Bandwidth (group velocity)	🙂	😀	😀	😀😀	😀😀
Sensitivity to tolerances	😀	🙂	😀😀	🙂	🙁
Loss in the metal	😀	🙂	😀😀	🙁	🙁

Figure 1.14: Different unit cell elements geometry used to realize a MTS antenna and some figures of merit [2]

generally be categorized according to the spatial dimension (Figure 1.15) as:

1. **0-D problems**:
   When all the dimensions are smaller than wavelength, it is possible used circuit theory by using a lumped model. Kirchhoff's laws are used to solve such problems.

2. **3-D problems**:
   When all dimensions are comparable to wavelength λ. This kind of problem describes properties of homogeneous (or inhomogeneous) mediums with permittivity and permeability (or effective) ϵ, μ. Problem solution involves general mathematical tools based on Maxwell's equations.

3. **1-D problems**:
   Structures where transverse dimensions are negligible with respect λ can be analyzed by means of transmission line theory, where fields are described with forward and backward waves.

4. **2-D problems**:
   Structures where only one size is lower than λ, the problem becomes 2D and the a good characterization is done with effective surface susceptibilities $\bar{\bar{\chi}}_{ee}$ and $\bar{\bar{\chi}}_{mm}$. The EM problem is solved with the use of the Generalized Boundary Conditions (GBCs).

15

How do those kinds of Boundary Conditions (BCs) differ from the conventional ones?

Field discontinuities across engineered surfaces are designed in order to manipulate or transform EM waves, and these BCs are used to describe those field discontinuities. Conventional boundary conditions relate field discontinuity along the surface with current sources; the latter depends both on surface characteristics and on applied fields; current sources and fields are coupled together. Then, solving field discontinuities is not straightforward with classical boundary conditions.

It is possible through the GBCs to describe the field discontinuity directly with the surface characteristic, independently of the applied fields. Those surface characteristics are dependent on the material and geometry of the surface, but not on applied fields; they are able to force a certain EM discontinuity in the space within a surface. In this way, field discontinuities across surfaces are analytically computed starting from some applied fields with arbitrary propagation direction and polarization.
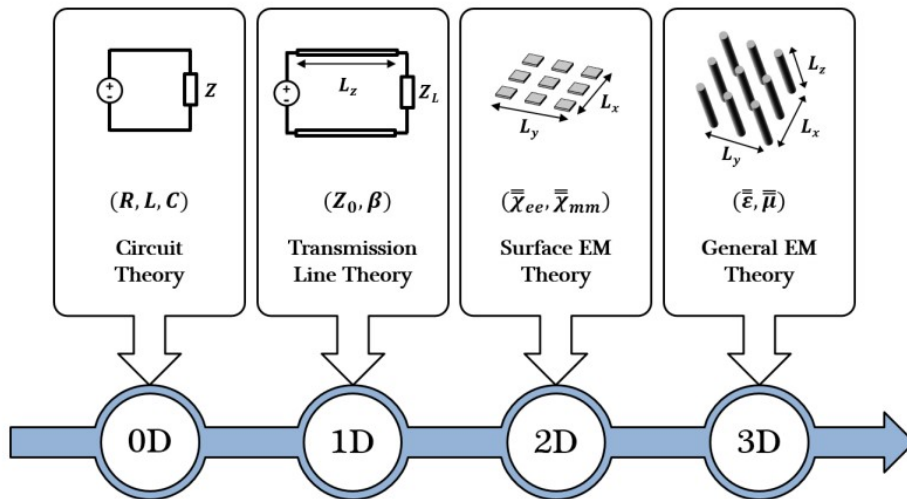
Figure 1.15: EM problem category in terms of spatial dimensions [25]

2D EM surfaces are usually made up of periodic (or quasi-periodic) elements, called unit cells. These unit cells exhibit features that characterize the electromagnetic surface. The main features are:

1. **Homogeneous impedance and spatial dispersion**:
   MTS are made of textured elements, the unit cells, which are periodically distributed as shown in Figure 1.16. However, if the scale of periodicity is much smaller than the wavelength λ, the surfaces can be modeled as

homogeneous effective mediums, and EM parameters are constants on the surface. Those parameters are the effective surface susceptibilities $\bar{\bar{\chi}}_{ee}$ and $\bar{\bar{\chi}}_{mm}$. With the increase in frequency, λ changes approaching p, making such an approximation not valid anymore. In this case, $\bar{\bar{\chi}}_{ee}$ and $\bar{\bar{\chi}}_{mm}$ become space-dependent, becoming spatially dispersive. Frequency Selective Surfaces (FSS) are a typical application of spatially dispersive surfaces with a period close to half wavelength.
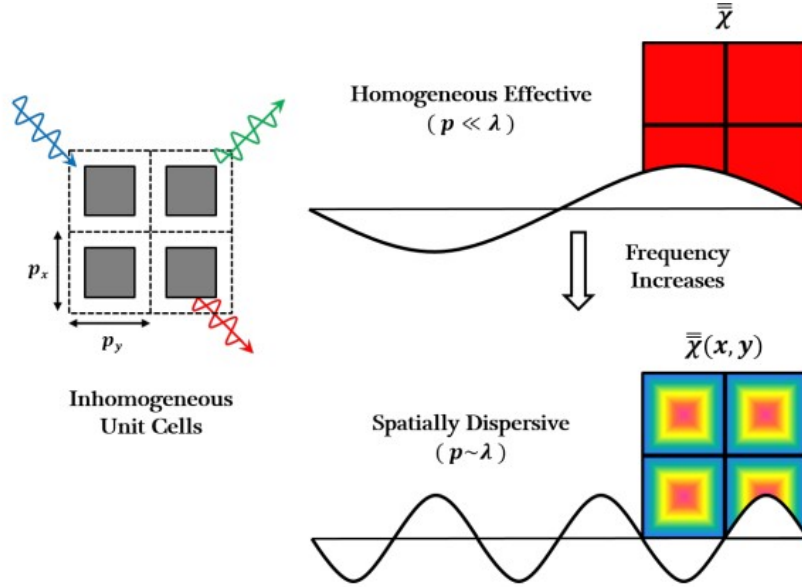
Figure 1.16: Homogeneous surface and spatially dispersive surface [25]

2. **Isolated Scatterers and Apertures**:
   Isolated scatterers surfaces involves a planar arrays made up of separated scatterers; isolated-apertures surfaces are made up of periodically spaced apertures, as shown in Figure 1.17.
   These structures are complementary and they realizes, also, complementary features. For example, FSSs isolated apertures realizes bandpass filtering while isolated scattering bandstop filtering.

3. **Isotropic and Anisotropic surfaces**:
   In 3D EM, isotropy means that applying a field in some direction doesn't modify fields in orthogonal directions; otherwise, they are anisotropic. In 2D EM, isotropic surfaces have the same meaning for TE and TM polarizations, and their scattering properties are not related to the angle φ (polar coordinates) of the propagation direction $\hat{k}$ but only to the elevation angle θ. On the contrary, anisotropic surfaces are dependent on φ, and mixed-polarization
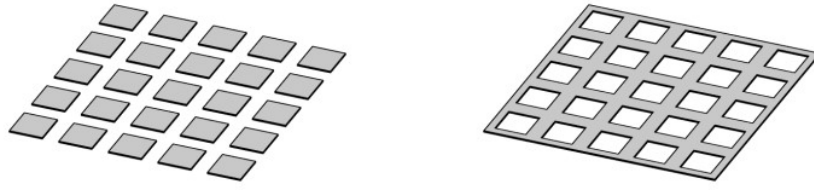
Figure 1.17: Isolated Apertures (right) and Isolated Scatterers (left) surface topology [25]

field contributions may arise both in scattering and transmission, as shown in Figure 1.18. It is useful to remember that when frequency is increasing, the wavelength is also modified, and anisotropy may arise due to spatial dispersion.
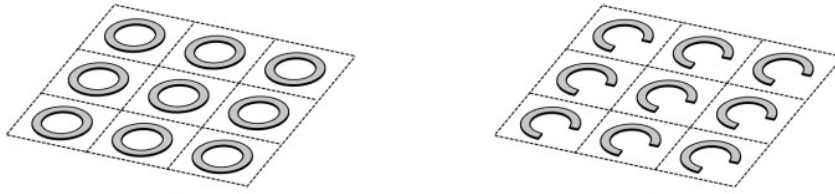
Figure 1.18: Isotropic (left) and Anisotropic (right) surface topology [25]

4. **Space and Surface waves modes**:
   2D surfaces can interact with EM fields of free space waves or surface waves, as shown in Figure1.19. Space waves need a reflection and transmission matrix to characterize their structure. In this case, the propagation constant along the normal direction to the surfaces, k_z, is purely real and means that EM fields can propagate along the $\hat{z}$ direction. On the contrary, surface wave fields exponentially decay along the $\hat{z}$ direction, and k_z is purely imaginary; field propagation is constrained only to the surface. Surface waves can be modeled as special cases of space waves, where the incident angle θ is equal to $\pi/2 + j\theta$. The unknown value of θ is determined by both surface EM parameters and working frequency.
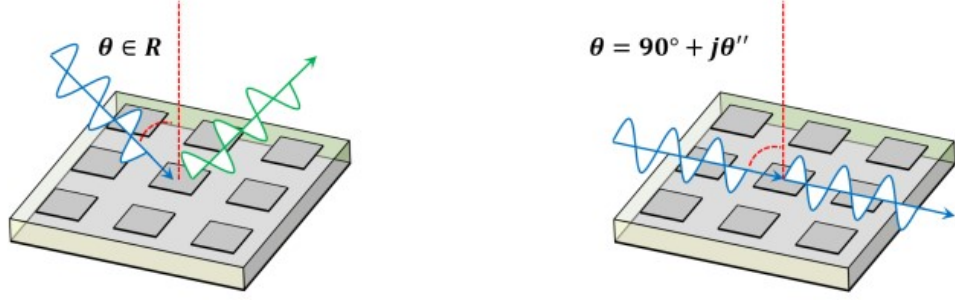
Figure 1.19: Space wave (left) and Surface wave (right) surface [25]

1.4 Boundary Conditions and Scattering properties

GBCs describe the relationship between field discontinuity across a boundary and current sources on that boundary (located at $z = 0$), as in Equation 1.9.

$$\vec{Js}_e = \hat{z} \times (\vec{H_2} - \vec{H_1})$$
$$\vec{Js}_m = \hat{z} \times (\vec{E_2} - \vec{E_1})$$

(1.9)

$\vec{H_2}$, $\vec{E_2}$ are the total magnetic and electric field on the region $z < 0$; $\vec{H_2}$, $\vec{E_2}$, the total magnetic and electric field on the region $z > 0$. $\vec{Js}_e$ and $\vec{Js}_m$ are the surface electric and magnetic current across the boundary and the fields. Generally speaking, both are non zero (even if in many material is assumed continuity of the tangential electric component) and depends always by the surface characteristic and impinging fields.

The fields discontinuity imposed by the 2D EM discontinuity is also characterized with the Impedance Boundary Conditions (IBCs), as in Equation 1.10.

$$\vec{E_{av,tan}} = \bar{\bar{Z}}_e \cdot \vec{Js}_e$$
$$\vec{H_{av,tan}} = \bar{\bar{Z}}_m^{-1} \cdot \vec{Js}_m$$

(1.10)

$\vec{E_{av}}$ and $\vec{H_{av}}$ are the average values of the total tangent fields in the two regions. This means that the EM surface imposes a specific relationship on the tangential field components on the surface; the two conditions have to be verified consistently, as in Equation 1.11.

$$\frac{\vec{E_{2,tan}} + \vec{E_{1,tan}}}{2} = \bar{\bar{Z}}_e \hat{z} \times (\vec{H_2} - \vec{H_1})$$
$$\frac{\vec{H_{2,tan}} + \vec{H_{1,tan}}}{2} = \bar{\bar{Z}}_m^{-1} \hat{z} \times (\vec{E_2} - \vec{E_1})$$

(1.11)

19

Generally, $\bar{\bar{Z}}_e$ and $\bar{\bar{Z}}_m$ are non-diagonal square matrices; isotropic structures imply that they are diagonal and describe with diagonal components the polarization TE/TM of the fields, which however does not mix. In order to simplify analysis, in our specific case for the antenna design, the scattering elements (unit cells) are made up of PEC elements, and it is possible to assume that tangential electrical fields are continuous across the electrically thin surface. Those conditions hold true for metallic elements realized on a dielectric substrate and lead to no magnetic impedance. $\bar{\bar{Z}}_m$.

In the literature, there is a good explanation of the relationship between the scattering properties of the structure and the impedance and susceptibilities [25]; the latter are not reported here, but the main difference between the two descriptions is that, assuming isotropic structures, the impedance tensor depends on the incident angle of the field on the surface, while the susceptibilities do not. However, susceptibilities are described with a three-dimensional tensor, adding huge complexity when the surface is anisotropic. In the case of isotropic structures, one can determine the susceptibility tensor of the structure (together with the PEC assumption of the scatterers) with a set of measurements and use the results for an arbitrary field incident to determine the scattering properties of the structure. GSTCs have been studied in literature to overcome the problem that conventional field boundary conditions relate the field to the neighborhood of the discontinuity (i.e., $z = 0^{\pm}$), but not to the discontinuity (i.e., $z = 0$). Indeed, Stokes and Gauss theorems derive conventional BCs assuming field continuity in all the regions, including the interfaces, whereas the fields may be discontinuous in the presence of sources [26]. Then, MTSs can be represented equivalently by sheet impedance (IBCs) or surface susceptibilities (GSTC) [25]. Using IBCs, EM surfaces relate to the circuit models shown in Figure 1.20, and it is useful to analyze complex problems as multiple-layer MTS by means of cascading networks from circuit theory. It is noted that the values of sheet impedance depend on the impinging field, which makes the evaluation of arbitrary incident angles difficult with only a set of measurements. On the contrary, surface susceptibilities are characteristic parameters that do not vary with the impinging fields, but GSTCs are appropriate for MTSs with single-layer structures and unsuitable for more realistic multiple-layer problems.

This is why IBCs are used for the design process of the antenna, together with the fact that it is possible to numerically solve Maxwell's equation by means of an integral formulation of the problem to compute far-field radiation [7]. All the results above are related to EM surfaces surrounded by vacuum. Practical metasurfaces are realized on a dielectric grounded support that is very easy to manifacture and allows coaxial feeding, which is one of the most popular feedings for practical MTS antennas. They are called opaque IBC, as shown in Equation 1.12, when the field relation is expressed only on one side of the surface (ignoring the field on the other
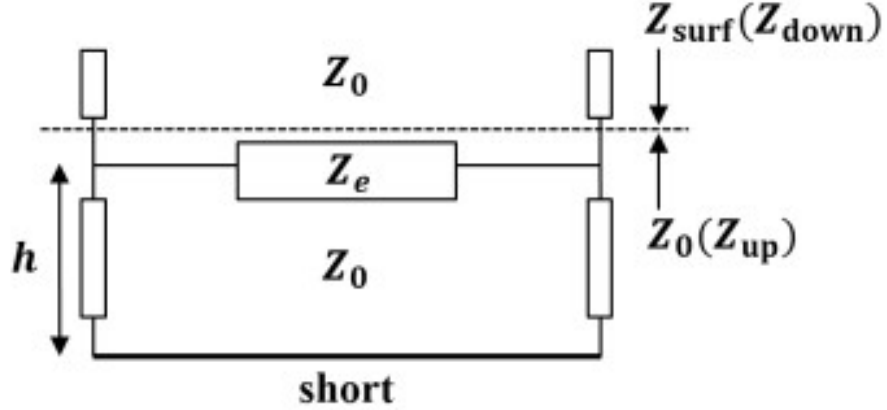
Figure 1.20: Transmission line equivalent model for the MTS and the grounded dielectric support [24]

side).

$$\vec{E_{tan}} = Z_{surf}^{=}\hat{z} \times \vec{H} \tag{1.12}$$

This kind of IBC is not suitable for the numerical integral formulation of Maxwell's equations since it leads to an ill-conditioned matrix for the numerical method. Transparent IBCs in Equation 1.11 ignore the spatial dispersion of the dielectric slab that must be taken into account but lead to a well-conditioned numerical problem. Method of Moment (MoM) formulation of the electric field integral equation (EFIE) to solve the EM problem of the structure, given the geometry of the surface and arbitrary feeding, is proposed, together with useful information on the validity of the numerical methods retrieved for transparent and opaque boundary conditions[7]. The opaque and transparent admittance equation, according to the transmission line model, is indicated in Equation 1.8 again. Validity of IBCs has been largely studied in literature as well [27]. In this thesis work, the IBCs are used to describe the MTS. This concept is not only used to characterize surfaces in terms of the equivalent transmission line model or solve the numerical EM problem associated with sources, but also to allow a faster modal analysis of the structures by means of the transverse resonant technique [22][18]. The transverse resonance condition is a powerful tool that can be used to derive the guidance condition of a mode in a layered medium or more complex waveguides (i.e., rectangular, dielectric waveguides, surface waves, etc.). The condition is related to the fact that, at cutoff frequency, the transverse field on the waveguide becomes a standing wave. This phenomenon can be modeled with an equivalent transmission line circuit operating at resonance. It is also possible to relate the scattered fields on the surface with

the surface impedance by means of two TE/TM illuminations orthogonal to the surface [24]. This is a fundamental result for this thesis work since the simulation of the surface impedance evaluated for each parameter combination of the unit cell is evaluated in this way, starting from the scattering matrix of the surface [22]. Fundamental results for this evaluation are reported in Chapter 2.3.

Chapter 2

Background information

2.1 The problem description

In this section, we briefly introduce the elements of theory that have been used to develop the thesis work. One of the most challenging topics in the research area of CPE (Advanced Computing, Photonics, and Electromagnetics) is focused on automating the design of such complex structures given an arbitrary radiation pattern. The LINKS foundation is currently working on this topic, and the research team is developing its own optimized code for each design step using the MATLAB development environment before a future porting towards more performing technologies (i.e., Python). A recent publication delivered by the team that followed me in my thesis work [8] gives an effective solution for the algorithm that performs the optimization process for the evaluation of the impedance profile of the surface.

The complementary part of the latter work involves the development of an algorithm that is able to create a "good" database of cell elements by fixing a given geometric shape of the cell element and the working frequency. This thesis work is focused on this part of the design of the MTS antenna.

This database of points represents the set of impedance points and the associated parameters of its geometry that it is possible to use to make the textured elements of the antenna. In general, the realized profile is different from the desired one since it takes the nearest points in the cell database. It is not straightforward to understand what combination of parameters realizes a certain impedance point because it is a very complex process; indeed, impedance values are evaluated starting from a scattering matrix of the structure through a PSSM (Chapter 2.3) software module and from some fundamental theoretical results [22]. Furthermore, the impedance points are not scalar values but a triad, since they involve an anisotropic behavior of the structure. It is not trivial to define what "good" means for this kind of

purpose. Practically speaking, the database of points should be dense enough in a volume where the points of the desired impedance surface profile lie. This is a very general constraint: it is not known how and where the image of the function will distribute a priori because it changes with the geometry of the unit cell and the choice of the parameter combination that characterizes the geometry. The general numerical output of the impedance $Z(X)$ has the following form:

$$Z(X) : R^n \rightarrow R^3$$
$$X : (x_1, x_2, ..., x_n) \in R^n \qquad (2.1)$$
$$Z(X) : (X_{rr}, X_{rp}, X_{pp}) \in R^3$$

With X being the combination of the parameters that realizes physically the unit cell (i.e., lengths or angles) and $Z(X)$ the associated impedance output value, that is identified by the scalar values X_{rr}, X_{rp}, and X_{pp}. This is possible thanks to some properties of the structures, such as passivity (a symmetrical matrix with purely imaginary components). Scalar unit cells (i.e., circular unit cells) also have an impedance tensor Z diagonal with equal principal components. The impedance tensor Z depends also on frequency, but it is assumed to be fixed in this frame as the working frequency of the antenna; the sensitivity of $Z(X)$ with respect to the frequency and X are also fundamental knowledge for practical realization (i.e., choosing a suitable insensitive unit cell with respect to manufacture and frequency tolerances) but are out of the scope of this work.

It is possible to define a multivariable constrained optimization problem for $Z(X)$ to minimize the distances between the set of points desired Z_{ideal}. However, this method has been observed to be not so effective in reducing the distance with respect to desired points while using MATLAB built-in solutions (i.e., "fmincon"). Due to the high irregularity of the numerical output function $Z(X)$, it is very difficult to use effectively gradient methods; heuristic algorithms such as the Genetic Algorithm (GA) may be convergent, but they are inherently too slow and find only a single impedance point, then they are not suitable to build a database. Furthermore, it is not trivial to invert an unknown numerical output and understand if the image of the function exists near the impedance points desired.

Indeed, it is very common to find that the numerical output $Z(X)$ does not have an image of the values of the set of ideal points Z_{ideal}; even if it does, it is very difficult to understand what X point realizes those values.

The approach that has been used in constructing the impedance points database so far has consisted of uniform sampling of the parameter space X. Each component of $x_1, x_2, ...x_n$ is limited by some upper and lower boundary value, and it is sampled uniformly (i.e., max size according to unit cell periodicity and min size due to tolerances): all the possible combinations of the parameter components were taken. This approach, however, seems to be effective to build a database only if the database is very dense and only if the image of the function $Z(X_{grid})$ evaluated on

the grid X_{grid} distributes near the set of points Z_{ideal}.

This is, of course, not verified in general; further, one does not have any control over where to refine the point density in the $Z(X)$ domain volume: that is the main task of the developed algorithm for the thesis work.

Indeed, they have identified two main specifics for the Search Algorithm:

1. It is best to distribute as uniformly as possible the image of $Z(X)$ by sampling properly the parameter space X.

   This helps to understand the range of the possible values that that unit cell geometry can realize at that frequency, and it could eventually help the optimization algorithm that finds the desired points Z_{ideal}, since it forces the optimization algorithm to find solutions only near realizable points and not using the usual upper and lower boundary for X_{rr}, X_{rp}, X_{pp} components;

   Uniform distribution also means that the distance between all couples of points is equal, and then the maximum error when using database points instead of desired values is half this (average) distance;

2. Once Z_{ideal} is available from the optimization process, representing the values that realize the desired radiation pattern under some feeding assumptions (i.e., coaxial feeding) and antenna geometry (i.e., circular), it is best to refine the search around those Z_{ideal} ideal values by choosing the proper X parameter points. In this way, even if the image of the function $Z(X)$ does not cover the ideal points, we are sure to take the nearest points possible to them.

The first condition is the hardest to meet, practically impossible in real cases: the image of the impedance $Z(X)$ can be distributed non uniformly in the impedance space. However, the algorithm developed will always take points in the most uniformly distributed way at parity of simulated points, and it is valid for any cell geometry we are able to define. The second condition is more easily realized, and it is achieved by restricting the point search around the desired ones.

2.2 Typical design process

Typical design process [8][5][26][9] for this kind of antenna does not involve a full wave analysis, but it is done with a simplified model to fasten the design. In general, the design process starts with defining some geometrical boundaries for the antenna and constraints on the radiation pattern. A full wave analysis of the multi-scale structure like the MTS involves intrinsically millions of unknowns, and it is performed only at the end to check the correctness of the radiation pattern constraints. A well-known publication in the literature [5] proposes a mathematical model based on the adiabatic Floquet expansion for the surface wave electrical

field, in which the wavefront is shaped according to the IBCs under the assumption of ideal monopole feeding at the center of the structure. A mathematical model of the aperture field is used to evaluate far-field radiation, from which it is possible to constrain the radiation pattern. However, the aperture field depends on some physical parameters (i.e., the propagation constant of the surface wave) that are assumed to be known or approximated. Furthermore, the model is valid only for circular antennas. Another work proposes another different mathematical model for the design, always using the IBCs to characterize the MTS structure [9]. A recent publication [8] from the team that followed me in my thesis work gives a very general method to solve the numerical EM problem associated with a generic-shaped surface characterized by IBCs and some feeding without any mathematical assumption on the surface wave field shape. The validity of the numerical method has also been tested in the paper for well-known theoretical results. This is based on the EM numerical solution of the surface problem-based electrical field integral equation, discretizing the surface domain by the Method of Moments.

Under some assumptions, the IBCs are sufficient as a boundary conditions to solve the problem and give a unique solution for the aperture field. Transparent IBC has been demonstrated more effectively in modeling spatial dispersion effects due to the dielectric grounded support, leading to a stable numerical method [7]. An optimization algorithm [8] proposed in the same work is able to find the best coefficients for the electrical current distribution on the surface that minimize the error with respect to the radiation pattern constraints. Since the IBCs assumptions are given, it is possible to find a relationship between current coefficients and impedance surface values. Radiation pattern constraints are given in terms of mask type, usually on directivity or gain. The dissertation is very complex, and it will not be discussed further.

The scope of this thesis is to deal with the complementary part of this work, the impedance database generation. Once the desired impedance point values for the surface have been found, it is necessary to physically realize the unit cells that match those values. This is done by finding the nearest points to the desired ones in a pre-computed database of impedance points. This pre-computed database, so far, has been evaluated by taking the unit cell parameters geometries and dividing the parameter ranges (according to the physical constraints of the cell) in a uniformly dense way: a grid of parameter points, where each point represents a combination of all the parameter values. This represents uniform sampling for the parameters that generate the impedance database; this does not mean that the impedance points are distributed uniformly in the image. The function $Z(X)$ that associates the impedance point values with some combination of the unit cell parameters is numerically evaluated through some simulation (see 2.3) to be more accurate; indeed, interpolation of impedance values is often not effective if the image of $Z(X)$ is under sampled in the domain, something that happens generally speaking.

They are reported in Figure 2.2 and 2.1, the outcome for the realized radiation pattern and mask with associated IBCs from numerical simulation from some numerical results [6]. In the latter work, it is assumed the impedance is scalar; generally speaking, the impedance is a 2D tensor and gives more flexibility for arbitrary polarization realization. Pattern mask imposes in the plane cut $\varphi = 90°$ a main lobe region between $\theta \in (-3°,3°)$ and side lobe region going from $\theta = 15°$, with side lobe level under -15 dB for a circular antenna of radius $10\lambda_0$, yielding 25.5 dB of directivity.

Starting from the desired IBCs, it is possible to physically realize the unit cell by choosing the nearest values in the impedance database. Some unit cells could realize scalar impedance, depending on the geometry and symmetry of this one; one must choose the best cell kind according to the polarization and radiation pattern requirements. At the end, it is checked if the realized antenna satisfies the radiation pattern constraints with both integral numerical formulation analysis (approximated results but fast computation) and full wave analysis (slower but more accurate results). This kind of design process has been demonstrated to be very effective for a variety of well-known structures with respect to theoretical results and full wave analysis [6][8].

2.3 PSSM Software Module

PSSM (Periodic Surface Spatial-Spectral Modeler) solver is an EAML (European Antenna Modelling Library) software module that is able to evaluate the scattering problem for an incident plane wave on the user-described structure geometry. The structure could be defined in two different ways:

1. Composed of metallic conductor; these can be embedded in a layered medium, with the possible presence of a backing infinite (unperforated) plane. ("ground" plane); the plane is usually a perfectly conducting electric (PEC) plane, but the possibility of magnetic conductor has also been incorporated.

2. Composed of apertures in an infinitely extended perfectly conducting (PEC) plane.

Typical applications regard Frequency-Selective Surfaces (FSS) applications [28], modeling of grid reflector surfaces, analysis/design of the single cells of reflectarrays, as well as the approximate analysis of very large finite arrays. FSS are used to achieve some spatial filtering of the incoming EM incident wave, analogous to the microwave filters according to the circuit theory. Filtering characteristics of FSS could be categorized into four well-known kinds of pass bands: stop band, low pass, and high pass, according to the operative frequency band. Several kinds of applications are possible for such structures. The main difference between the MTS
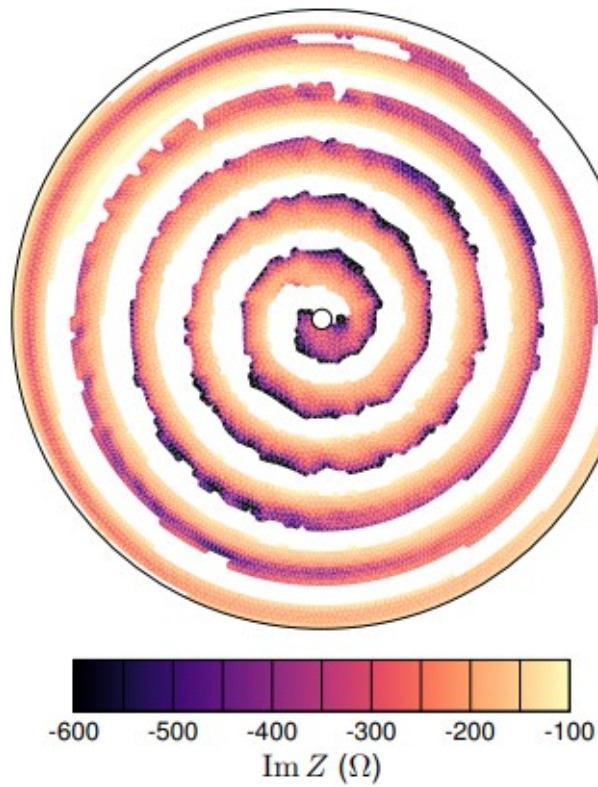
Figure 2.1: Impedance boundary condition (IBC) for scalar impedance distribution of the surface retrieved with some numerical method discussed in [6]
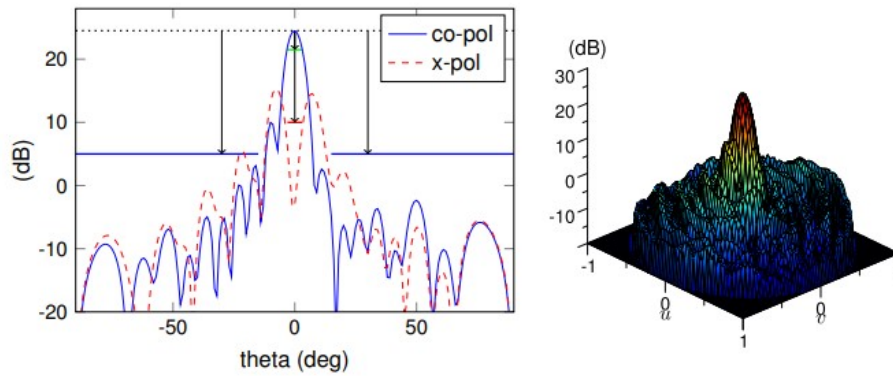

Figure 2.2: Radiation pattern mask constraints in the $\varphi = 90°$ and realized radiation pattern with IBC (left); 3D radiation pattern in the u,v plane (right)

and FSS is the spacing between adjacent elements, which is usually higher than the wavelength in FSS. Indeed, spatial filtering is achieved thanks to the spatial dispersion of the surface. Typical FSS applications involve EM absorbers, radar cross-section control, electromagnetic interference (EMI) reduction, radome, EM cloaking, and the capability to work at very high frequencies up to THz bands. It is possible to describe a MTS with such PSSM software, since it imposes a unit cell periodicity that is lower than wavelength.

In our applications, aperture radiation engineering is done by imposing the impedance boundary conditions on the surface (IBCs). Those conditions characterize the EM discontinuity that is represented physically by the MTS. Then, a software module is needed to extract the equivalent impedance of the periodic MTS, and a grounded dielectric is needed to complete the design process. This tool should also be faster in computation compared to full wave analysis tools since the structure is inherently multi-scale. Because the structure is quasi-periodic, it is possible to simulate its effective surface impedance using a single unit cell with a periodic boundary condition. The PSSM uses Floquet expansion to solve the EM scattering problem of the structure; the theoretical framework used to solve the structure is out of the scope of this thesis, and the PSSM is given as a black box tool. This results in faster computations for impedance values $Z(X)$. It is useful to understand that if the unit cell impedance values are slowly varying, it is possible to design non-uniform surfaces by just simulating another parameter X combination with the same periodicity hypothesis. Simulation time depends both on the mesh step and the metallic pattern shape complexity (i.e., the number of mesh vertices and faces). In our simulations, the mesh step has been fixed to a fraction of the guided wavelength, which represents the best trade-off between simulation time and accuracy results. The input of this PSSM software module is the mesh of the single unit cell metallic shape, EM parameters, and the structure description of the layered medium; these will not be discussed further, and they are generated properly by some MATLAB scripts according to the structure description.

The output is a scattering matrix $S(\varphi_{inc}, \theta_{inc}, f)$, which depends on the $\varphi_{inc}, \theta_{inc}$ incident plane directions (polar coordinates) and the working frequency f. The database is built assuming a fixed frequency and unit cell shape (but varying parameters of its geometry) in this frame, and if the incident angle for the plane wave it is needed for our purpose is normal to the surface, then $\varphi_{inc} = 0°, \theta_{inc} = 0°$. Indeed, according to the fundamental results presented in the literature [18][22], it is possible to extract the admittance tensor that describes the MTS according to the equations in 2.6. The problem description is reported in Figure 2.4. In order to extract the admittance tensor, it is needed to have two orthogonal TE and TM surfaces. According to the structure definition, the TE and TM incident fields and

29
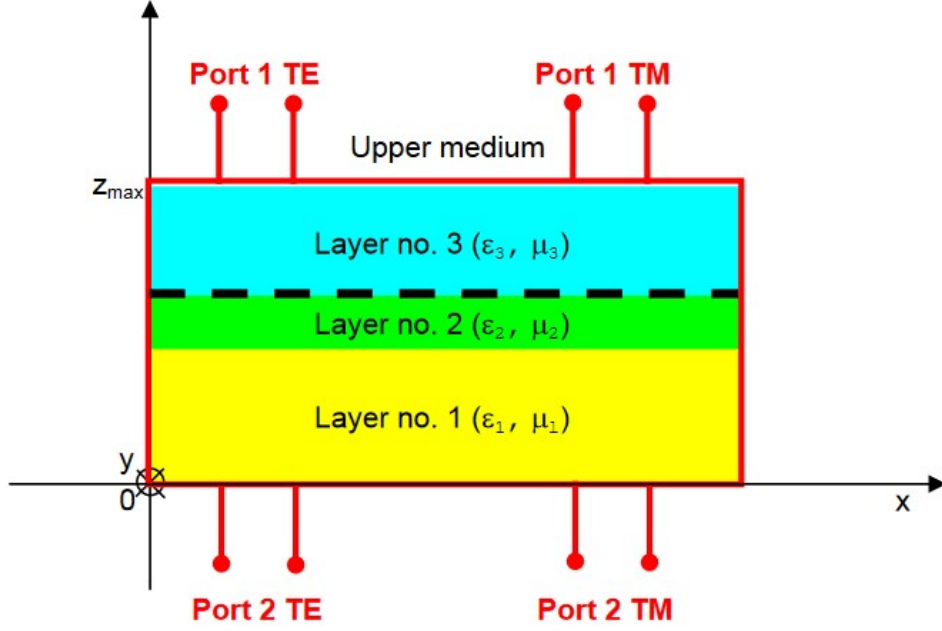
Figure 2.3: Layered structure definition for the PSSM. Unit cell is at top of the surface, ground plane at bottom.

reflected fields are defined as in Equation 2.2.

$$
\begin{aligned}
E_i^{TE}(z) &= V_{TE}^I e^{jk_2 z} \hat{y} \\
E_i^{TM}(z) &= V_{TM}^I e^{jk_2 z} \hat{x} \\
E_r^{TE}(z) &= V_{TETM}^R e^{-jk_2 z} \hat{x} + V_{TETE}^R e^{-jk_2 z} \hat{y} \\
E_r^{TM}(z) &= V_{TMTM}^R e^{-jk_2 z} \hat{x} + V_{TMTE}^R e^{-jk_2 z} \hat{y}
\end{aligned}
\tag{2.2}
$$

Where V_{TETM}^R, V_{TETE}^R and V_{TMTM}^R, V_{TMTE}^R are unknown but are proportional to V_{TE}^I, V_{TM}^I amplitudes through some scattering coefficients that are evaluated by PSSM simulation. It is highlighted that, due to the generality of the MTS structure, it is possible to have mode mixing in reflection (indeed, the tensor could be non-diagonal), as is clear from the polarization of the reflected fields. This effect could be wanted or unwanted depending on the kind of application; in our case, it could give more flexibility for arbitrary polarization of the desired far field. The magnetic field H is evaluated with the well-known plane wave relation $\bar{H} = \frac{k_z \hat{z} \times \bar{E}}{Z_2}$, with $Z_2 = \sqrt{\frac{\epsilon_2}{\mu_2}}$. The output of the PSSM module is a reflection matrix that describes

the MTS surface and the grounded dielectric:

$$\begin{bmatrix} V_{TE}^R \\ V_{TM}^R \end{bmatrix} = \begin{bmatrix} S_{11} & S_{12} \\ S_{21} & S_{22} \end{bmatrix} \begin{bmatrix} V_{TE}^I \\ V_{TM}^I \end{bmatrix} \tag{2.3}$$

Where $V_{TE}^R = E_r^{TE}(z = 0)$, $V_{TM}^R = E_r^{TM}(z = 0)$. The relation between fields and voltages on the top of the surface $z = 0$ is given by Equation 2.4.

$$\begin{aligned}
\bar{E}_R^{TE} &= V_{TE}^R \hat{u}_{TE} + V_{TM}^R \hat{u}_{TM} = S_{11} V_{TE}^I \hat{u}_{TE} + S_{12} V_{TM}^I \hat{u}_{TM} \\
\bar{E}_R^{TM} &= V_{TE}^R \hat{u}_{TE} + V_{TM}^R \hat{u}_{TM} = S_{21} V_{TE}^I \hat{u}_{TE} + S_{22} V_{TM}^I \hat{u}_{TM} \\
\bar{E}_I^{TE} &= V_{TE}^I \hat{u}_{TE} \\
\bar{E}_I^{TM} &= V_{TM}^I \hat{u}_{TM} \\
\bar{E}^{TE} &= \bar{E}_R^{TE} + \bar{E}_I^{TE} = V_{TE}^I(1 + S_{11})\hat{u}_{TE} + S_{12} V_{TM}^I \hat{u}_{TM} \\
\bar{E}^{TM} &= \bar{E}_R^{TM} + \bar{E}_I^{TM} = V_{TM}^I(1 + S_{22})\hat{u}_{TM} + S_{21} V_{TE}^I \hat{u}_{TE}
\end{aligned} \tag{2.4}$$

Where $\hat{u}_{TM} = \hat{x}$, $\hat{u}_{TE} = \hat{y}$. Total fields are TE and TM illumination, which are the sum of incident and reflected waves. It is clear from Equation 2.3 and 2.4 that the non-diagonal terms S_{12} and S_{21} represent, respectively,the TM illumination that generates a TE reflected field on the $\hat{y}$ direction and the TE illumination that generates a TM reflected field on the $\hat{x}$ direction. This phenomenon is typical of anisotropic EM media. Dielectric grounded support does not directly have such an EM characteristic, but the periodic pattern layer of metallic conductors (the unit cells are made up of the surface) makes the equivalent total impedance surface anisotropic. It is possible to de-embedding the periodic array contribution (MTS) and the dielectric grounded substrate considering an equivalent transmission line model, as shown in Figure 1.20. The transmission line model for TE and TM modes for dielectric grounded substrate is given by well-known theoretical results, and the equivalent impedance is equal for both modes without mixing terms because of the full symmetry of the structure. The MTS impedance sheet is described by a lumped impedance that is in parallel to the dielectric grounded line. The lumped model is justified by the fact that the MTS is electrically thin. The total surface admittance can be written as:

$$\bar{\bar{Y}}_{surf} = \begin{bmatrix} Y_{xx}^{sheet} & Y_{yx}^{sheet} \\ Y_{yx}^{sheet} & Y_{yy}^{sheet} \end{bmatrix} + \begin{bmatrix} -jZ_1 \cot k_1 h & 0 \\ 0 & -jZ_1 \cot k_1 h \end{bmatrix} \tag{2.5}$$

Where d is the thickness of the dielectric, Z_1, and k_1 is the characteristic impedance and propagation constant in the dielectric. The matrix components $\bar{\bar{Y}}_{sheet}$ are extracted from the total fields component (reflected plus incident) on each direction, thanks to the PSSM information and some fundamental theoretical results [22]

31

that are reported in Equation 2.6.

$$Y_{xx}^{surf} = \frac{E_y^{TM} H_y^{TE} - E_y^{TE} H_y^{TM}}{E_x^{TM} E_y^{TE} - E_x^{TE} E_y^{TM}}$$

$$Y_{xy}^{surf} = \frac{E_x^{TE} H_y^{TM} - E_x^{TM} H_y^{TE}}{E_x^{TM} E_y^{TE} - E_x^{TE} E_y^{TM}}$$

$$Y_{yx}^{surf} = \frac{E_y^{TE} H_x^{TM} - E_y^{TM} H_x^{TE}}{E_x^{TM} E_y^{TE} - E_x^{TE} E_y^{TM}} \quad (2.6)$$

$$Y_{yy}^{surf} = \frac{E_x^{TM} H_x^{TE} - E_x^{TE} H_x^{TM}}{E_x^{TM} E_y^{TE} - E_x^{TE} E_y^{TM}}$$

It can be shown that the input amplitude of the electric fields for the two illuminations TE and TM, V_{TE}^I and V_{TM}^I, will not affect the evaluation since they will simplify out the ratio. Then, they will normalize to one in the evaluation of the total surface admittance $\bar{\bar{Y}}_{surf}$. This not only represents the MTS contribution but also the grounded dielectric. The sheet admittance $\bar{\bar{Y}}_{sheet}$ is evaluated as shown in Equation 2.5. The impedance tensor of the MTS sheet is evaluated as the inverse of the admittance tensor $\bar{\bar{Z}}_{sheet} = \bar{\bar{Y}}_{sheet}^{-1}$. The PSSM module is used together with
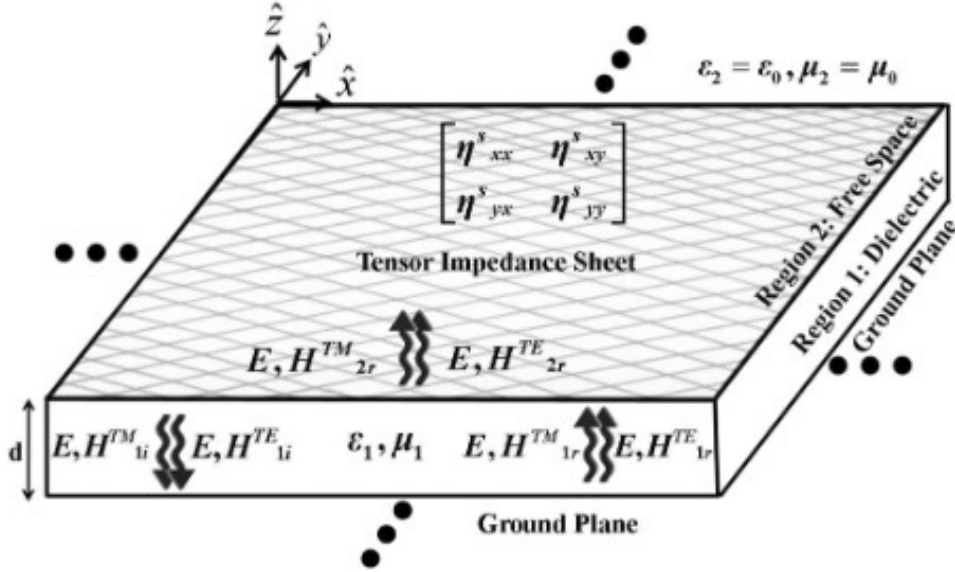

Figure 2.4: Problem description for the impedance extraction [22]

some MATLAB functions to extract the impedance tensor, which describes the MTS sheet during the impedance database generation. Each time, a new unit cell defined by the X parameter point is needed to be evaluated. Indeed, the $Z(X)$

value is not interpolated, but it is preferred to be evaluated with direct simulation due to the high complexity of the structure. Then, this PSSM module is called a number of times that is equal to the number of points that have been found in the database generation (see later in Chapter 3). For this reason, typical database generation could take many hours up to a couple of days for a very large database (i.e., more than 10,000 points). PSSM simulation time of a single unit cell strictly depends also on the unit cell geometry complexity and the mesh step size; in this setup (AMD RAM, 16 GB RAM), the simulation time of a single unit cell is about 3 seconds; impedance database generation could last even several days, depending on the number of points generated and the unit cell complexity. At least, the PSSM software module does not allow to define an incident wave from above since the geometrical references for the electric field it uses have a fixed sign for the incoming wave on the positive $\hat{z}$ axis and the absolute value of k_z is determined only by the polar coordinate θ angle. It is well known that the latter angle range is between zero and ninety degrees. Theoretical results have been evaluated in Equation 2.4 and 2.6, but for the incident wave that comes already from above, namely with $-\hat{z}$. However, PSSM software evaluates results for $\hat{z}$ direction for incident waves; apparently, it is not possible to define incident waves that come from above. In order to solve this problem, it has been evaluated using the same matrix but with $-\hat{z}$ for the unit vector. Understating how the output scattering matrix is influenced by that is now straightforward because it is sufficient to substitute the definition of the versor $\hat{u}_{TE}$ with $-\hat{u}_{TE}$ ($\hat{u}_{TE} = \hat{z} \times \hat{u}_{TM}$).

This leads to inverting the sign of the scattering matrix components on the outside of the diagonal. Verifying the PSSM properties, functionalities, and output scattering matrix with the corrections to the MATLAB code for the evaluation of the impedance tensor has been an active part of this thesis work, together with the impedance database algorithm generation that is presented in Chapter 3.

Chapter 3

Impedance Database Generation Algorithms

In this section, the algorithms that have been used to implement impedance database generation are described. Main features of the algorithms are presented together with some explicative figures and the proposed pseudo-algorithms for implementation.

3.1 Box Search Function

In this section, the "Box Search" algorithm has been developed for this thesis work is presented. According to what is discussed in Chapter 2, a heuristic approach is used for the sampling of the space parameter X and the generation of the corresponding impedance points $Z(X)$.

The idea behind the algorithm is to use a division of the impedance domain into search boxes. Each search box is then explored; it is checked if the interpolant $Z_{interp}(X_{query})$ built with only the nearest points to the box and evaluated on some X_{query} points has an image in the box. If this is verified, the corresponding subset X_{found} of X_{query} (according to the minimum number of points required for each search box) is taken as valid for the database, and the corresponding $Z(X_{found})$ impedance points are evaluated using the PSSM module (see Chapter 2.3).

The database is then iteratively updated for each search box explored. The search starts with a coarse database $Z(X_{start})$ that is evaluated with the PSSM, uniform sampling the parameters space X_{start}. Of course, this approach relies on the fact that the evaluated $Z(X_{found})$ points belong to the search box. This condition could be difficult to meet for several reasons:

1. $Z(X)$ has not image in the current search box;

2. Interpolant can be locally inaccurate when the database has few points, typically when the database is coarse or when it is not uniformly distributed;

3. Interpolant can be very inaccurate due to the irregularity of the numerical output $Z(X)$ (i.e., the high gradient around some points);

However, this does not represent a real issue since it would be sufficient to take $Z(X_{found})$ points in the neighborhood of the boxes, something that most likely happens in most cases when, eventually, enough points are generated.

The linear interpolant is evaluated with the nearest points to the search box using the in-built MATLAB solution 'griddatan', which is able to fit the hypersurface components X_{rr}, X_{rp}, X_{pp} with scattered X data using a Delaunay triangulation for the query X_{query} points.

The function works with N-D scattered data that is suitable for the general setting; however, no extrapolation of data is possible outside the triangulation with this solution. For this reason, the X_{query} points have been taken as a dense grid between the maximum and minimum of the component values X_{interp} are used to evaluate the local interpolant.

Then, they are selected only a part of these points (i.e., 10) in order to keep simulation time reasonable; they are taken as valid the corresponding X_{found}, and they are simulated the associated $Z(X_{found})$ value with PSSM module and some coding. X_{found} points are selected randomly among the X_{query} that has image $Z_{interp}(X_{query})$ in the current box.

These functionalities have been implemented by a function called "BoxSearch". This function takes as input a "param" structure that fully describes the unit cell database (EM parameters, type of cell, name of parameters, etc.), the input parameter points X_{start} with the associated impedance points $Z(X_{start})$, and some other fundamental parameters that will be detailed later. The number of points X_{start} have to be enough to properly start the search with interpolant; for example, 343 points have been used for 3-D parameter space X databases that have been considered in this work (7^3, dividing each parameter range in 7 points and taking all the combinations of them).

They are reported as the input parameters for the "BoxSearch" function that has been developed for the "Search Algorithm":

1. $Z(X_{start})$, X_{start} input database points evaluated on a low-density grid of the input parameters range;

2. *data* EM structure parameters for the PSSM simulation and impedance $Z(X)$ evaluation;

3. The number of points N_{point} that ideally have to be found in each search box;

4. The centers of the boxes $center_{points}$ in the Z impedance domain;

5. The lengths of the rectangular search boxes $lengthcube_x$, $lengthcube_y$, and $lengthcube_z$;

6. A number $numGrid$ that indicates the division of each range of the parameters for the construction of the query grid X_{query};

7. The minimum number of points used for the interpolation $minpoints_{interp}$

8. A matrix $coeff$ that is used to rotate the output of the impedance domain Z after each PSSM simulation (see Chapter 3.2);

They are resumed the main steps that are iterated for each search box. Each box is defined by its own center point; lengths are equal for all boxes.

1. It is checked if the database Z_{update} has less than N_{points} inside the search box; if that happens, it is tried to take N_{points} with local interpolation inside the box otherwise, it is passed to the next box;

2. They are found at least $minpoints_{interp}$ near the search box center to build the interpolant Z_{interp}.

3. Interpolant is evaluated with 'griddatan' on the query grid X_{grid}. It is checked if $Z_{interp}(X_{grid})$ has an image in the search box; if that happens, N_{points} are randomly selected inside the image; otherwise, it is passed to the next search box.

4. The subset of the parameters (X_{grid}) points, namely X_{found}, is added to the database points; $Z(X_{found})$ is simulated with the PSSM module and added to the database as well;

These steps are repeated until they have explored all the search boxes; at the end, a full-box exploration of the impedance domain is obtained and the corresponding database points are generated.

At least, a pseudocode for the 'Box Search' implementation is given in Appendix A. A flow chart is reported as well in Figure 3.1.

3.2   Search Algorithm Function

In the previous section (Chapter 3.1), it has been described the fundamental block on which the developed Search Algorithm for this thesis work is based.
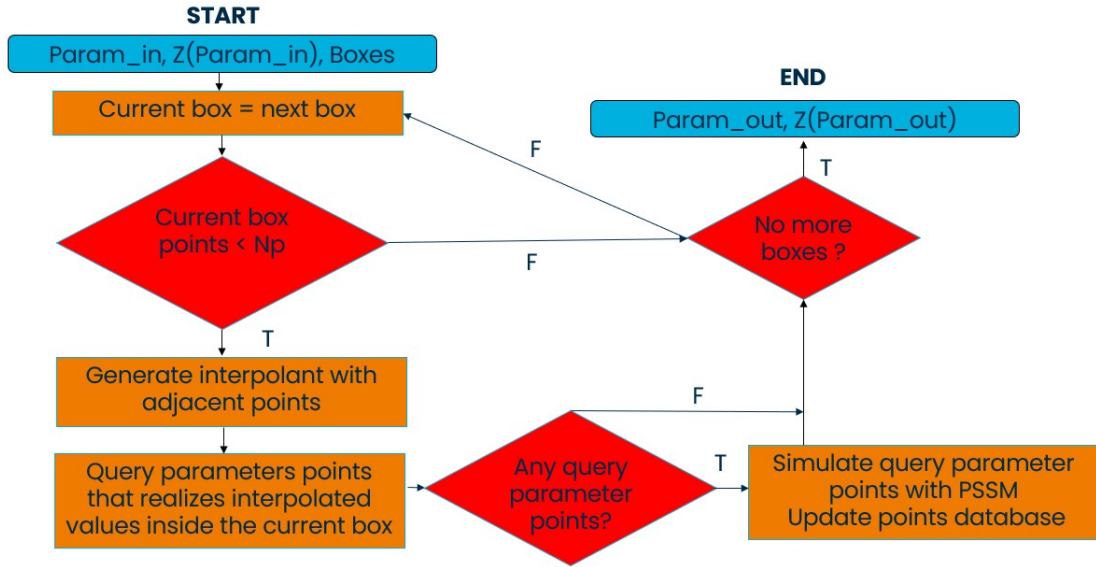
However, some important questions still remain:

Figure 3.1: Flow chart proposed for the Box Search implementation

1. The impedance point search is based on rectangular (boxes) division of the $Z(X)$ impedance domain; this may not be so effective for some convex hull shapes (i.e., narrow, rotated hulls) because many of the boxes could be outside the hull and smaller boxes would be required to discretize effectively the image of $Z(X)$.
   Is it best to perform the search not directly on the original domain but by applying some linear transformation in order to make the box division more suitable?

2. Center points and lengths of search boxes are given, but how should they be chosen to have a "good" discretization of the impedance domain?

3. An effective database is built iteratively on successive Box Searches, but what are the conditions that should be met to stop the overall search?

Domain rotation is a feature that has been developed after the first version of the Search Algorithm. Indeed, the first version was able to explore the image of the function $Z(X)$, but not effectively as expected: some subvolumes of the impedance were empty. By only refining the box division, this effect is mitigated, but with the consequence of increasing simulation time.
A Principal Component Analysis (PCA) MATLAB tool: 'pca' has been used to evaluate the matrix coefficients for the domain rotation, starting from the input impedance points Z_{start}.
This domain rotation is particularly suitable for a rectangular box division of the

search domain, since rotating the database points on its principal plane will always make the points distributed on a volume that resembles, as much as possible, a rectangular domain on the new axis, with the consequence of having boxes that enclose more effectively the convex hull. Furthermore, whenever they are given the desired impedance points $Z_{desired}$, available as design process outcome (Chapter 2.2), it is possible to rotate the domain according to these points, achieving the database refinement necessary to the final goal of reducing the average distance between database points and desired points (see Chapter 4).

The center points and lengths of boxes have to be chosen according to the image of $Z(X)$, which is however unknown a priori.

Some considerations that have been empirically observed during the development of the algorithm are reported:

1. Ideally, it is best to have point centers that lie inside the convex hull of $Z(X)$. However, at first, the database of points is very coarse, and they are given few impedance points (i.e., about 300). A good estimation of the convex hull is not possible, together with the fact that the $Z(X)$ function has an image that is generally only some subdomain of the convex hull.
   Further, those starting points could be crowded in some regions, leaving most of the convex hull empty. For this reason, it is decided to take the centers inside the cubic domain volume defined by the min and max of each component of the starting points Z_{start}; the centers are regularly spaced inside this cube; those boxes are not overlapping and generated by some functions (Chapter 3.3). After a first "Box Search" performed according to the boxes defined on these centers, it is possible to take further "Box Searches" with boxes into the convex hull since it is assumed to have enough points, after a first search, to properly estimate the convex hull.

2. The lengths of boxes should be chosen, ideally, as small as possible, to have a uniform and dense point impedance distribution in the generated database. Practically, having small boxes is not a good idea because local interpolant is not accurate enough to generate all points inside the box, with the consequence of skipping most of the search boxes and then increasing simulation time, also due to the high number of search boxes (see Appendix 1). Further, lengths should be normalized according to the range of $Z(X)$ components, unknown a priori. For this reason, it has been proposed a method for the division, starting from the rotated domain, that involves a user-defined number of divisions for the maximum range of the $Z(X)$ component (i.e., $N = 10$; the maximum range of $Z(X)$ is divided into 10). The other components division are automatically estimated in such a way that smaller ranges have the finest division (inverse proportional to the higher range), with some caps to avoid the generation of too many boxes. This has been empirically observed as very

effective in generating proper box lengths; it seems that narrower ranges need more refinement to be properly explored.

3. Once it is performed a first search on those boxes, iterative searches follows to refine more uniformly possible the database. In the first version, iterative searches have been done on the same previously defined box division. However, the method has been observed to be not so effective since only a few points would be taken on each complete exploration of all boxes, and, worst of all, they were not uniformly distributed on graphical inspections.

   This is due to the fact that boxes may contain the required minimum number of points and are skipped for the search, together with the fact that previously founded points may be clustered in some regions; a new box division of the impedance domain is needed.

   The idea that has been implemented to solve such an issue is to generate randomly sampled center points for boxes inside the convex hull, a good amount of them (i.e., 2000), in order to cover statistically all the convex hull volume.

   This helps to avoid taking boxes outside the convex hull, where very probably $Z(X)$ has no image, and also to generate points in the most uniform way. Indeed, taking random search boxes into the convex hull implies that generated impedance points lie in their vicinity, statistically homogenizing the distribution of simulated points when enough boxes are used.

Stop conditions for the Search Algorithm should consider a trade-off between simulation time and the number of points the user wants to generate in a single search. Furthermore, a number of maximum iterative searches have to be considered in order to force convergence of the algorithm if the minimum number of points wanted is not found. This phenomenon never happens in our numerical simulations, but it is a good practice to insert such a condition.

At least, it may be useful to insert a condition that considers a minimum increment point increment between two consecutive Box Searches: if it is too low (i.e., lower than 200), it may not be worthy to perform other Box Searches indicating that in each box are present at least the minimum number of points defined by the user.

This section ends with a brief explanation of how to use the developed Search Algorithm.

A "Blind Search" is first performed without having constraints on sub-volumes or desired points. This is typically done whenever it is not available a pre-computed database of impedance points (coarse as well) that does not explore all the image of $Z(X)$ in a "uniform" way (points clustered in some regions); It takes a good amount of points, but it is not dense (i.e., 5k points minimum) in order to keep simulation time low while generating a good amount of points.

This "Blind Search" database can be used both to inspect graphically the point

distribution and to have a good sampling of all the images of $Z(X)$; generally, this does not happen with the database generated by uniformly sampling the parameters. Furthermore, this database gives a first idea of the realizable values of the points $Z(X)$ with that kind of geometry and parameter points X for that specific unit cell at a fixed frequency; it may be used at the optimization process design step. Indeed, it may help the optimization process to realize desired values that are a trade-off between the radiation pattern constraints and the realizable database points. The user can perform another run of the Search Algorithm with such constraints to refine the impedance database around specific subvolumes that are of interest.

"Refinement Searches" involves generating more points (i.e., 10k) but only confined to some region of interest, practically near the desired points, in order to generate a uniform and dense distribution around them since it is practically unfeasable (no solution for the counter image) to find the exact parameter points $X_{desired}$ that realize all the desired values $Z_{desired}$. Generate the impedance points in such a way as to decrease the average distance to the desired points.

This is the method proposed together with the developed Search Algorithm for this thesis work, obtaining the results reported in Chapter 4.

They sum up the inputs of the "SearchAlg" function:

1. $Z(X_{start})$, X_{start} coarse input database of points;

2. "*data*" EM structure parameters needed for the PSSM simulation and impedance $Z(X)$ evaluation;

3. Z_{ideal} are the desired points of search. If it is empty, the domain rotation is done according to the $Z(X_{grid})$ points; otherwise, according to the Z_{ideal} points;

4. *hullsearch* flag indicates if the iterative box searches should be on boxes whose centers lie in the convex hull of the rotated domain or on centers that lie between the minimum and maximum impedance values of the rotated domain.

In this thesis work, it has been observed that after a "Blind Search", the generated database with refinement, according to a domain rotation around the $Z_{desired}$ points, gives the best results in terms of lower average distances with respect to the case where the domain rotation is performed according to the input impedance points. This is due to the fact that the search is restricted near the $Z_{desired}$ desired points and the search boxes are generated effectively around those points.

The *hullsearch* flag can be an arbitrary set; in this work, it has been preferred to choose "true" for a "Blind" searches and "false" and for "Refinement" searches because on the latter, it is required to take boxes around only the desired points.

They are briefly reported the main operative steps of the "SearchAlg":

1. Initialize parameters described in Chapter 3.1 and Appendix 1.

2. Rotate the search domain according to whether it is provided by Z_{ideal}.

3. Generate the first search boxes (Figure 3.3).

4. Perform a first Box Search with the "SearchBox" Algorithm (Appendix 1), exploring all the boxes, and update the database of points (Figure 3.5).

5. Perform iterative Box Searches (Appendix 1) on new boxes generated randomly in the convex hull of the current database or between minimum and maximum values of current impedance database points (Figure 3.4); iterative searches are performed if they are not found at least *minpoints* for the database. Iterative searches end when End-Of-Loop (EOL) conditions are not met. The database is updated after each iterative Box Search.

6. Save the updated final database (Figure 3.6).

At least, it reported a pseudo code for the implementation of the "SearchAlg" in Appendix A. A flow chart is reported as well in Figure 3.2.

3.3 Support functions for the implementation

The PSSM module has been provided as a black box tool; it will not be discussed further. Information about the functionalities is given in 2.3.
The PSSM module is called by some MATLAB scripts and functions that are able to extract the impedance according to the theoretical framework explained in 2.3 as well. Those scripts have been given since they were used yet to construct a database by Uniform Sampling the parameter space X. Of course, those were not suitable for our purpose, and the files have been properly modified and some features added, such as:

1. Major fixes in the impedance points formula implemented to the code (see 2.3);

2. Major fixes to the code in order to have up to N-D optimization possible;

3. Generate new unit cell descriptions for the database, such as elliptical, circular, and rectangular;

4. Clean efficiently workspace from generated iteratively by the PSSM module and some optimization in memory allocation;
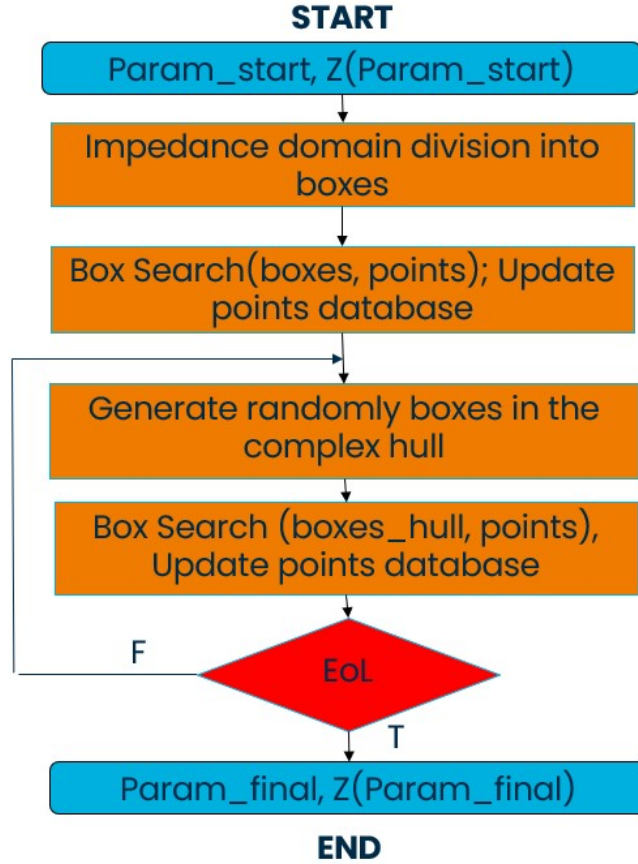
Figure 3.2: Flow chart proposed for the Search Algorithm implementation

Support functions for Search Algorithm implementation, "createBox" and "search-NearPoints," have been developed to help the "SearchBox" function developed for this thesis work.

The first function generates the centers and sizes of the impedance domain division boxes according to the N number of divisions of the maximum range and the minimum and maximum values of the cubic impedance domain that encloses the starting impedance points.

The second function searches for at least $minpoints_{interp}$ points near the input box $Box_{current}$ among all the actual database impedance points Z_{update} for the local interpolation.

Pseudo codes are not reported since the functions are very simple and do not add any additional information about the developed algorithm.
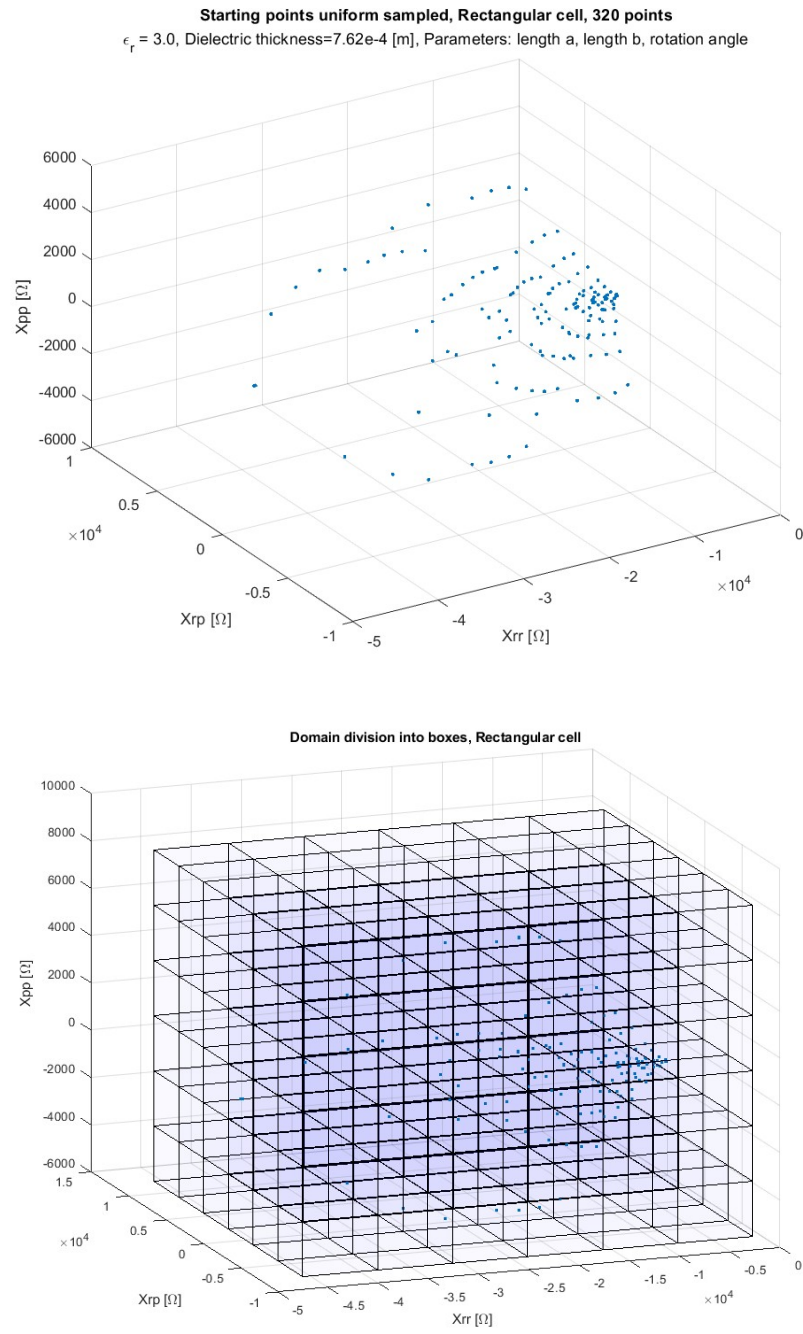
Figure 3.3: First Search Boxes; division of the rotated impedance domain according maximum and minimum values of the starting impedance points
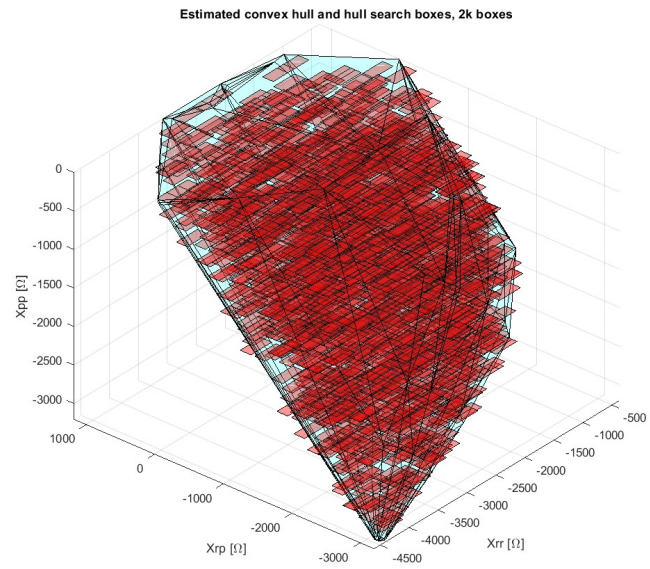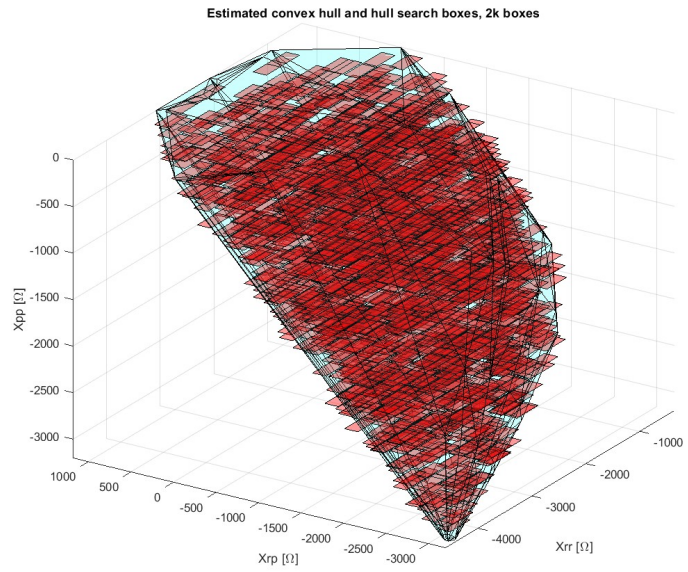
Figure 3.4: Iterative Search Boxes; two different realizations of the rotated impedance domain division according random generated boxes inside the convex hull (2k boxes here)
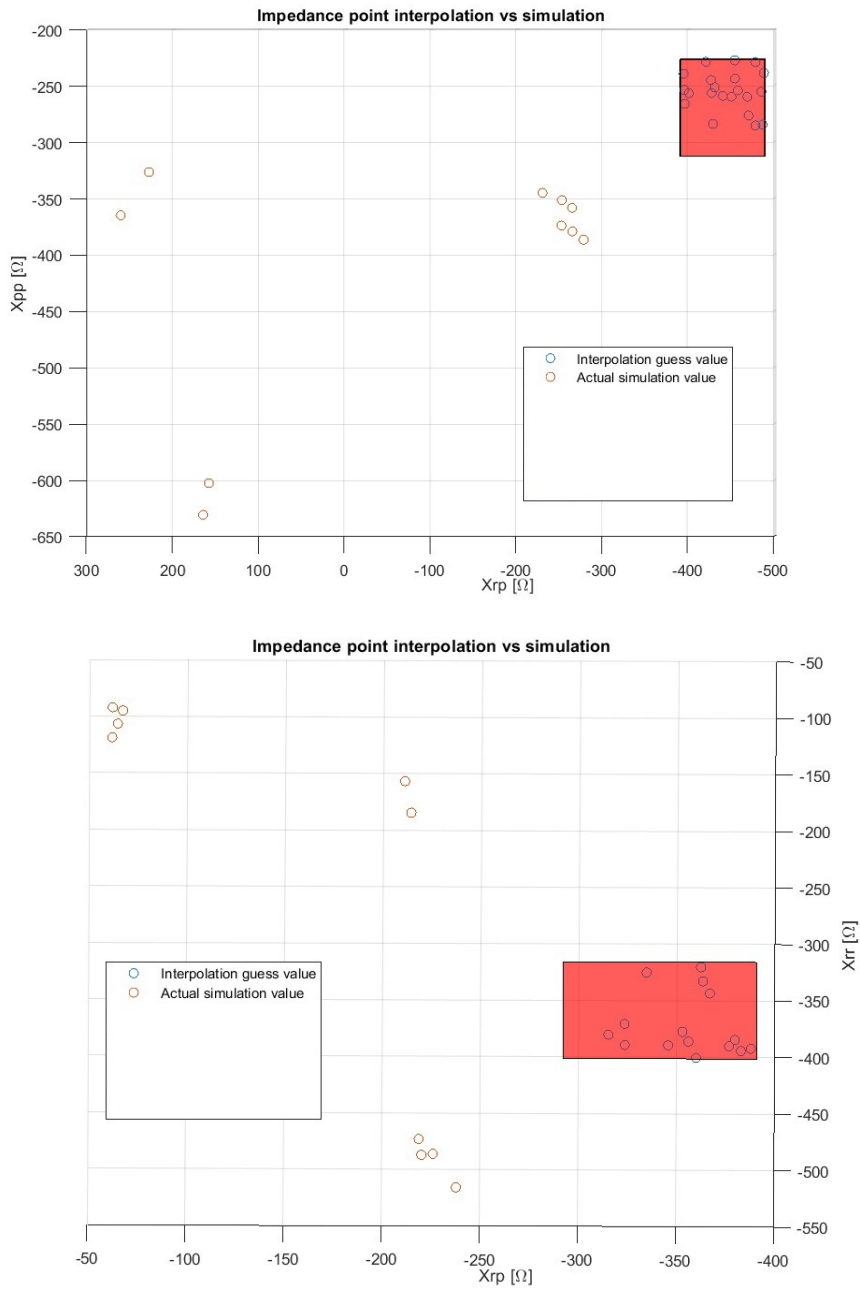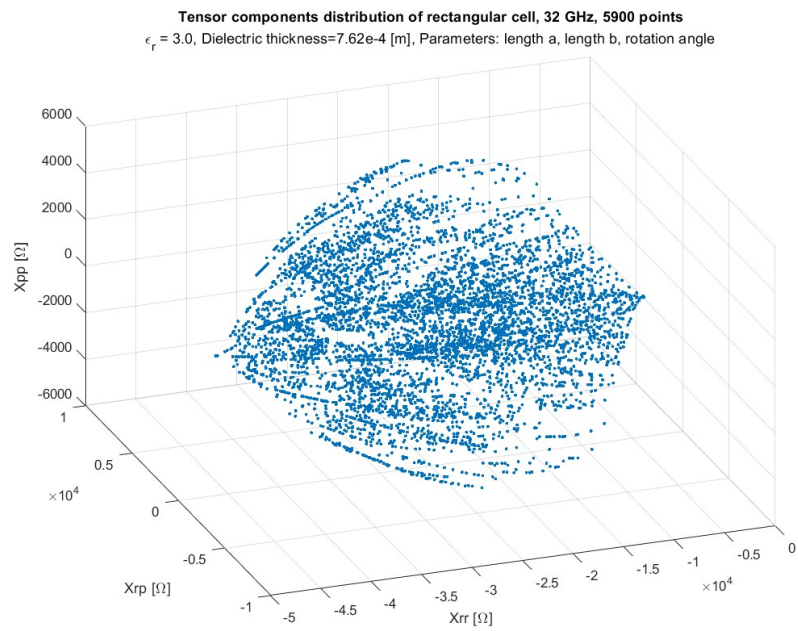
Figure 3.5: Interpolated Impedance Points into boxes and PSSM simulated points; some cases showing the dispersion of the actual PSSM impedance (orange) points around the interpolated ones (blue)

45
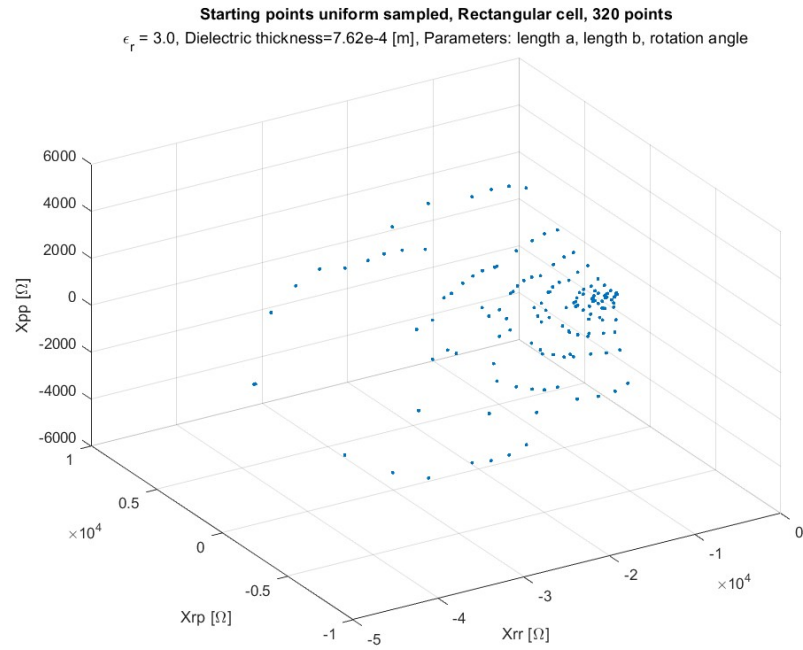
(a) Starting database, 320 points

(b) Final dense database, 5900 points

Figure 3.6: "Blind" Search for a rectangular unit cell database, 32 GHz

Chapter 4

Numerical Results

In this section, the main results for the impedance databases generated by the developed Search Algorithm are reported, and they are given a fair comparison with respect to the Uniform Sampling method, which has been used as a solution so far for the impedance database creation.

A first database is generated with a MATLAB script: in this script are inserted the information about the unit cell mesh, EM structure, and PSSM parameters listed previously. This database of points is empty, but it contains all the data needed to generate the first coarse database that is always used as first input for the "SearchAlg." This empty database is then updated with the points found by the developed algorithm.

At the end of this first search, a "Blind" search has been performed since it regards a first-wide exploration of the impedance image $Z(X)$, but it is performed limiting the number of points to be found. This is necessary in order to have a starting database of points that is sufficiently sampled almost everywhere on its image, on which it is possible to refine the point search, potentially in every subvolume of interest.

Indeed, a second search, called the "Refinement" search, is performed starting from the "Blind" database, and, whenever the desired points are available, it is possible to refine the search of the points only in the interested subregion (see Chapter 3.2).

The combination of those two kinds of searches has been used to generate the impedance points and associated parameters effectively for the antenna. Some IBCs surface constraints have been assigned in this thesis work, as shown in Chapter 4.3, and the database is build around the desired points.

4.1   Format of the Impedance Database

The database is given as a MATLAB structure that we will call 'data' for simplicity. The database "*data*" is defined by the following fields:

1. EM: it contains information about minimum and maximum working frequency ($fmin$, $fmax$), the number of frequencies analyzed ($Nfreq$), the vector of frequencies, pulsation analyzed ($frequency$, $omega$), dielectric constant and permeability in the free space (ϵ_0, μ_0), the speed of light, wavelength and wave number in free space ($vlight$, λ_0, k_0), the free space impedance (eta_0);

2. layer: the relative dielectric and permeability constants (ϵ_r, μ_r), the height ($thickness$), and the characteristic impedance (eta) of the grounded dielectric support;

3. pixels: the name of the database ($filename$) and the width of the unit cell ($width$);

4. pixels.sim: the simulation parameters of the PSSM module as the incidence angle of the plane wave ($\theta_i nc$, $\varphi_i nc$), the vectors ϵ and μ which describes the layers of the structure, the number of layers of the structures $Nlayer$, the vector of layers height $layer$, the mesh step simulation ($Hmesh$), the shape of the metallic element of the unit cell ($cellfun$), the names of the parameters of the metallic metallic element of the unit cell ($paramname$), the number of the parameters of the metallic metallic element of the unit cell ($Nparam$), the vectors containing the minimum and maximum of the parameters values ($paramLB$, $paramUB$), the number of parameters have been found ($paramN$), the vector of the parameters have been found ($param$) and the impedance points vectors have been found, also in matricial form (Xrr, Xrp, Xpp and $Xtensor = [Xrr, Xrp, Xpp]$).

4.2   "Blind" searches

It is reported that the graphic results for the point distribution have been found with the developed "SearchAlg" compared with the uniform sampling database impedance points. Parameters of the structures are indicated in the figures; the mesh step for the PSSM will always be set to $\lambda_g/30$, a good trade-off between simulation time and accuracy of results. The unit cell width is also set on $\lambda_0/10$, less than a wavelength, to allow homogenization of the surface impedance; the working frequency is 32 GHz. The coarse database point input of the Search Algorithm, since all the searches in this work involve three components for the parameter point X, has 343 points (7^3, each range of parameters is divided into 7

points).

Simulation results comparison for the Search Algorithm and the Uniform Sampling for the coffee bean (Figure 4.1), double anchor (Figure 4.3), elliptical (Figure 4.5), rectangular (Figure 4.7), and circular (Figure 4.9) unit cells have been reported. The associated parameters sampled from the databases and the definition of the cell geometry are also reported for the coffee bean (Figure 4.2), double anchor (Figure 4.4), elliptical (Figure 4.6), rectangular (Figure 4.8), and circular (Figure 4.10) unit cells.

In all the reported figures, a graphical comparison of the impedance points database generated with the same number of points is shown in order to have a fair comparison. It is graphically clear for the unit cells of coffee beans and double anchor that the distribution of points in the impedance space is way more uniform with the use of the Search Algorithm than with uniform sampling of the parameter space. Indeed, uniformly sampling the parameter space is not always the best way to build a database since the generated points will not cover the entire image of $Z(X)$. Orange impedance points (Uniform Sampling of parameters) tend to be distributed in a specific subregion, preventing a good part of the image of $Z(X)$ from being covered. On the contrary, search algorithm-founded points (blue points) are distributed as uniformly as possible into the image of the numerical output $Z(X)$, allowing the best sampling of the impedance domain.

In the rectangular and elliptical cells, the results are also very similar due to the fact that the shape and geometry of the two metallic elements are similar (also for the covered impedance volume), and they show the same kind of results previously discussed. The results for the circle unit cell are similar in uniform sampling and Search Algorithm database: this is a special case since the optimization parameter has only one dimension and the point distribution is already most likely uniform in the impedance space.

In all cases, it is clear that the Search Algorithm (blue points) does not perform a uniform sample of parameters; the parameter points will be taken mostly in some sub-regions of the parameter space in order to let the distribution of the associated impedance points $Z(X)$ be as uniform as possible.

At this point, the "Blind Searches" databases are suitable to get a refinement, potentially, in every subregion. Indeed, a good amount of impedance points for local interpolation are present almost everywhere now. The refinement is done in the sub-regions of impedance where the desired impedance points, given by the design process of the MTS antenna (see Chapter 2.2), are present. The Search Algorithm parameters for the "Blind" searches (see Chapter 3.2) are:

1. $N \leftarrow 10$

2. $secondsearchMax \leftarrow 10$

3. $minpoints \leftarrow 5 * 10^3$

4. $boxinhull \leftarrow 2 * 10^3$

5. $maxIncrement \leftarrow 200$

6. $Z_{ideal} \leftarrow empty$

7. $hullsearch \leftarrow true$

These parameters have been used for all the databases reported in this work and they have been observed empirically the best ones for the "Blind" searches.

4.3   "Refinement" searches

In this section, numerical results are reported for databases of double anchor cells that have been refined properly in some subregions, according to the desired input points from the design steps. This is the usage of the Search Algorithm for its final goal, then sampling the parameter space in such a way that it is given a dense impedance point $Z(X)$ distribution around the wanted values in order to minimize the error (distance) between the realizable set of points and the desired ones. It is reminded that the algorithm is not able to understand exactly what parameter combination realizes some impedance point $Z(X)$ value; this could be solved with some heuristic optimization algorithm, but eventually (simulation time) and without the guarantee that this value could be assumed by the image of $Z(X)$. Then, this is not a suitable method to build a dense database of impedance points for our purpose.

The best we can do is try to take many impedance points in the neighborhood of the desired ones in the most uniform way possible around them (that is what the developed algorithm has been designed for); this statistically helps to reduce the mean distance with the target points. This also helps to compensate for another important issue regarding the fact that the intersection between the image of the $Z(X)$ function and some (even all) of the desired points could be empty. Generally speaking, the best one can do is to generate a database of impedance points as close as possible to the desired ones, in the most uniform way it is possible.

In Figure 4.11 are reported the ideal profile values for a circular 10 λ_0 diameter MTS antenna they are needed to realize a radiation pattern that satisfies the mask constraints given in Figure 2.2, with a circular polarization and broadside beam. It is recalled that the different values for the impedance surface values X_{rr}, X_{rp}, and X_{pp} are realized by varying a subset (or all) of the unit cell parameters, then the parameter point X that realizes the double anchor unit cell (see Figure 4.4). The working frequency is 22 GHz; the EM structure parameters are also different and indicated on the figures, as well as the parameter combinations that define the geometry. The unit cell width (lattice periodicity) is set to $\lambda_0/6$.
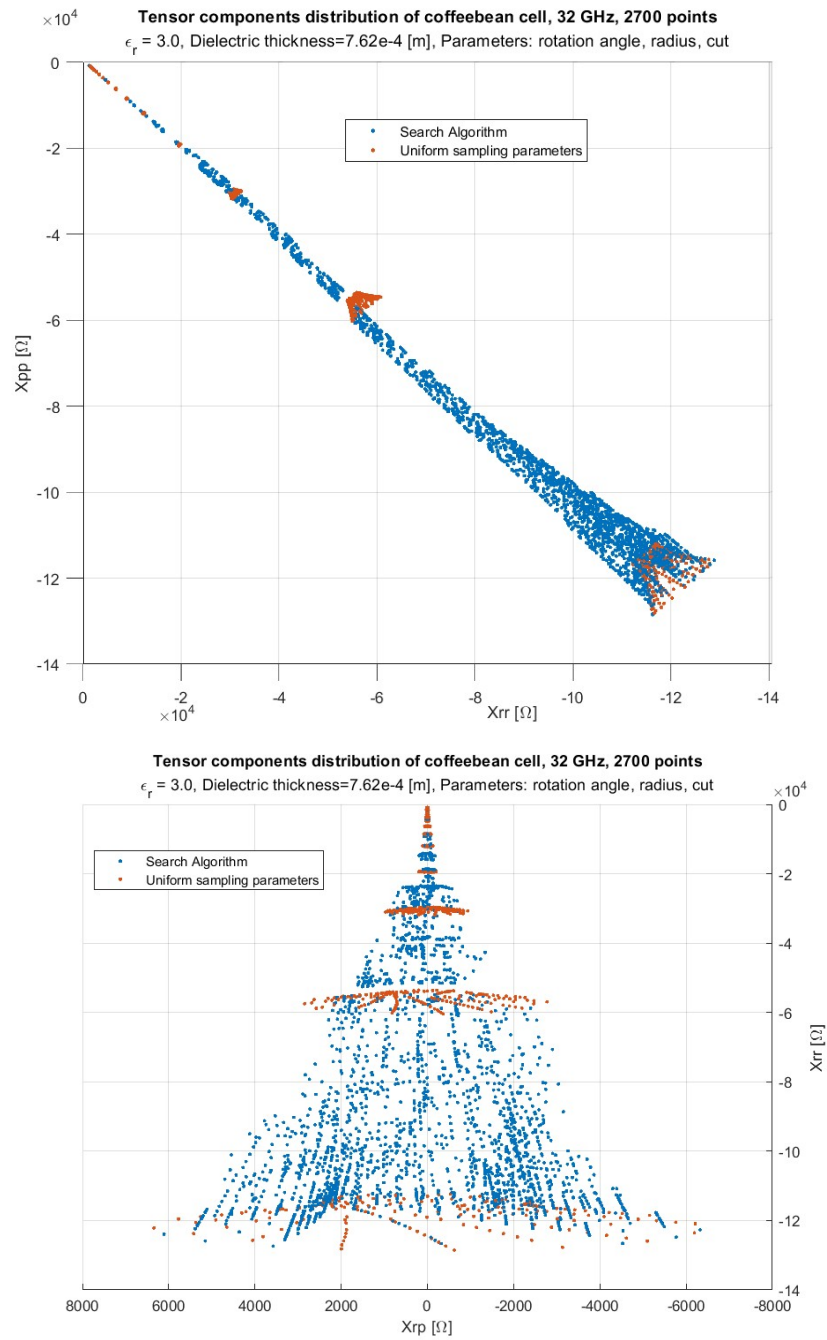
Figure 4.1: Impedance Points comparison for the coffee bean unit cell shape; Search Algorithm (blue) and Uniform Sampling Parameters (orange)

In Figure 4.12 are shown the fair comparison (same number of simulated points) for the "Blind" search and uniform parameter sampling for such a database. Once again, it can be observed a non-uniform distribution for the impedance points in the domain in the uniform sampling case, preventing truly a full exploration of the image of $Z(X)$. Starting from the "Blind" search database, it is possible to select only the points belonging to a certain sub-region (around the desired points) and start a new search that also gives the desired points. In Figure 4.13 are reported the results for the "Coarse Refinement" search, with $minpoints = 5*10^3$ for such a search. The $Z_{desired}$ matrix represents the desired points, and it is the outcome of the design process for some radiation pattern mask constraint; it is used to focus the impedance point search truly around the desired points (see Chapter 3.2). Typical parameters for the "Refinement" Search Algorithm are:

1. $N \leftarrow 10$

2. $secondsearchMax \leftarrow 10$

3. $minpoints \leftarrow 5*10^3$ or $minpoints \leftarrow 10*10^3$

4. $boxinhull \leftarrow 1*10^3$ or $boxinhull \leftarrow 600$

5. $maxIncrement \leftarrow 200$

6. $Z_{ideal} \leftarrow Z_{desired}$

7. $hullsearch \leftarrow false$

According to $minpoints$, it is possible to take less or more points around the wanted $Z_{desired}$ points. Of course, it is best to take the most possible points in order to have a good statistical coverage of the neighborhood of the desired points; however, this will dramatically increase simulation times. For this reason, $minpoints$ has been limited to some value (i.e., $5*10^3$) that experimentally has been observed to be the best trade-off between simulation time and impedance domain covering. As an example, the "Refinement" search with $minpoints = 5*10^3$ lasted about 15 hours, and the other with $minpoints = 10*10^3$ lasted about 20 hours on this PC setup (16 GB RAM, AMD RADEON). For this reason, they have been referred to as "Dense Refinement" ($10*10^3$) or "Coarse Refinement" ($5*10^3$), according to the number of generated points from the Search Algorithm. "Blind" searches also lasted about 15 hours, depending on the mesh complexity of the unit cell. Generally speaking, simulation time depends mostly on the number of impedance points in the database the user wants to generate and the mesh complexity of the metallic unit cell element.
In Figure 4.14 are reported the parameter points sampled for "Coarse Refinement"

which are always crowded into a certain subvolume compared to the uniform sampling.

In Figure 4.15 are reported the results for the "Dense Refinement" database, around 10k points. In Figure 4.16 are also reported the corresponding parameter values sampled in the two cases. It is clear that, in this case, uniform sampling of the parameter space X in a more dense way tends to distribute the $Z(X)$ impedance points towards the desired point region, which is found in the upper part of the domain. Indeed, it is expected that there will be a lower average distance between the desired points and the Uniform Sampling database points due to the high point density around the desired region; however, this is a special case and not a general rule.

4.4 Projection error on desired points and realized radiation pattern

Since our goal is to focus the impedance point search around the $Z_{desired}$ for our generated databases, they have been evaluated and reported as the average distances between the nearest database points and the desired points on the antenna surface for both Uniform Sampling (Figure 4.18a) and "Coarse Refinement" (Figure 4.18b) Search Algorithm databases.

It is clear from these results that the developed algorithm is very effective in minimizing the average distance between the $Z_{desired}$ and the generated database of points, with an average distance of about 22 Ω for the "Coarse Refinement" vs. the 71 Ω given for generating the database Uniform Sampling the parameter space. This means about three times lower average distances for the impedance points generated with the Search Algorithm.

One can think to refine the search by increasing the number of points and see if things are improved since we are performing a stochastic search in the subdomain of interest with the Search Algorithm: refinement means taking more (different) points, and it is theoretically possible to cover all the subvolume eventually. Of course, this is extremely time-intensive at this point, without any guarantee that the average distance is lowering as more points are generated, due to the fact that the image of $Z(X)$ could have an empty intersection with some of the desired points. Then, a minimum "saturation" value for the average distance is expected as the generated points increase.

The impedance points have been found to be truly distributed only near the desired points, as shown graphically in Figure 4.17. All the 4913 founded points by the algorithm (blue) are inside the cubic impedance region limited by the shown axis, while the uniform sampling points (black) are only 669 in the same region; the uniform sampling is not effective at all for our purpose in this case.

In Figure 4.19 are shown the points inside the previously defined cubic impedance region, which contains all the database points generated with the Search Algorithm (11024 points); uniform sampling database points are only 1489 inside the region of interest. It is clear graphically that the number of impedance points generated is as close as possible to the desired impedance points $Z_{desired}$.

In Figure 4.20a and 4.20b are reported the results for the distances and the average distance for the two database points. Even numerically, it is clear that the average distance is lower, even if the improvement is lower compared to before, due to the fact that the image of $Z(X)$ seems to not reach all the desired points. Indeed, the average distance between the Search Algorithm database and the desired one is about 18 Ω, compared with the 30 Ω value of the uniform sampling database: about x1.5 improvement factor in terms of average distance. In both the "Dense Refinement" and "Coarse Refinement", it is graphically clear that the image of $Z(X)$ is not reaching the points at the center of the rings defined by the desired points $Z_{desired}$; this is the case above mentioned, where the intersection between the image of $Z(X)$ and the desired points $Z_{desired}$ is (most likely) empty in some regions.

4.5 Conclusions

In this section, they have analyzed the main numerical results for the database impedance generation with the developed Search Algorithm, and it has given a fair comparison, both graphically and numerically, between the two ways to generate impedance database points.

The first way is simply to sample the parameter space in a uniform way and generate the associated $Z(X)$ points. The proposed technique for this thesis work aims to sample the parameter points in a more reasonable way, ideally taking the parameter points X in such a way that the corresponding $Z(X)$ impedance points are as uniform as possible distributed in the impedance domain, with the consequence of exploring the image of $Z(X)$ at best, avoiding down sampling effects. Further, the developed algorithm, once the user has a suitable, well-distributed impedance database of points, is able to refine the database in the subregion where the desired impedance points are present. In this work has been shown, for the double anchor unit cell (see,4.3), that the results in terms of average distance between the two data sets ($Z_{desired}$ vs Search Algorithm) are improved in both cases of coarse (5k points) and dense (10k points) databases. The average distance is always lower compared to the Uniform Sampling databases which have the same number of points generated.

This Search Algorithm is able to satisfy the constraints on minimizing the average distances between the desired points with those data, meaning that the physically

realized MTS antenna (ignoring manufacture tolerances) will have a lower error on the realized IBC profile. This will have consequences for a more reliable realization of the radiation pattern mask constraints that have been imposed during the design process.

This is evident from the comparison between the ideal radiation pattern realized with desired impedance points on the MTSs and the actually realized MTS antenna with generated database points in Figures 4.27 and 4.25. From the latter, it is evident that by generating a dense database (11024 points here) around the desired points, it is sufficient to get results very close to the ideal radiation pattern that represents the final goal. Indeed, cross-polarization, SLL levels, directivity, and aperture efficiency are really close (or equal) to the ideal values, while antennas realized with uniform sampling (Figures 4.28 and 4.26) have higher discrepancies.

It is also possible to make a comparison between the "Refinement" and the uniform sampling databases, as shwon in Figure 4.22 and 4.24. Results for realized electrical current distribution on the MTS antenna with the "Coarse Refinement" (Figure 4.21) and for the "Dense Refinement" (Figure 4.23) databases are reported as well. The improvement in terms of efficiency is evident since the directivity is slightly higher for the "Coarse Refinement" database, together with lower SLL levels and cross-polarization lobes. Aperture efficiency remains always higher with the Search Algorithm generated databases, together with lower cross-polarization side lobe levels.

The final goal of finding an algorithm for sampling the space parameter X to generate a database of points $Z(X)$ that effectively minimizes as much as possible the average distance with the desired points $Z_{desired}$ has been reached, making possible the realization of radiation patterns closer to the ideal one.

At the end, it is shown in Figure 4.29 a simplified draw of the complete antenna realized with the "Dense Refinement" database, according each element parameter combination that realizes the closer desired IBCs on the surface.
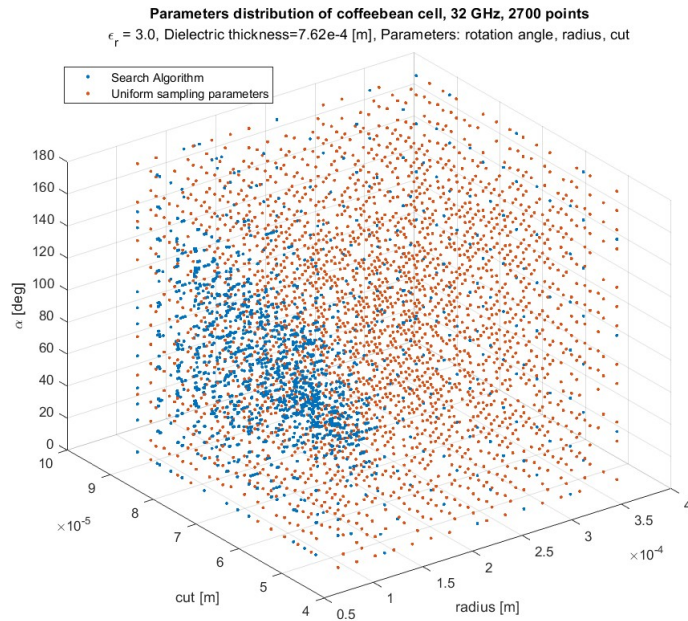
(a) Parameters points comparison for the coffee bean unit cell shape; Sampling points resulting from Search Algorithm (blue) and Uniform Sampling Parameters (orange)
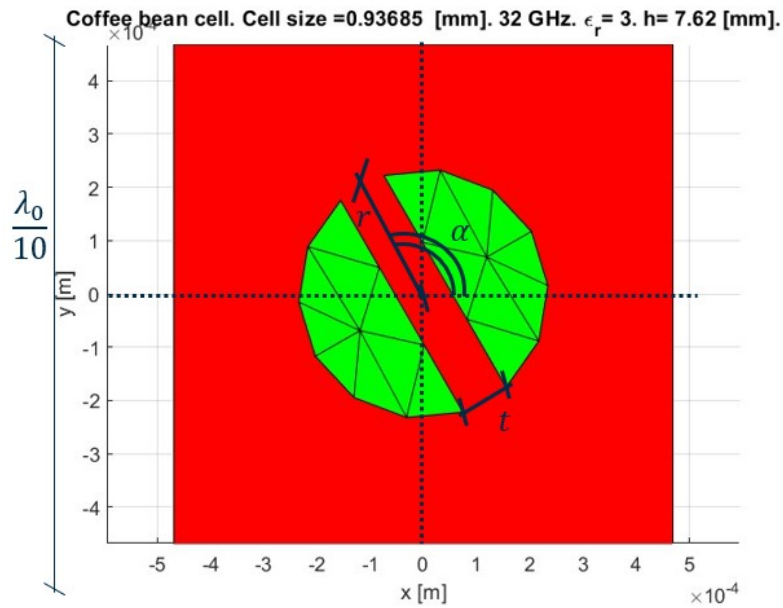
(b) Coffee bean unit cell defined by radius r, cut t and rotation angle α; Metallic printed element (green) and dielectric (red)

Figure 4.2: Parameters Coffee Bean unit cell
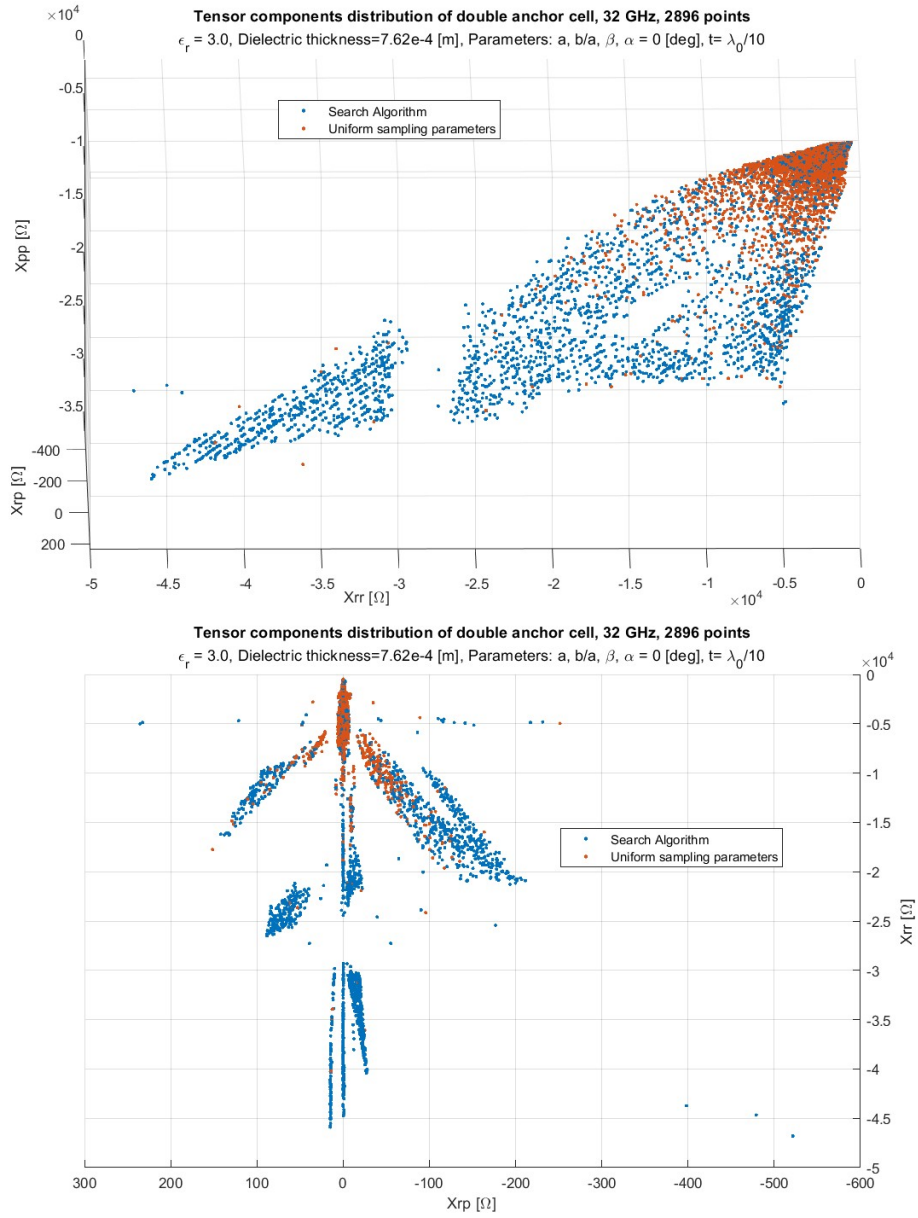
Figure 4.3: Impedance Points comparison for the double anchor unit cell shape; Search Algorithm (blue) and Uniform Sampling Parameters (orange)

57
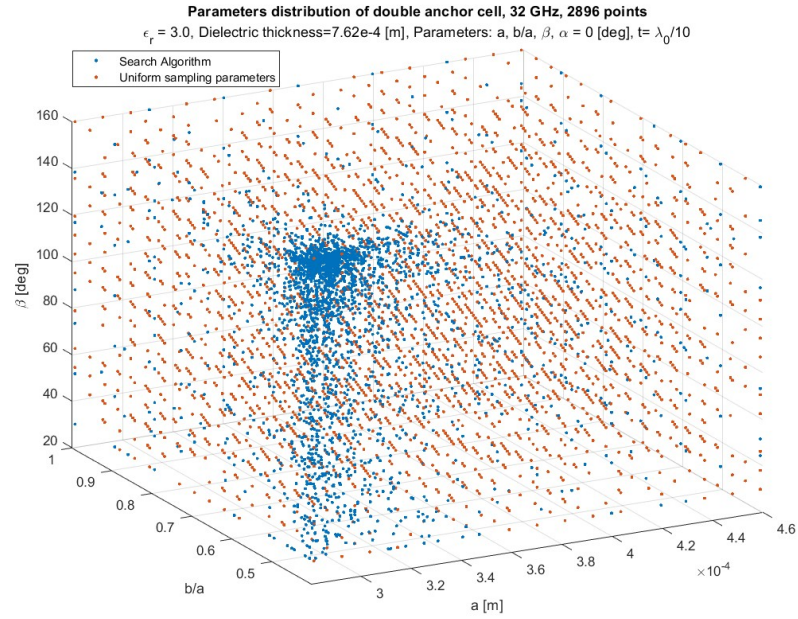
(a) Parameters points comparison for the double anchor unit cell shape; Sampling points resulting from Search Algorithm (blue) and Uniform Sampling Parameters (orange)
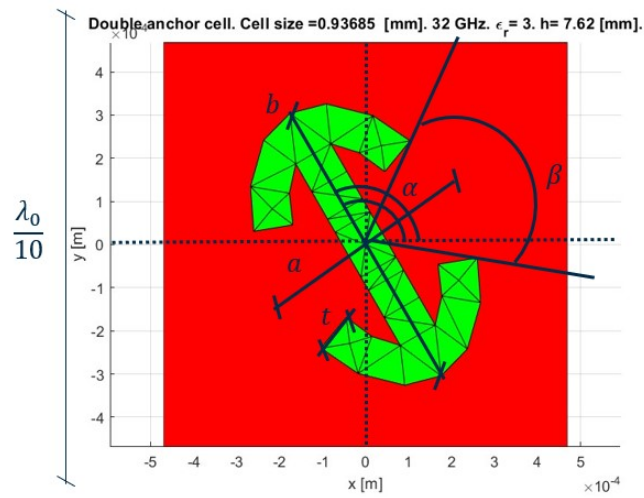
(b) Double Anchor cell defined by sizes a, b, t, angle β and rotation angle α; Metallic printed element (green) and dielectric (red)

Figure 4.4: Parameters Double Anchor unit cell
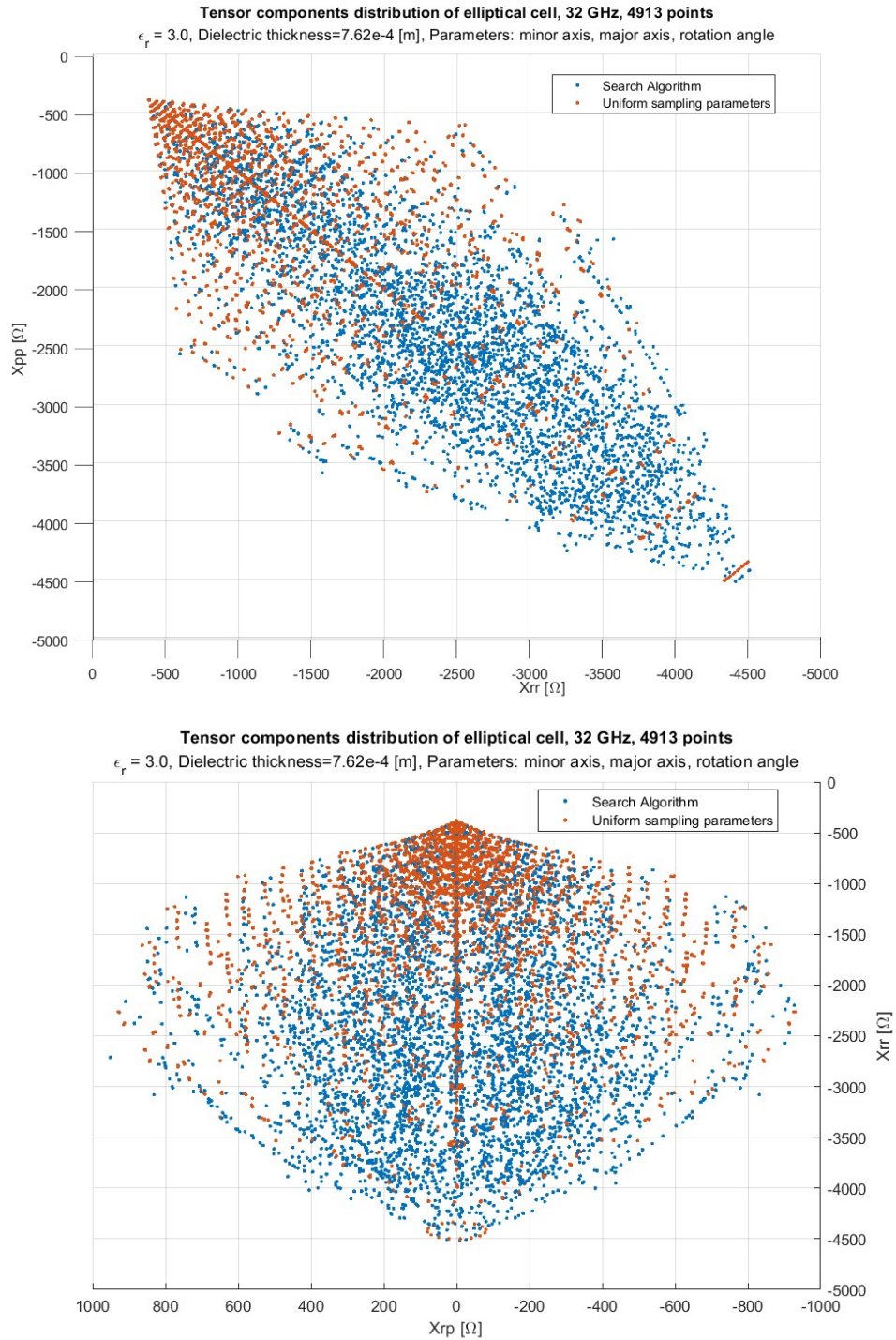
Figure 4.5: Impedance Points comparison for the elliptical unit cell shape; Search Algorithm (blue) Uniform Sampling Parameters (orange)

59
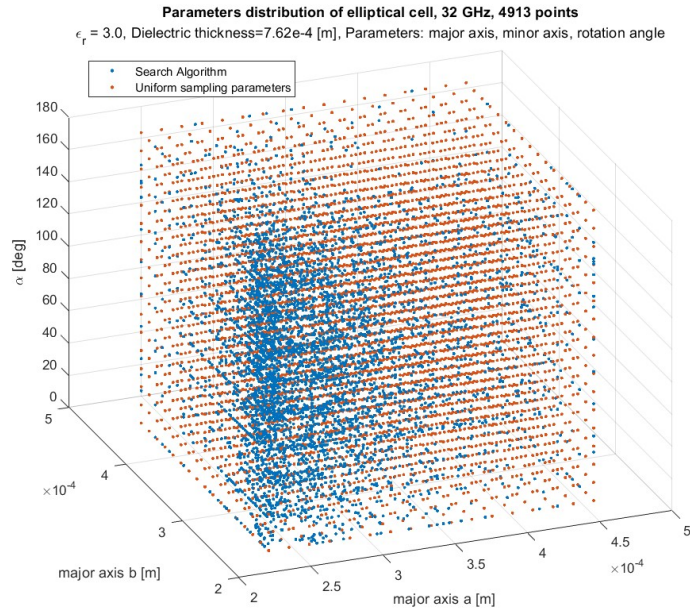
(a) Parameters points comparison for the elliptical unit cell shape; Sampling points resulting from Search Algorithm (blue) and Uniform Sampling Parameters (orange)
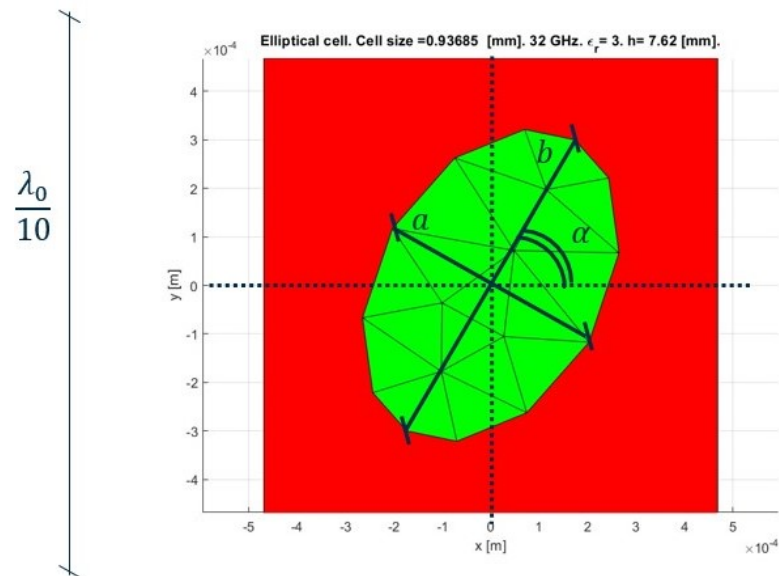
(b) Elliptical unit cell defined by sizes a, b and rotation angle α; Metallic printed element (green) and dielectric (red)

Figure 4.6: Parameters Elliptical unit cell
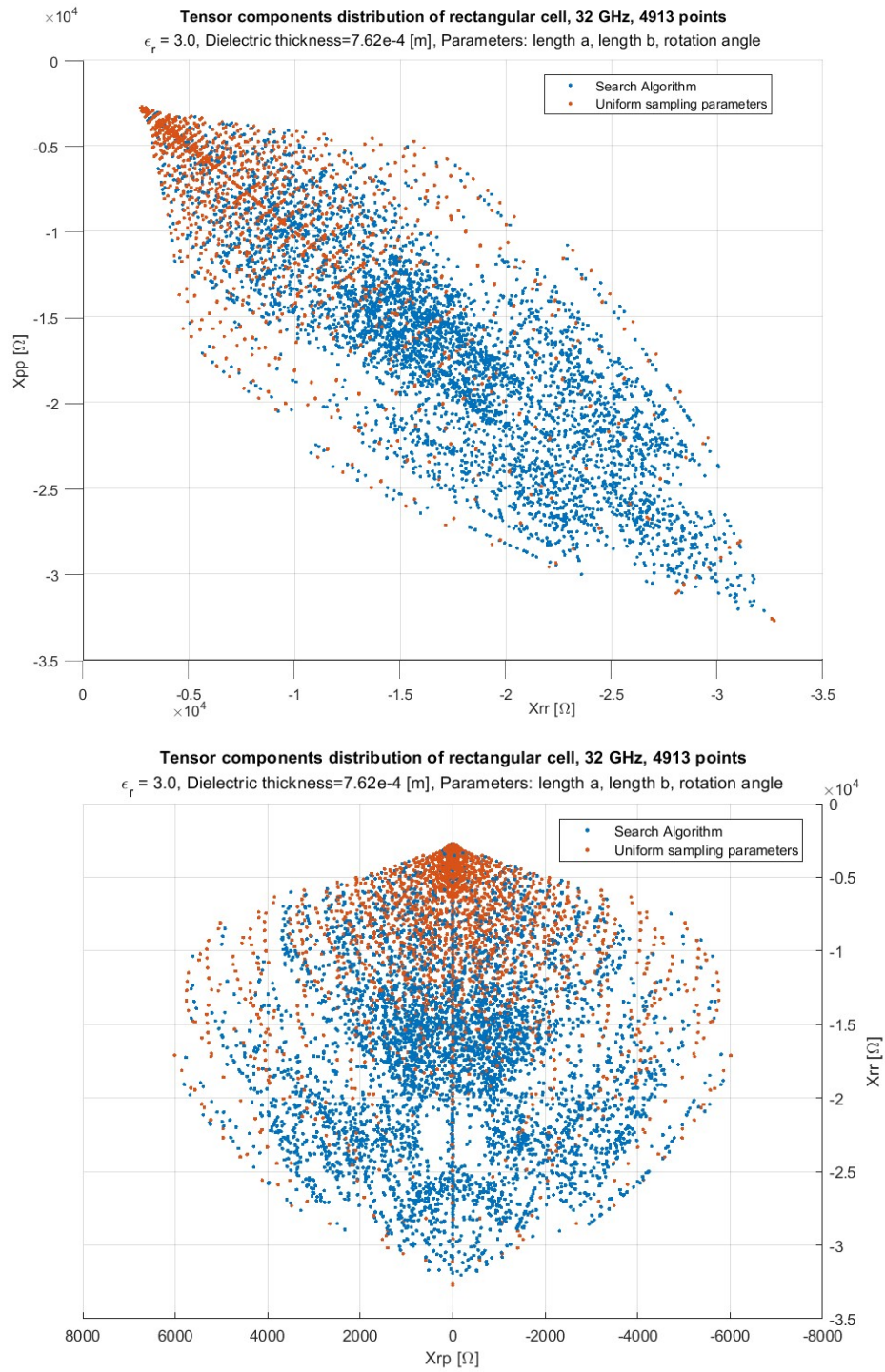
Figure 4.7: Impedance Points comparison for the rectangle unit cell shape; Search Algorithm (blue) and Uniform Sampling Parameters (orange)
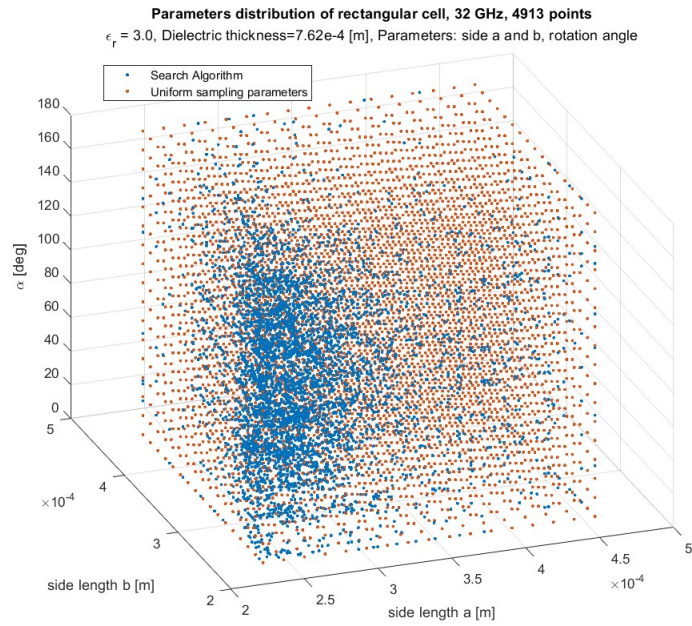
(a) Parameters points comparison for the rectangle unit cell shape; Sampling points resulting from Search Algorithm (blue) and Uniform Sampling Parameters (orange)
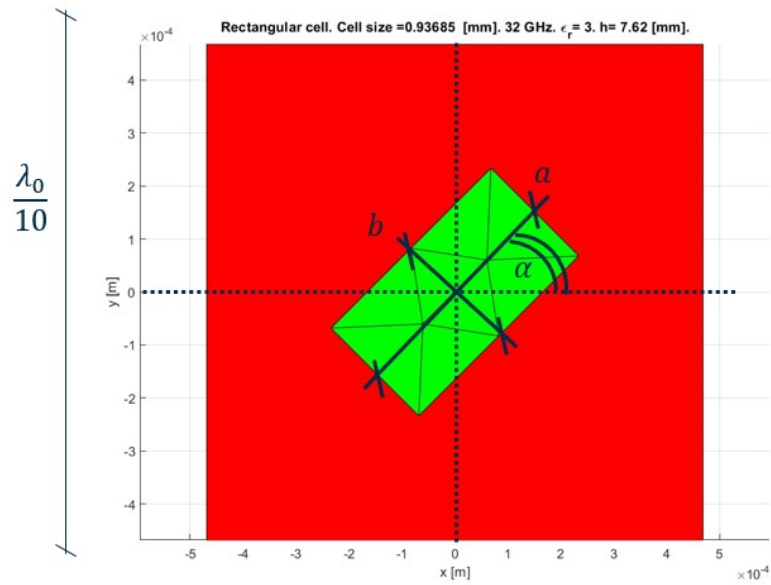

(b) Rectangle unit cell defined by sizes a, b and rotation angle α; Metallic printed element (green) and dielectric (red)

Figure 4.8: Parameters Rectangular unit cell
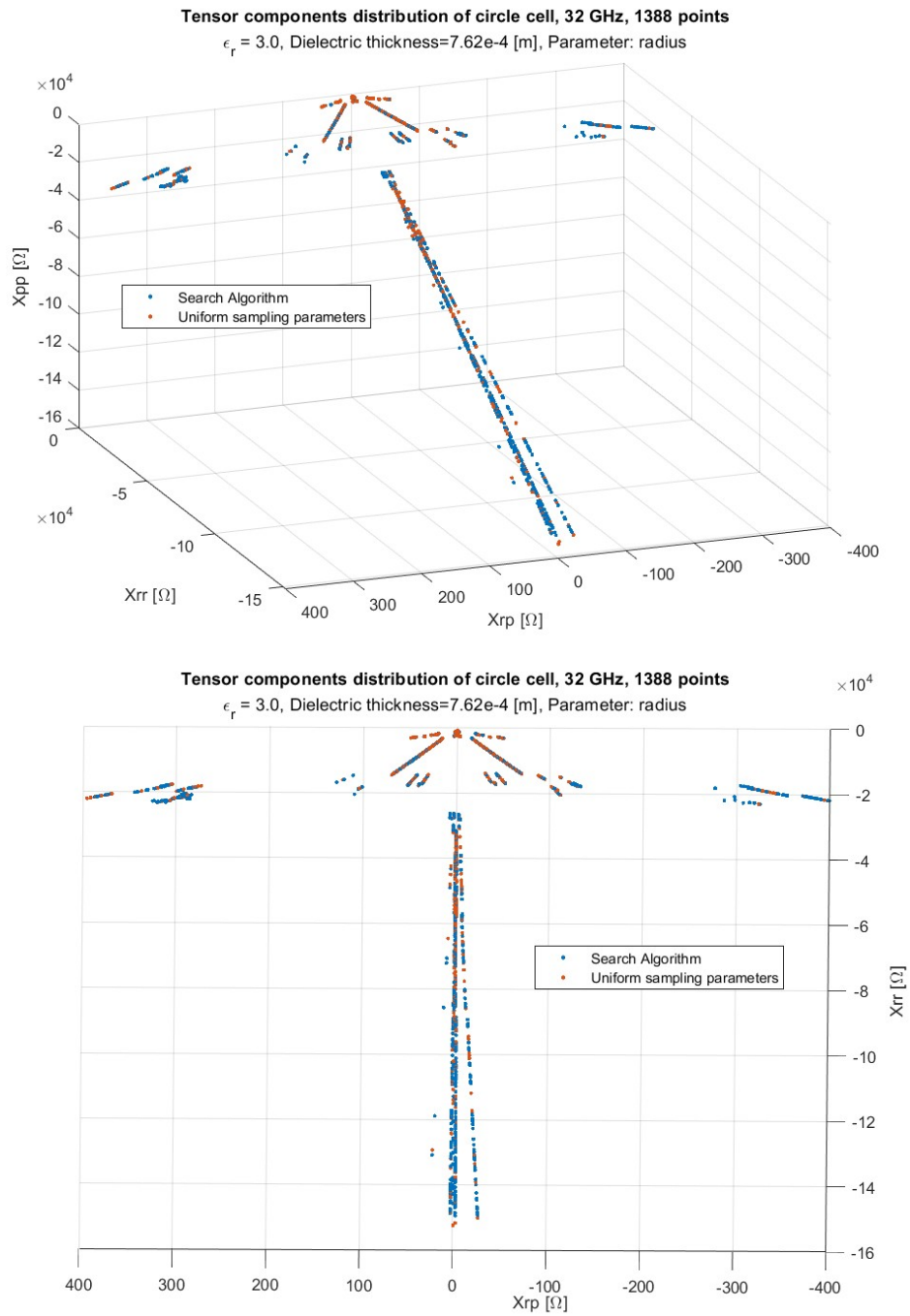
Figure 4.9: Impedance Points comparison for the circle unit cell shape; Search Algorithm (blue) and Uniform Sampling Parameters (orange)
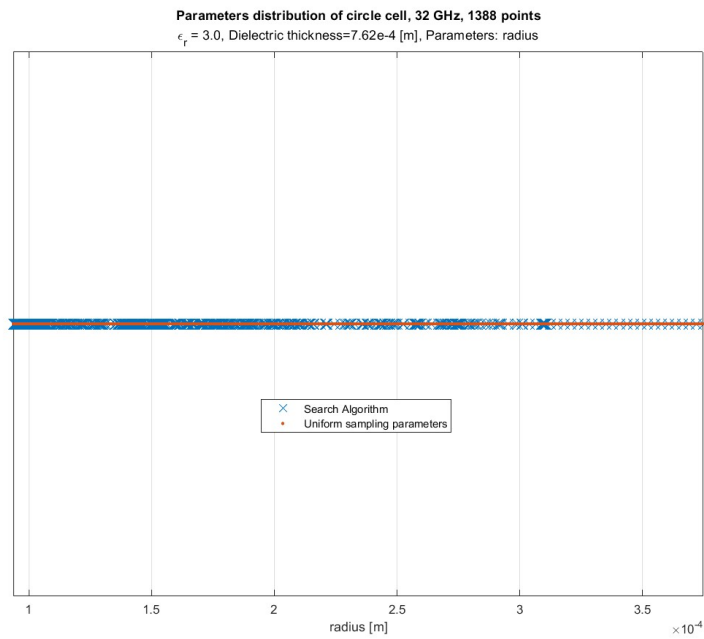
(a) Parameters points comparison for the circle unit cell shape; Sampling points resulting from Search Algorithm (blue) and Uniform Sampling Parameters (orange)
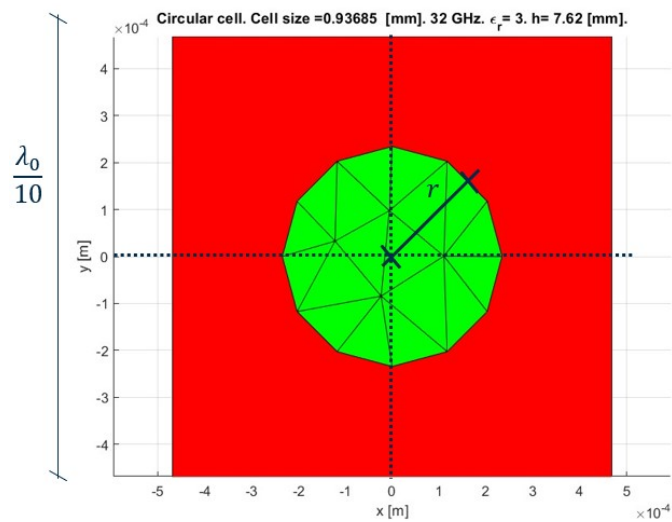
(b) Circle unit cell defined by size r; Metallic printed element (green) and dielectric (red)

Figure 4.10: Parameters Circular unit cell
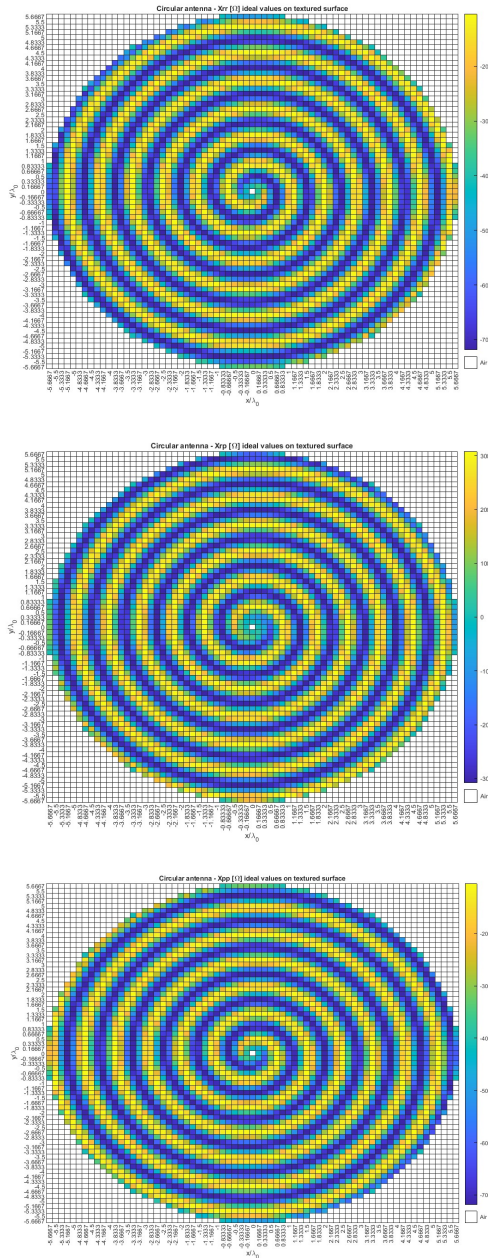
Figure 4.11: Ideal IBC profile on the MTS antenna surface, each textured elements represent a different double anchor unit cell and realize a different impedance value

65
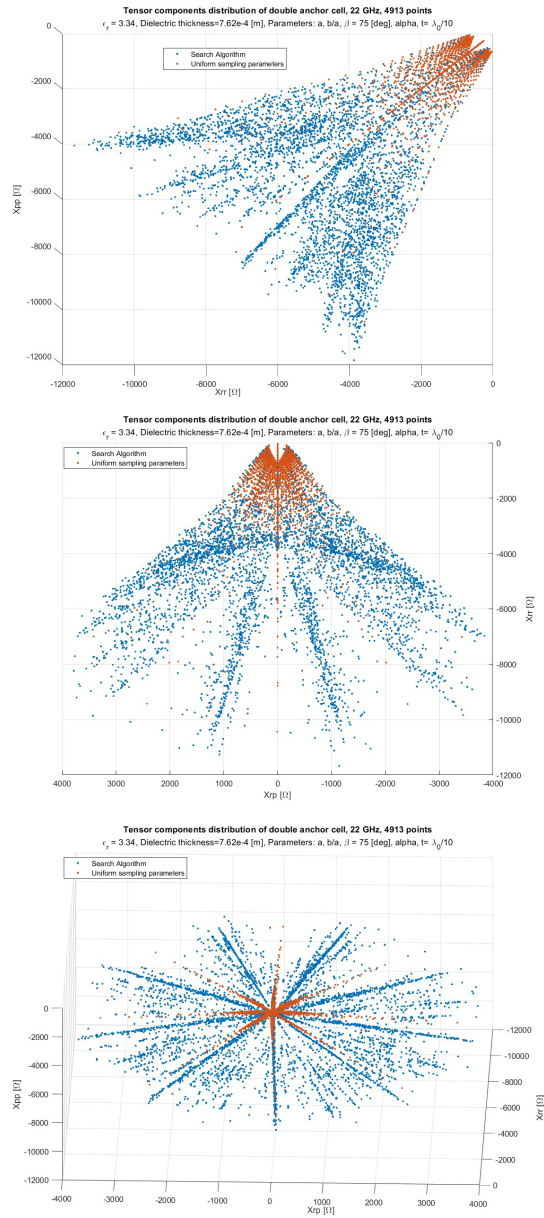
Figure 4.12: "Blind" Search Algorithm (blue) vs Uniform parameters sampling (orange) database
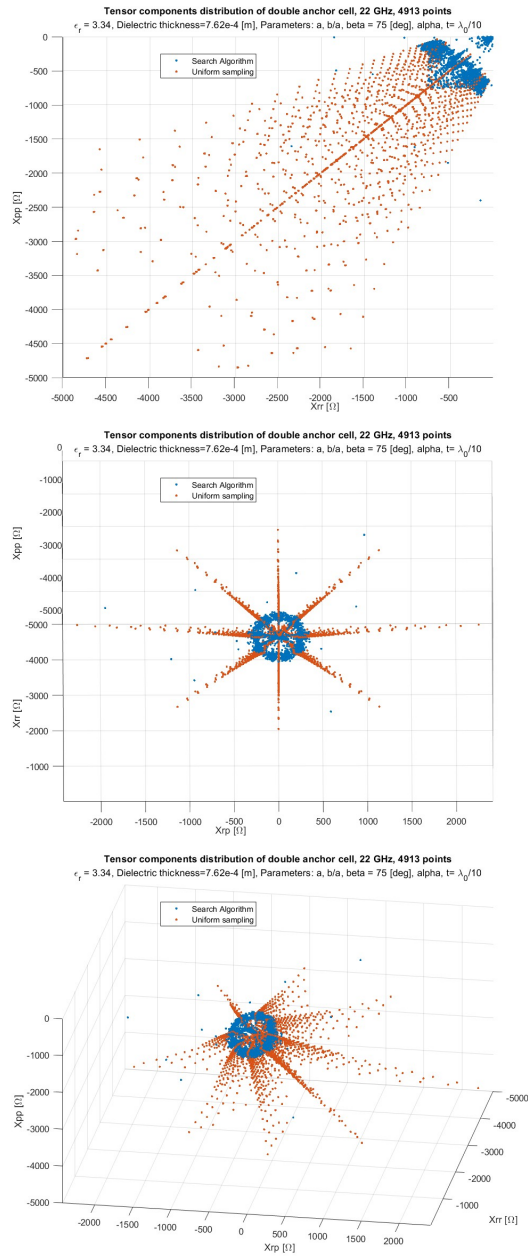
Figure 4.13: "Coarse Refinement" Search Algorithm (blue) vs Uniform parameters sampling (orange) 4913 points database
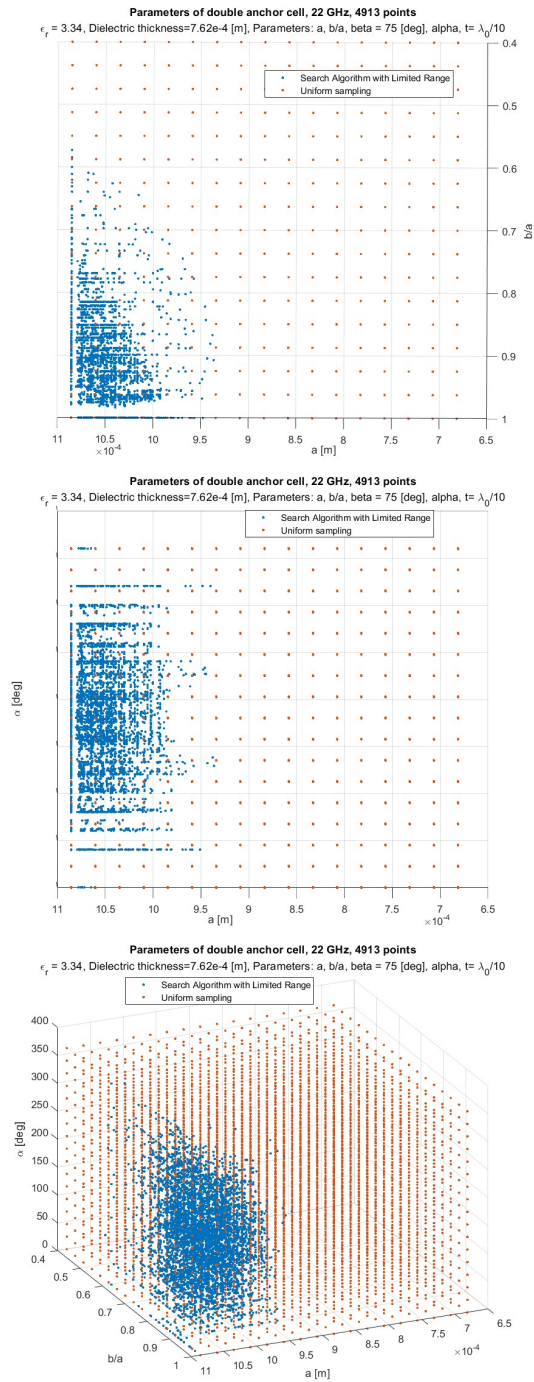
Figure 4.14: "Coarse Refinement" Parameters points comparison for the double anchor cell shape; Sampling points resulting from Search Algorithm (blue) and Uniform Sampling Parameters (orange)
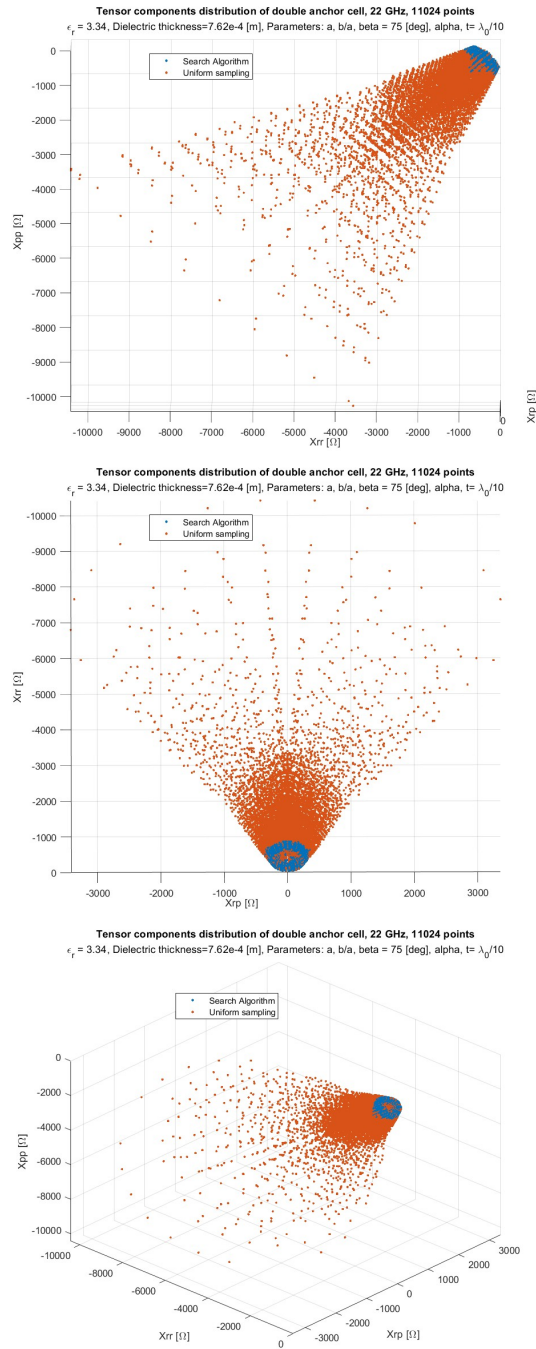
Figure 4.15: "Dense Refinement" Search Algorithm (blue) vs Uniform parameters sampling (orange) 11024 points database
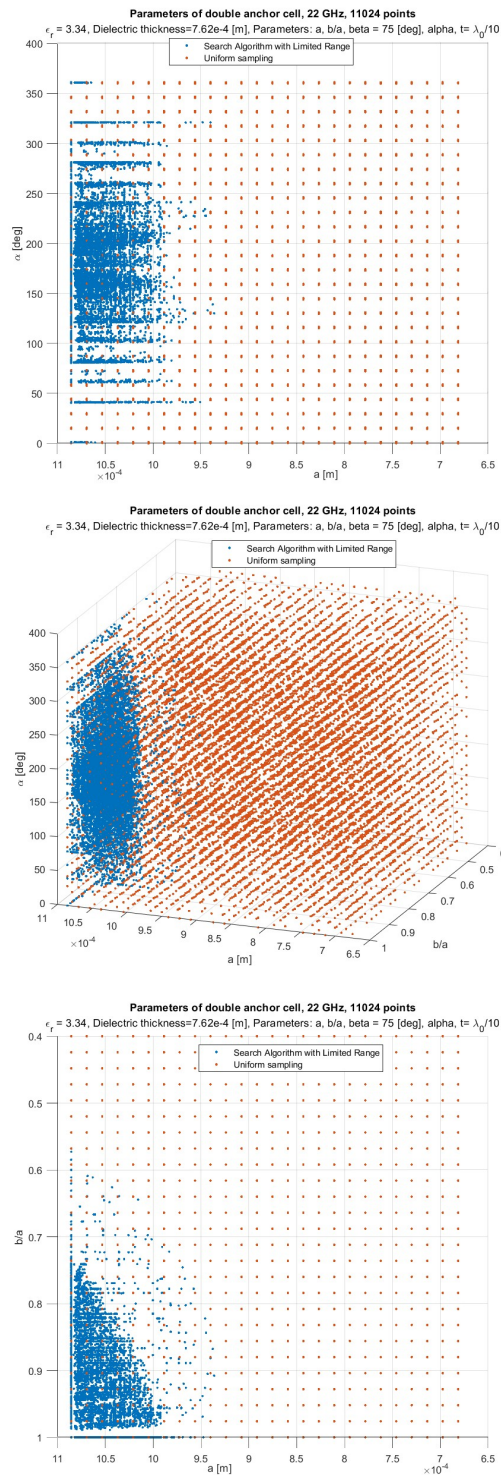
Figure 4.16: "Dense Refinement" Parameters points; Sampling points resulting from Search Algorithm (blue) and Uniform Sampling Parameters (orange)
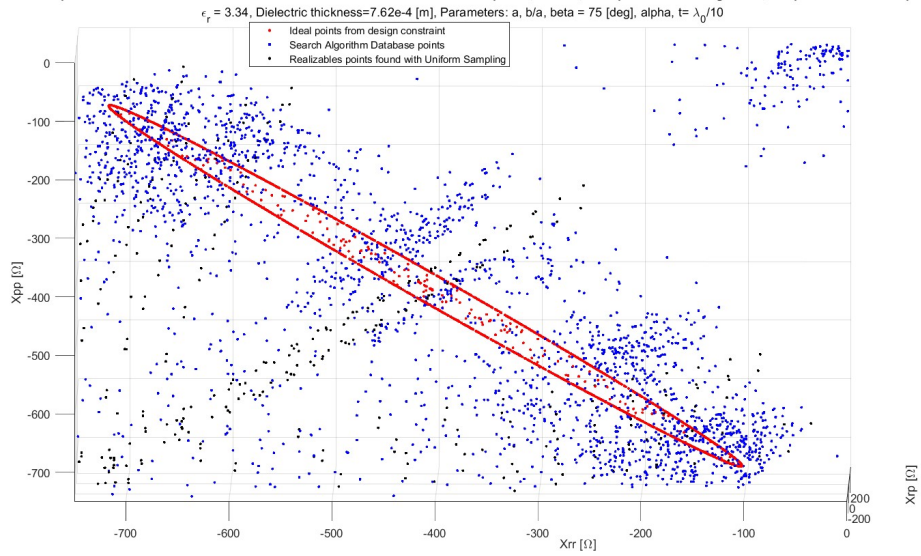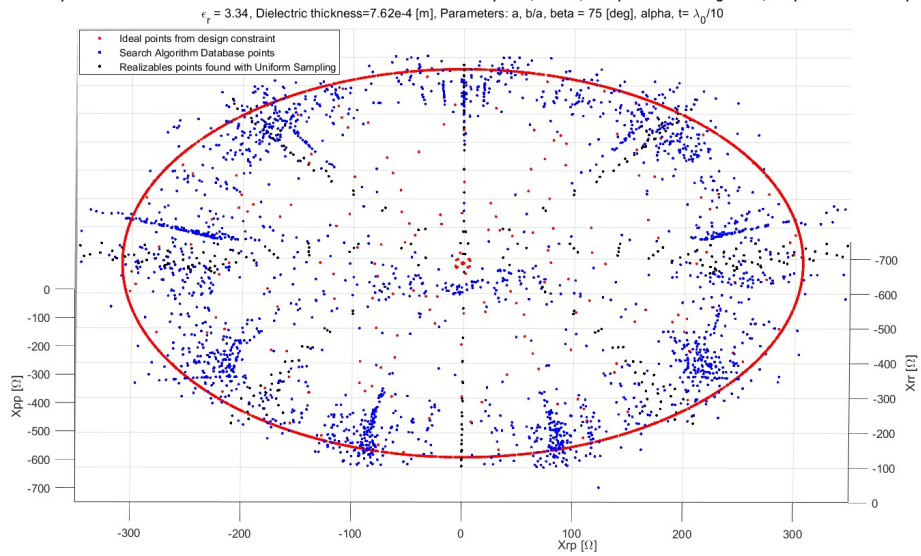
Figure 4.17: "Coarse Refinement" Search Algorithm (blue) vs. Uniform parameters sampling (black) vs. $Z_{desired}$ desired points (red), 4913 points databases
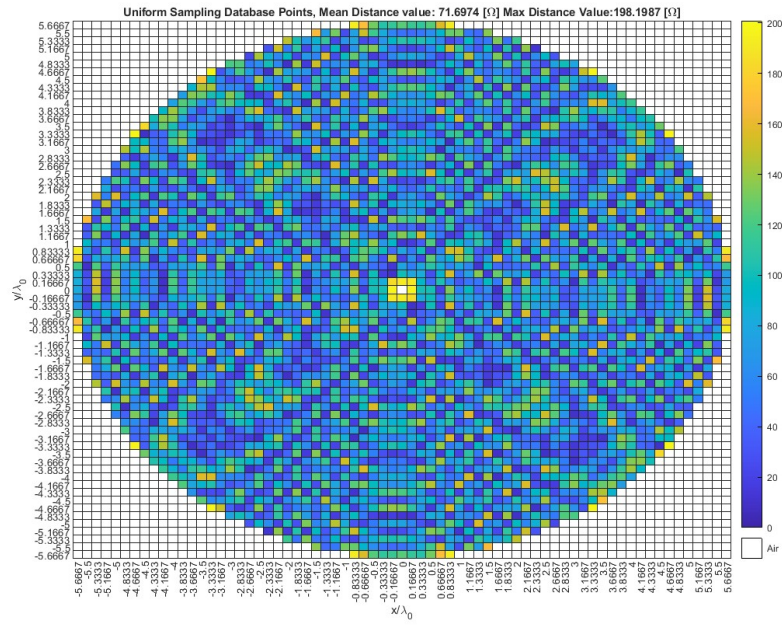
(a) Distance between $Z_{desired}$ and uniform sampling database points reported on the antenna surface, 4913 points
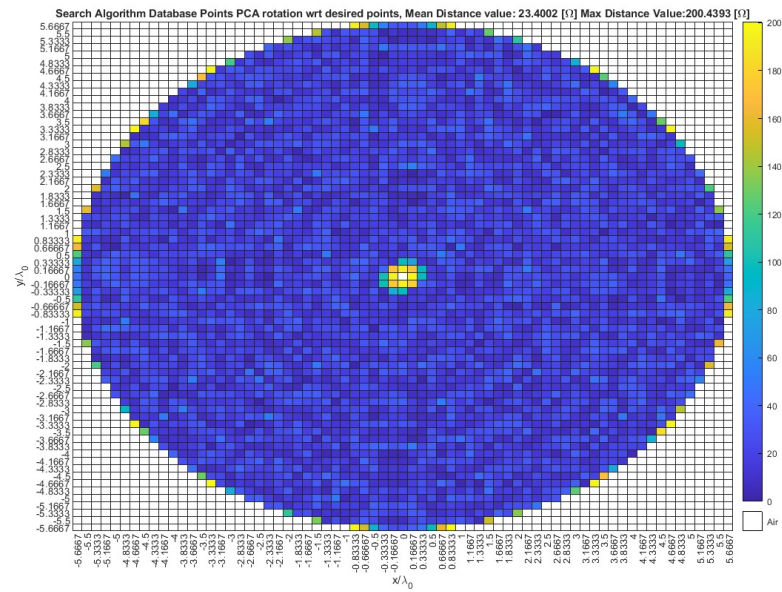
(b) Distance between $Z_{desired}$ and "Coarse Refinement" Search Algorithm database reported on the antenna surface, 4913 points
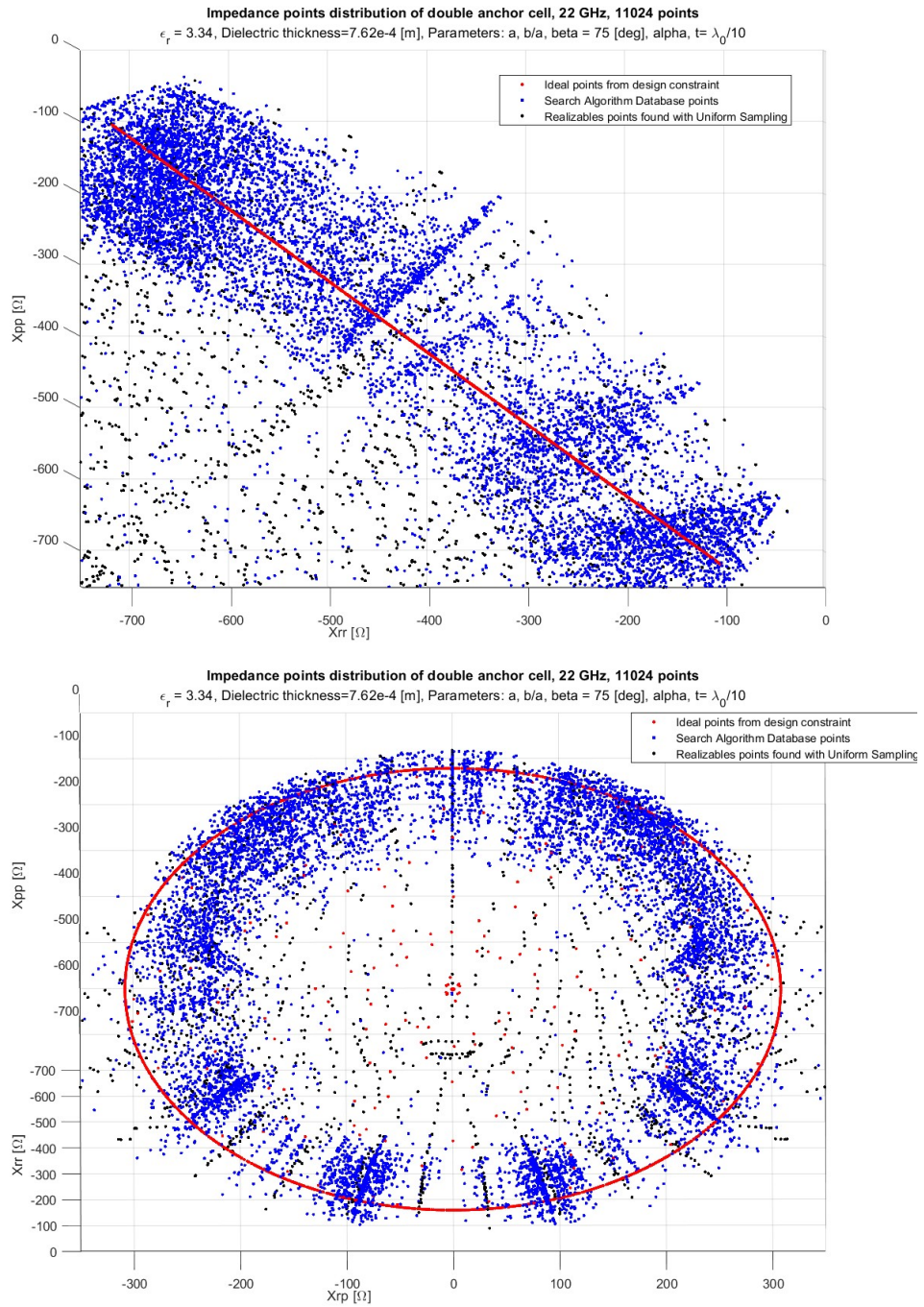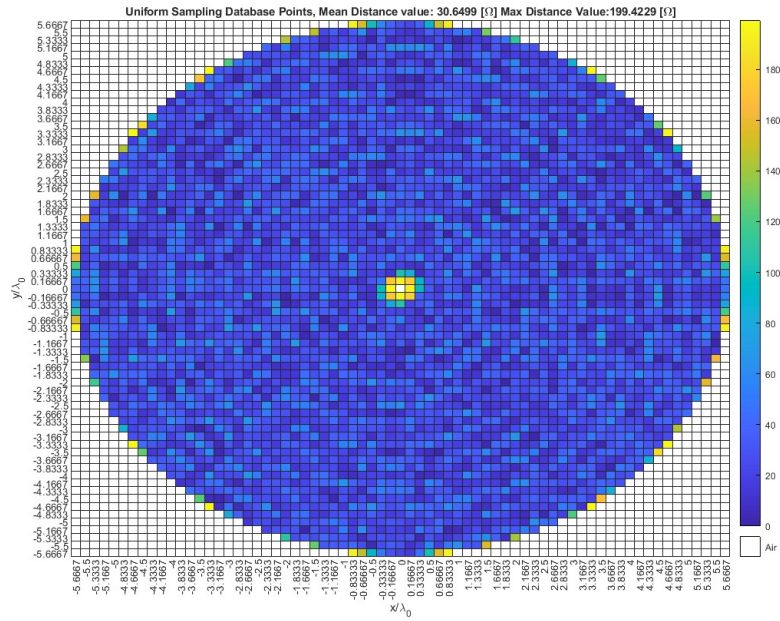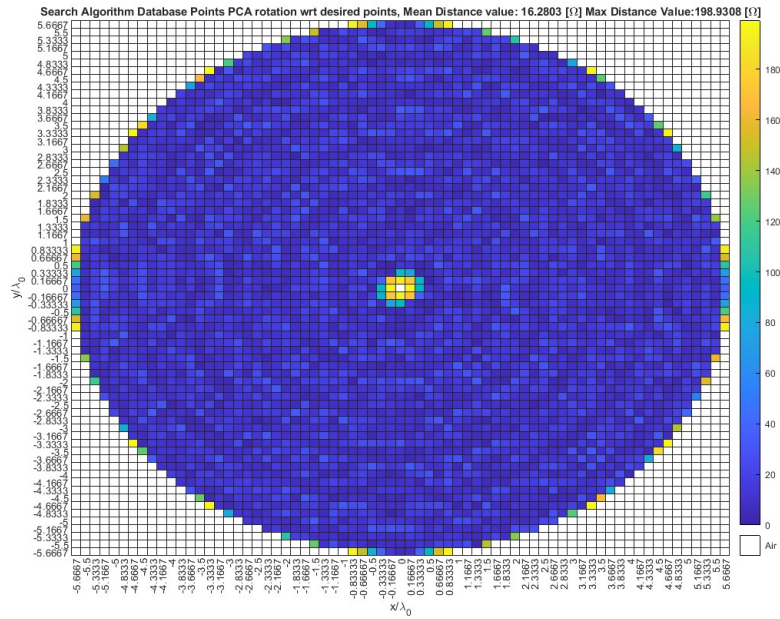
Figure 4.19: "Dense Refinement" Search Algorithm (blue) vs Uniform parameters sampling (black) vs. $Z_{desired}$ desired points (red), 11024 points databases

(a) Distance between $Z_{desired}$ and uniform sampling database points reported on the antenna surface, 11024 points


(b) Distance between $Z_{desired}$ and "Dense Refinement" Search Algorithm database reported on the antenna surface, 11024 points

Realized Electrical Current Distribution [A/m] with 'Coarse Refinement' 4913 points Database, 22 GHz, circular antenna diameter 10λ_0
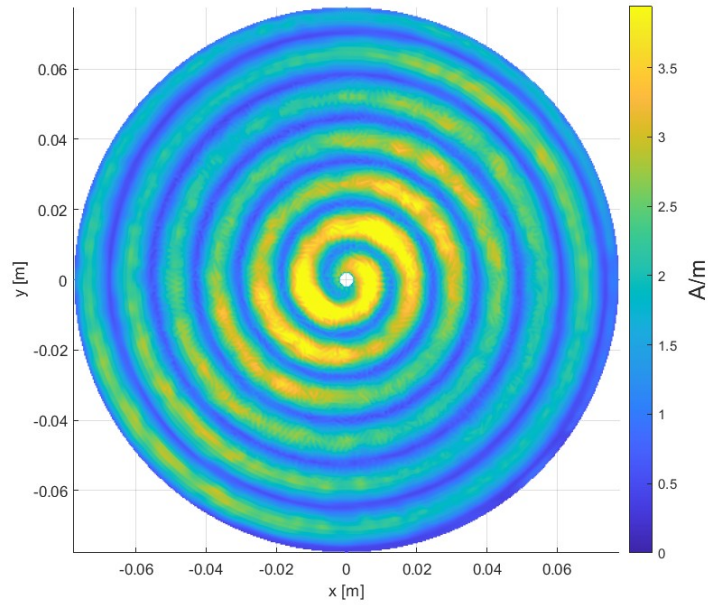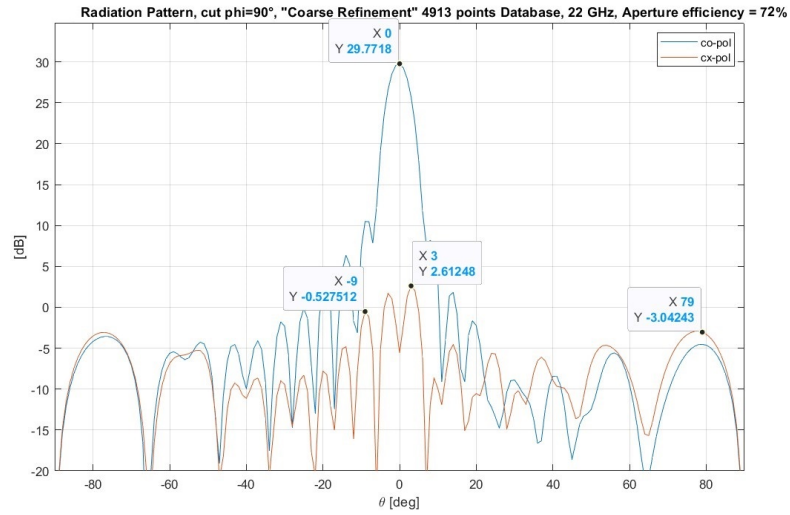

(a) "Coarse Refinement" database, 4913 points

Realized Current Distribution [A/m] with Uniform Sampling 4913 points Database, 22 GHz, circular antenna diameter 10λ_0
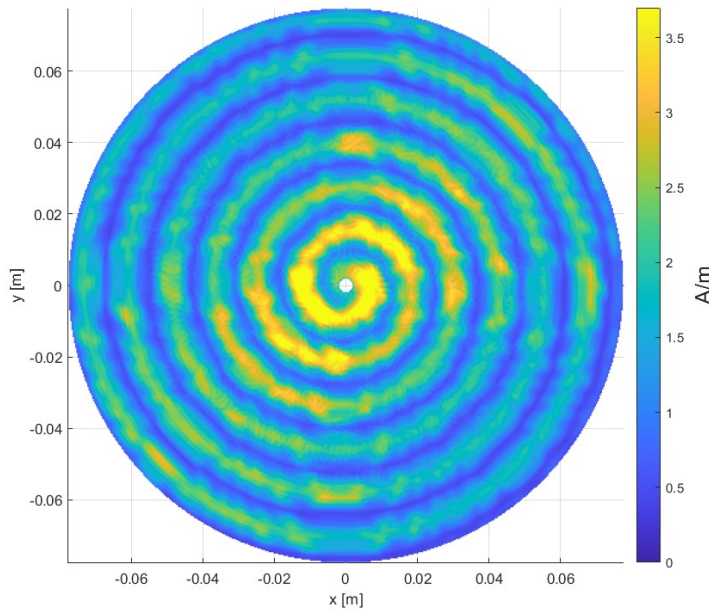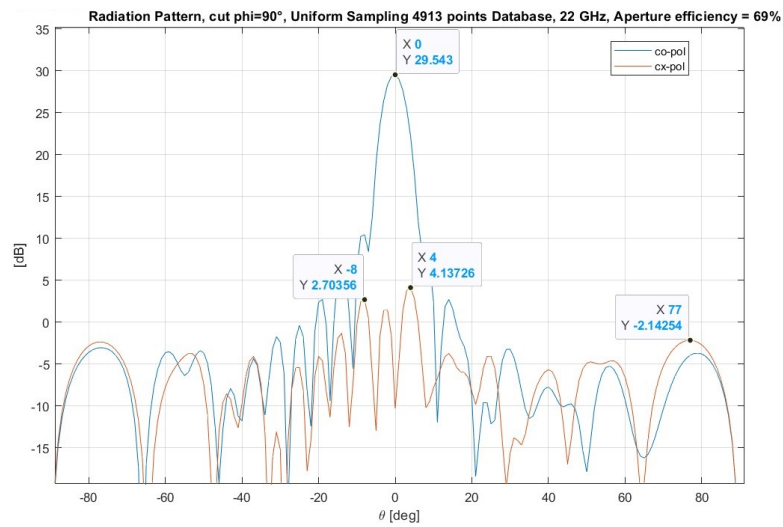

(b) Uniform sampling database, 4913 points

Figure 4.21: "Coarse" SA vs. "Coarse" Uniform Sampling Database current distribution
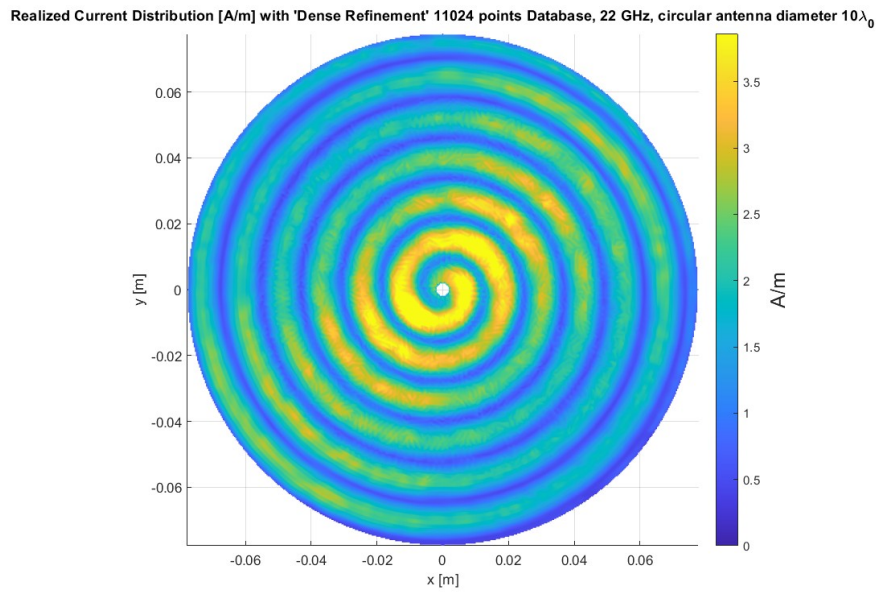
(a) "Coarse Refinement" database , 4913 points

(b) Uniform sampling database, 4913 points

Figure 4.22: "Coarse" SA vs. "Coarse" Uniform Sampling Database Radiation Pattern

Realized Current Distribution [A/m] with 'Dense Refinement' 11024 points Database, 22 GHz, circular antenna diameter 10λ_0

(a) "Dense Refinement" database, 11024 points

Realized Current Distribution [A/m] with Uniform Sampling 11024 points Database, 22 GHz, circular antenna diameter 10λ_0

(b) Uniform sampling database, 11024 points

Figure 4.23: "Dense" SA vs. "Dense" Uniform Sampling Database current distribution

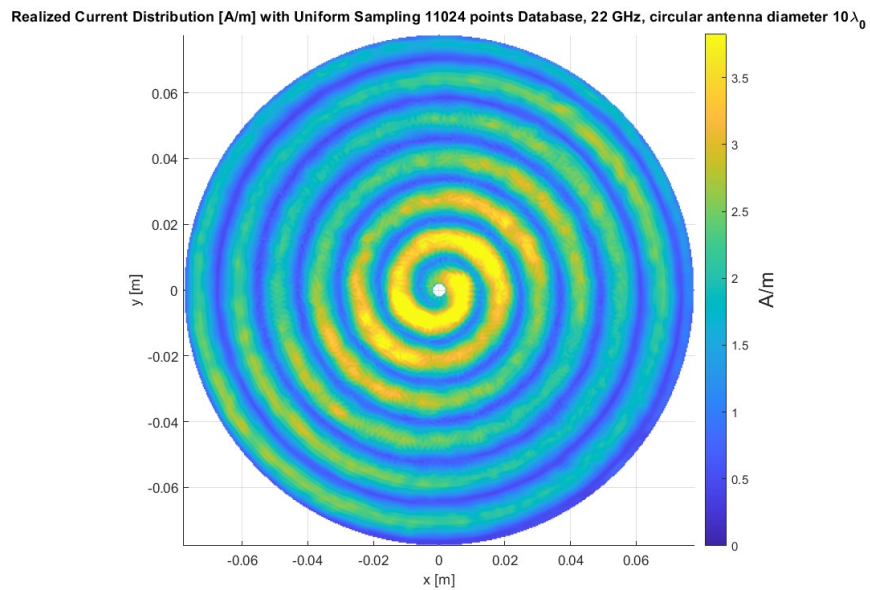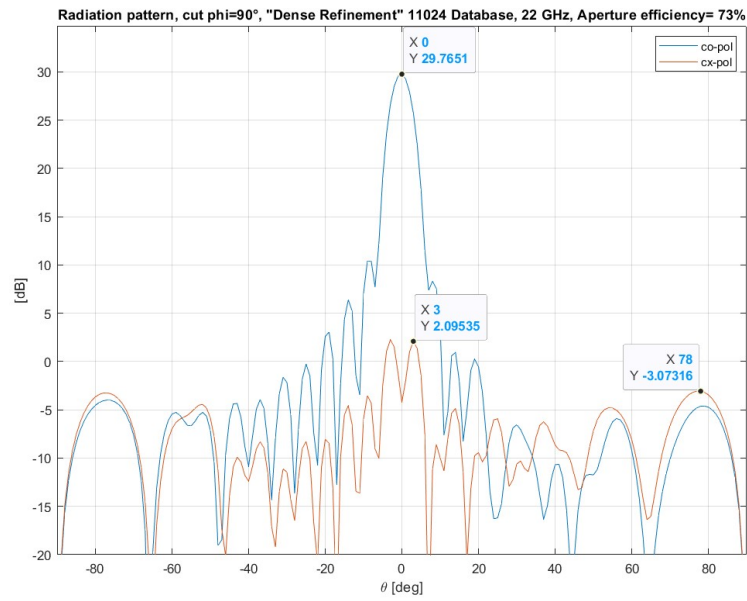**(a)** "Dense Refinement" database, 11024 points

(b) Uniform sampling database, 11024 points

Figure 4.24: "Dense" SA vs. "Dense" Uniform Sampling Database Radiation Pattern
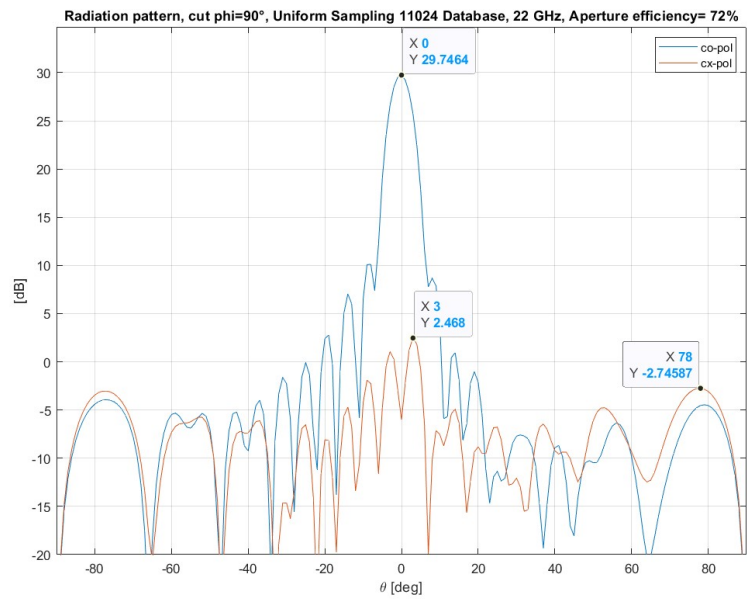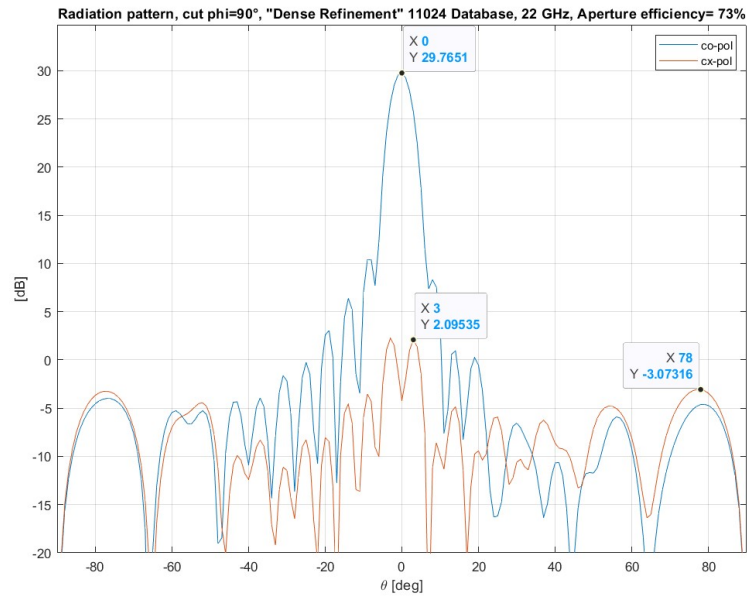
(a) "Dense Refinement" database, 11024 points
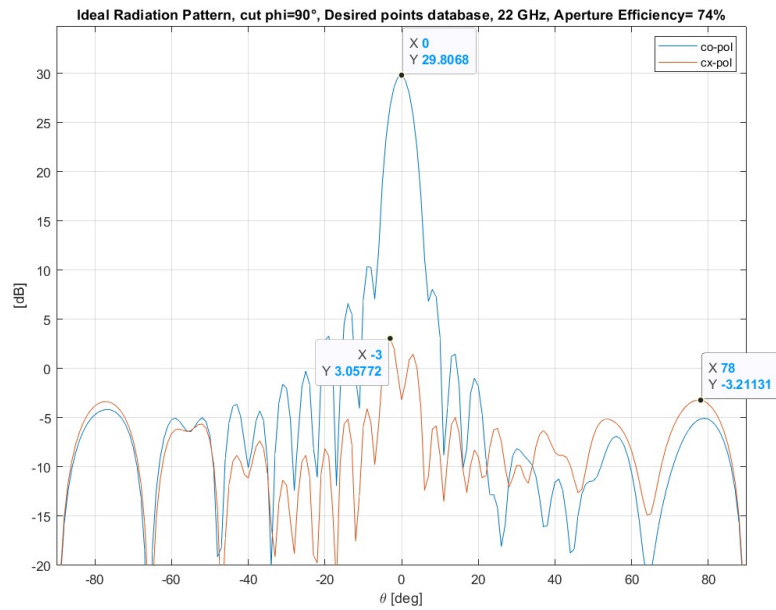
(b) Ideal radiation pattern realized with desired points

Figure 4.25: Ideal vs. "Dense" SA Database Radiation Pattern

(a) Ideal radiation pattern realized with desired points
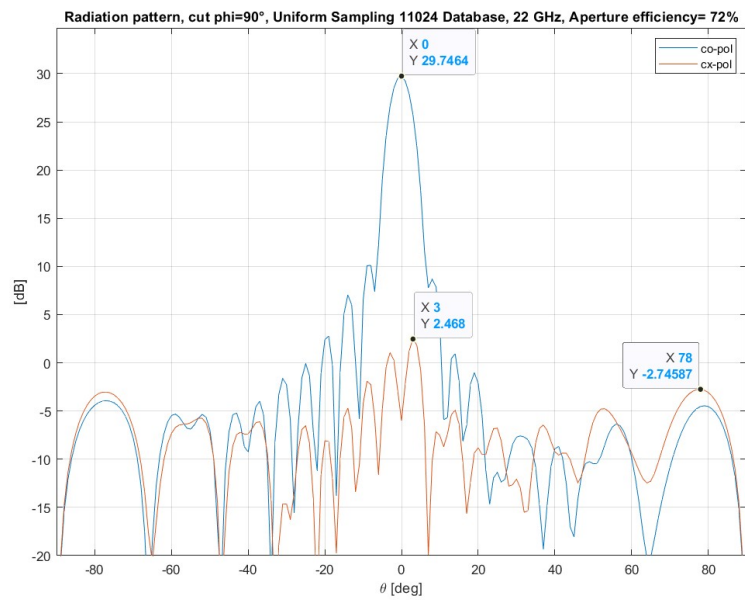
(b) Uniform sampling database, 11024 points

Figure 4.26: Ideal vs. "Dense" Uniform Sampling Database Radiation Pattern

80
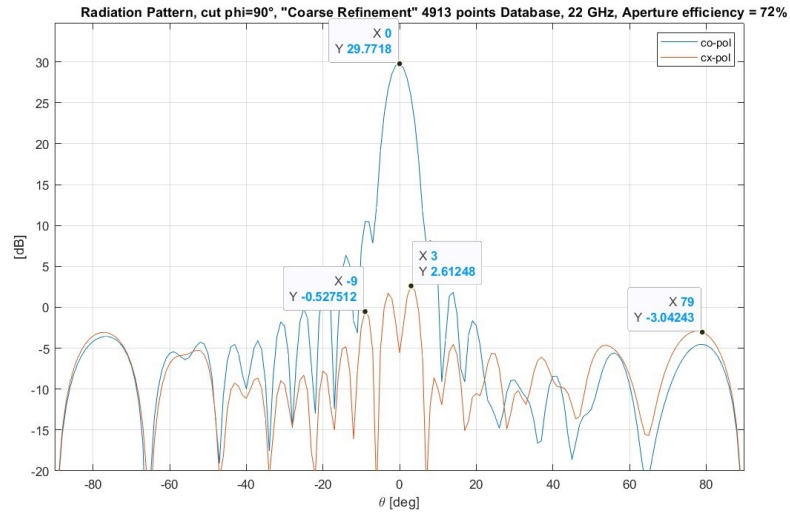
(a) "Coarse Refinement" database, 4913 points
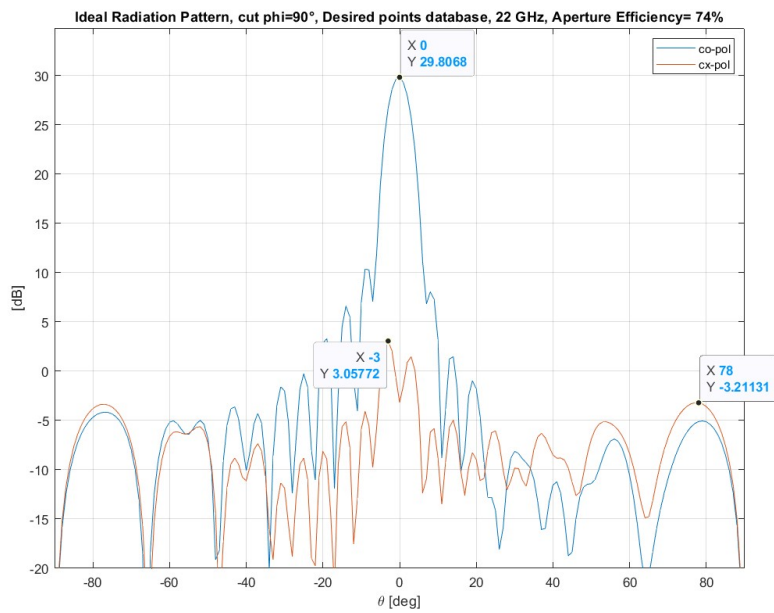
(b) Ideal radiation pattern realized with desired points

Figure 4.27: Ideal vs. "Coarse" SA Database Radiation Pattern

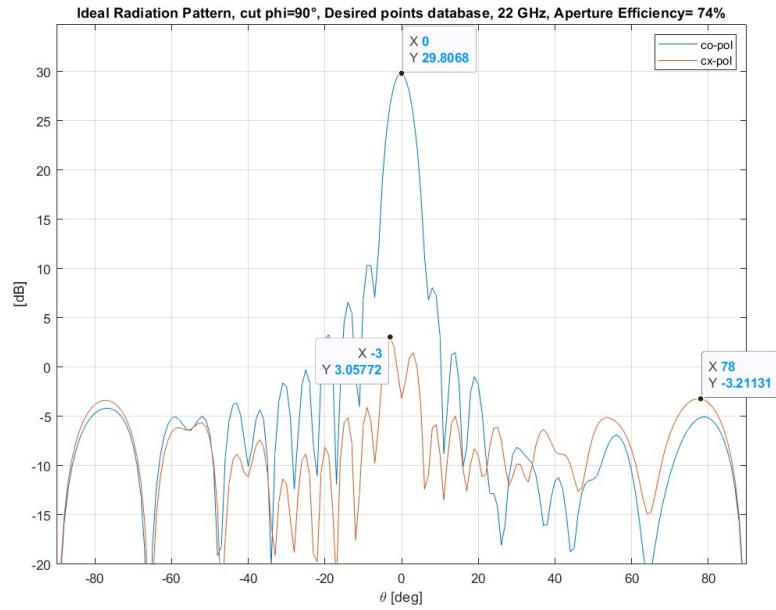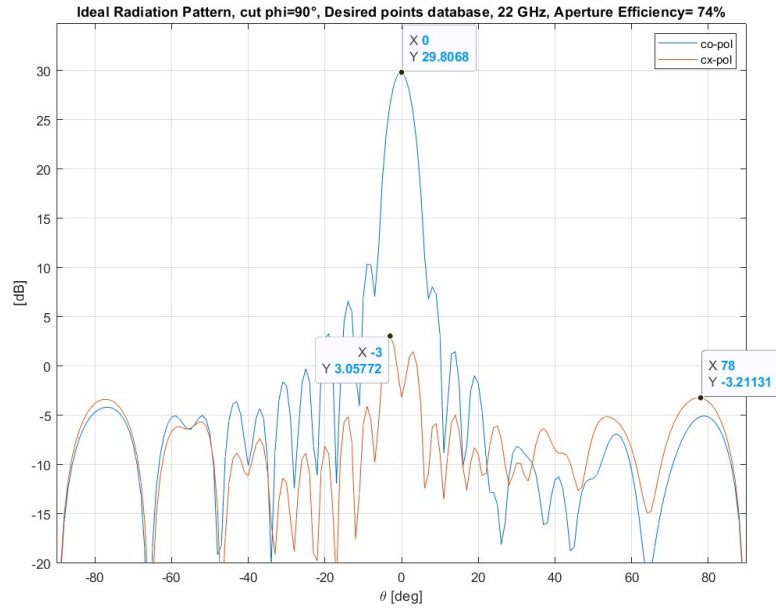**(a)** Ideal radiation pattern realized with desired points
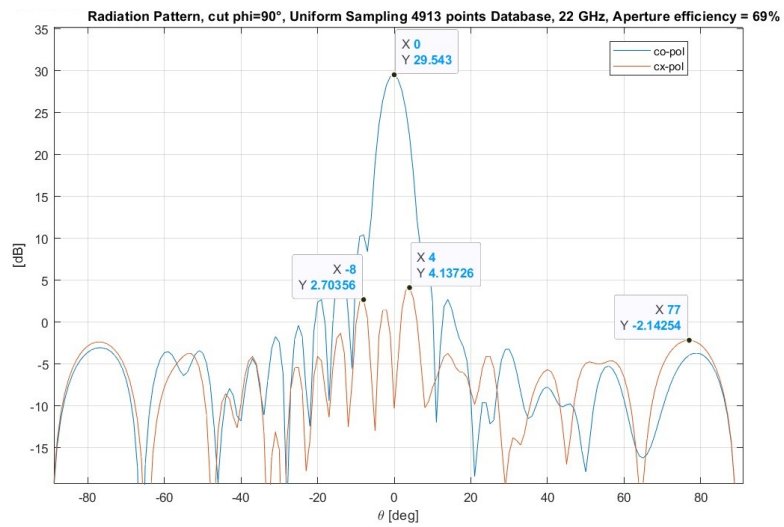
(b) Uniform sampling database, 4913 points

Figure 4.28: Ideal vs. "Coarse" Uniform Sampling Database Radiation Pattern

Circular MTS antenna realized with the "Dense Refinement" Database, 22 GHz, 10λ_0 diameter
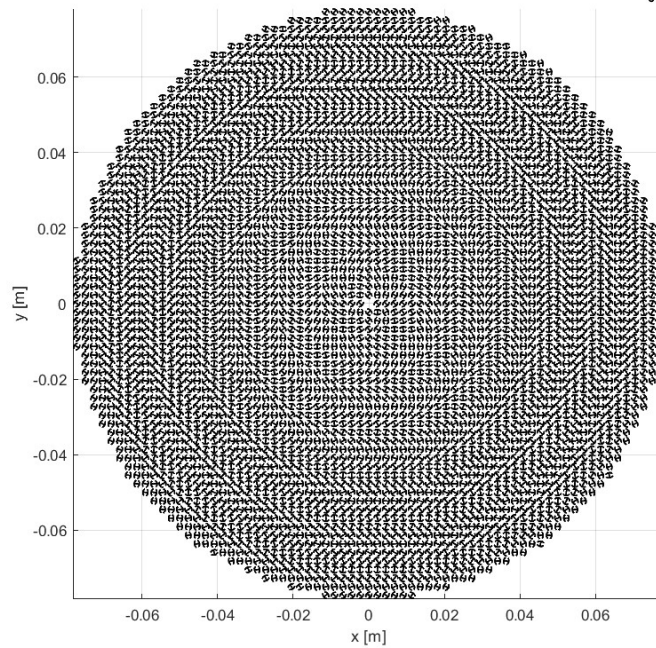
Circular MTS antenna realized with the "Dense Refinement" Database, 22 GHz, 10λ_0 diameter
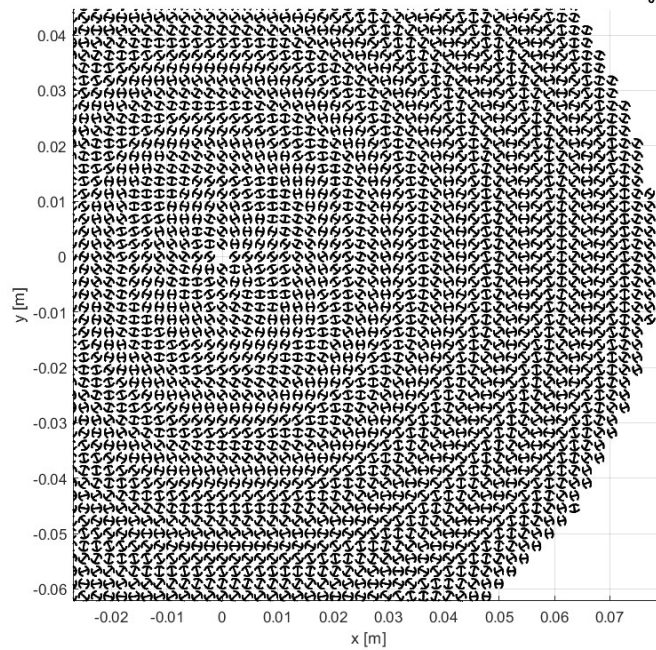
Figure 4.29: 10λ_0 circular MTS antenna made up of double anchor unit cells of different sizes and orientations that realize the IBCs on the surface

Chapter 5

Conclusions

In this thesis work, an overview of the main field of applications of MTS structures that could be found in the literature has been presented, along with some fundamental theoretical elements that have been studied in the last few years as analysis and design tools to deal with such complex EM structures.

It followed the specific problem description regarding this thesis work, together with a description of a typical design process for such an antenna. The goal was to realize a proper algorithm for the impedance database generation that is needed for the design process.

The proposed algorithm is based on local interpolation, using a built-in MATLAB solution, and samples the parameter space X according to the interpolated value of $Z(X)$. The search is performed on a box division of the impedance domain according to some fundamental defined parameters.

It has been distinguished between two kinds of searches it is possible to perform with this algorithm, namely "Blind" and "Refinement" searches, according to the features of the generated database.

Numerical results have shown an improvement with respect to the uniform sampling method for database generation in terms of a lower average distance between generated impedance points and desired points $Z_{desired}$ for a double anchor cell realizing a circular polarized and broadside beam (about 30 db directivity) for a 10 lambda circular MTS antenna with coaxial feeding at the center.

Appendix A

Algorithm Pseudo Codes

Algorithm 1 Box search

1: **procedure** BOXSEARCH($param$, X_{start}, $Z(X_{start})$)
2:     ▷ $param$ is a structure containing $data$,$coeff$, $center_{points}$, $lengthcube_x$, $lengthcube_y$, $lengthcube_z$, $minpoints_{interp}$, N_{point}, $numGrid$;
3:     ▷ X_{grid}, $Z(X_{grid})$ are input parameters and impedance database points;
4:     ▷ Initialization
5:     $param_{update} \leftarrow X_{start}$
6:     $Z_{update} \leftarrow Z(X_{start})$
7:     ▷ Assign starting values for database points
8:     ▷ Execution
9:     **for** each $center_{points}$ **do**
10:         ▷ Define current Box as function of center and lengths
11:         $Box_{current} \leftarrow Box(center_{points}, lengthcube_x, lengthcube_y, lengthcube_z)$
12:         Find num_{pixels} such as $Z_{update}(num_{pixels}) \in Box_{current}$
13:         **if** $num_{pixels} < N_{point}$ **then**
14:             ▷ Find at least $minpoints_{interp}$ points of Z_{update} near the current Box
15:             $index_{parents} \leftarrow SearchNearPoints(Box_{current}, Z_{update}, minpoints_{interp})$
16:             $NotCoplanar \leftarrow CoplanarCheck(param_{update}(index_{parents})$
17:             ▷ Coplanar flag check
18:             **if** $NotCoplanar$ **then**
19:                 ▷ Create X_{query} grid from parameters pointed by $index_{parents}$
20:                 $X_{query} \leftarrow Grid(param_{update}(index_{parents}), numGrid)$
21:                 $Z_{Interp} \leftarrow griddatan(Z_{update}(index_{parents}), param_{update}(index_{parents}), X_{query})$
22:                 ▷ Generate Z_{Interp} points evaluated on X_{query} from nearest points
23:                 Find $index_{query}$ such as $Z_{Interp}(index_query) \in Box_{current}$
24:                 **if** NotEmpty($index_{query}$) **then**
25:                     ▷ Random values among the $index_{query}$ to simulate only N_{point}
26:                     Find $index_{simulation} \leftarrow Random(index_{query}, N_{point})$
27:                     ▷ PSSM simulation of $X_{query}(index_{simulation})$
28:                     $Z_{new} \leftarrow OutPZM(X_{query}(index_{simulation}), data)$
29:                     ▷ Domain rotation of generated impedance points
30:                     $Z_{new} \leftarrow Z_{new} * coeff$
31:                     ▷ Update database of points
32:                     $Z_{update} \leftarrow Z_{update} \cup Z_{new}$
33:                     $param_{update} \leftarrow param_{update} \cup X_{query}(index_{simulation})$
34:                 **end if**
35:             **end if**
36:         **end if**
37:     **end for**
      return $Z_{update}, param_{update}$
38: **end procedure**

Algorithm 2 Search Algorithm

1: **procedure** SEARCHALG($data$, X_{grid},$Z(X_{grid})$,Z_{ideal},$hullsearch$)
2:     ▷ X_{grid}, $Z(X_{grid})$ are input parameters and impedance database points;
3:     ▷ Z_{ideal} input desired points, if any;
4:     ▷ Initialization
5:     ▷ Search Algorithm parameters, typical values for "blind" database creation
6:     $N \leftarrow 10$
7:     $secondsearchMax \leftarrow 10$
8:     $minpoints \leftarrow 5 * 10^3$
9:     $boxinhull \leftarrow 2 * 10^3$
10:     $maxIncrement \leftarrow 200$
11:     ▷ Box search parameters structure initialization. Those values are fixed.
12:     $paramsearch.NumQueryGrid \leftarrow 10$
13:     $paramsearch.N_{point} \leftarrow 10$
14:     $paramsearch.minpoints_{interp} \leftarrow 200$
15:     $paramsearch.data \leftarrow data$
16:     $numsecondsearch \leftarrow 0$;
17:     $numPointsStart \leftarrow length(Z(X_{grid}))$;
18:     ▷ Execution
19:     ▷ Rotation of search domain according Z_{ideal}, if any.
20:     **if** IsEmpty(Z_{ideal}) **then**
21:         $coeff \leftarrow pca(Z(X_{grid}))$
22:     **else**
23:         $coeff \leftarrow pca(Z_{ideal})$
24:     **end if**
25:     $points_{rotated} \leftarrow Z(X_{grid}) * coeff$
26:     ▷ Extracting min and max values for each components of rotated domain.
27:     $minZ \leftarrow min(points_{rotated})$
28:     $maxZ \leftarrow max(points_{rotated})$
29:     ▷ Evaluate number of division for each range
30:     $division \leftarrow Div(N, maxcomponentsZ, mincomponentsZ)$
31:     ▷ Evaluate box centers and lengths
32:     $center_{points} \leftarrow createBox(N, maxZ, minZ)$
33:     $lengthcube_x \leftarrow createBox(N, maxZ, minZ)$
34:     $lengthcube_y \leftarrow createBox(N, maxZ, minZ)$
35:     $lengthcube_z \leftarrow createBox(N, maxZ, minZ)$

36:     ▷ Assign parameters for Box search
37:     $paramsearch.coeff \leftarrow coeff$
38:     $paramsearch.center_{points} \leftarrow center_{points}$
39:     $paramsearch.length_x \leftarrow lengthcube_x$
40:     $paramsearch.length_y \leftarrow lengthcube_y$
41:     $paramsearch.length_z \leftarrow lengthcube_z$
42:     ▷ First search, update database
43:     $Z_{update} \leftarrow BoxSearch(paramsearch, points_{rotated}, X_{grid})$
44:     $param_{update} \leftarrow BoxSearch(paramsearch, points_{rotated}, X_{grid})$
45:     $incrementpoints \leftarrow length(Z_{update}) - numPointsStart$
46:     ▷ Perfoming iterative second searches on new boxes, if required
47:     **if** $incrementpoints < minpoints$ **then**
48:         ▷ Initialize flag for iterative searches
49:         $EOL \leftarrow true$
50:         **while** EOL **do**
51:             $prevsize \leftarrow length(param_{update})$
52:             $numsecondsearch \leftarrow numsecondsearch + 1$
53:             ▷ Generate randomly new center points for search boxes
54:             **if** $hullsearch$ **then**
55:                 $paramsearch.center_{points} \leftarrow CenterHull(Z_{update}, boxinhull)$
56:             **else**
57:                 $paramsearch.center_{points} \leftarrow CenterRange(Z_{update}, boxinhull, minZ, maxZ)$
58:             **end if**
59:             ▷ Iterative Box Search
60:             $Z_{update} \leftarrow BoxSearch(paramsearch, points_{rotated}, X_{grid})$
61:             $param_{update} \leftarrow BoxSearch(paramsearch, points_{rotated}, X_{grid})$
62:             $incrementpoints \leftarrow length(Z_{update}) - numPointsStart$
63:             ▷ End Of Loop conditions check
64:             $EOL \leftarrow CheckEOL(minpoints, secondsearchMax, maxIncrement)$
65:         **end while**
66:     **end if**
67:     ▷ Rotate points into the original domain
68:     $Z_{db} \leftarrow Z_{update} * coeff^{-1}$
69:     ▷ Return database of points
        return $Z_{db}, param_{update}$
70: **end procedure**

Bibliography

[1] Li Aobo Singh Shreya and Sievenpiper Dan. «Metasurfaces and their applications». In: *Nanophotonics* (2018) (cit. on pp. 2, 3).

[2] Faenzi M. Minatti G. David González-Ovejero Caminita F. Martini E. Della Giovampaola C. Maci S. «Metasurface Antennas: New Models, Applications and Realizations». In: *Nature* (2019) (cit. on pp. 2, 3, 14, 15).

[3] Khushboo Singh Foez Ahmed and Karu Esselle. «Electromagnetic Metasurfaces: Insight into Evolution, Design and Applications». In: *Crystals* (2022). Available at `https://www.mdpi.com/2073-4352/12/12/1769` (cit. on pp. 2, 11, 12).

[4] E. Martini S. Maci. «Theory, Analysis, and Design of Metasurfaces for Smart Radio Environments». In: *IEEE Xplore* (2022) (cit. on pp. 2, 4, 6–10).

[5] Minatti G. Caminita F. Martini E. Sabbadini M. Maci S. «Synthesis of Modulated-Metasurface Antennas With Amplitude, Phase, and Polarization Control». In: *IEEE Xplore* (2016) (cit. on pp. 2–4, 14, 25).

[6] Marcello Zucchi. «Numerical Techniques for the Automated Design of Metasurface Antennas». Available at `https://iris.polito.it/handle/11583/2972560.`. PhD thesis. Politecnico of Torino, 2022 (cit. on pp. 3, 4, 12, 27, 28).

[7] Vecchi G. Francavilla A.M. Martini E. Maci S. «On the Numerical Simulation of Metasurfaces With Impedance Boundary Condition Integral Equations». In: *IEEE Xplore* (2015) (cit. on pp. 3, 4, 12, 20, 21, 26).

[8] Zucchi M. Vernì F. Righero M. Vecchi G. «Current-Based Automated Design of Realizable Metasurface Antennas with Arbitrary Pattern Constraints». In: *IEEE Xplore* (2023) (cit. on pp. 3, 23, 25–27).

[9] M. Teniou H. Roussel N. Capet G.-P. Piau M. Casaletti. «Implementation of Radiating Aperture Field Distribution Using Tensorial Metasurfaces». In: *IEEE Xplore* (2017) (cit. on pp. 3, 25, 26).

[10] NIAMAT HUSSAIN SABA TARIQ SYEDA I. NAQVI and YASAR AMIN. «A Metasurface-Based MIMO Antenna for 5G Millimeter-Wave Applications». In: *IEEE Xplore* (2021) (cit. on p. 4).

[11] Nir Shlezinger George C. Alexandropoulos Mohammadreza F. Imani Yonina C. Eldar and David R. Smith. «Dynamic Metasurface Antennas for 6G Extreme Massive MIMO Communications». In: *IEEE Xplore* (2021) (cit. on p. 4).

[12] Lei Zhang1 Xiao Qing Chen Qiang Cheng and Tie Jun Cui. «Space-Time-Coding Digital Metasurfaces for New- Architecture Wireless Communications». In: *IEEE Xplore* (2022) (cit. on p. 4).

[13] Sepideh Fallahzadeh Keyvan Forooraghi Zahra Atlasbaf. «A polarization-insensitive metamaterial absorber with a broad angular band». In: *IEEE Xplore* (2012) (cit. on p. 5).

[14] Suresh Chejarla Sreenath Reddy Thummaluru Sachin Kalraiya Raghvendra Kumar Chaudhary. «Polarization-angle insensitive metamaterial absorber for wide incident angles». In: *IEEE Xplore* (2018) (cit. on p. 5).

[15] Michael Selvanayagam and George V. Eleftheriades. «Discontinuous electromagnetic fields using orthogonal electric and magnetic currents for wavefront Manipulation». In: *Optical Society of America* (2013). Available at `https://opg.optica.org/oe/fulltext.cfm?uri=oe-21-12-14409&id=257011` (cit. on p. 5).

[16] Jan Mietzner Robert Schober Lutz Lampe Wolfgang H. Gerstacker and Peter A. Hoeher. «Multiple-Antenna Techniques for Wireless Communications – A Comprehensive Literature Survey». In: *IEEE Xplore* (2009) (cit. on p. 6).

[17] Francesco Monticone and Andrea Alu. «Leaky-Wave Theory, Techniques, and Applications: From Microwaves to Visible Frequencies». In: *IEEE Xplore* (2015) (cit. on p. 8).

[18] Amit M. Patel. «Controlling Electromagnetic Surface Waves with Scalar and Tensor Impedance Surfaces». Available at `https://deepblue.lib.umich.edu/handle/2027.42/97954`. PhD thesis. University of Michigan, 2013 (cit. on pp. 9, 13, 21, 29).

[19] Gabriele Minatti Francesco Caminita Massimiliano Casaletti and Stefano Maci. «Spiral Leaky-Wave Antennas Based on Modulated Surface Impedance». In: *IEEE Xplore* (2011) (cit. on p. 9).

[20] E. Martini M. Mencagli Jr. and S. Maci. «Metasurface transformation for surface wave control». In: *The Royal Society* (2015). Available at `http://dx.doi.org/10.1098/rsta.2014.0355` (cit. on pp. 11, 12).

[21] Christopher L. Holloway and Edward F. Kuester. «Generalized Sheet Transition Conditions for a Metascreen—A Fishnet Metasurface». In: *IEEE Xplore* (2018) (cit. on p. 12).

[22] Patel A.M. Grbic A. «Modeling and Analysis of Printed-Circuit Tensor Impedance Surfaces». In: *IEEE Xplore* (2013) (cit. on pp. 13, 21–23, 29, 31, 32).

[23] Henry J. Bilow. «Guided Waves on a Planar Tensor Impedance Surface». In: *IEEE Xplore* (2003) (cit. on p. 13).

[24] Patel A.M. Grbic A. «Effective Surface Impedance of a Printed-Circuit Tensor Impedance Surface (PCTIS)». In: *IEEE Xplore* (2013) (cit. on pp. 14, 21, 22).

[25] Xiao Liu Fan Yang Maokun Li Shenheng Xu. «Generalized Boundary Conditions in Surface Electromagnetics: Fundamental Theorems and Surface Characterizations». In: *Applied Sciences* (2019) (cit. on pp. 14, 16–20).

[26] Karim Achouri Mohamed A. Salem and Christophe Caloz. «General Metasurface Synthesis Based on Susceptibility Tensors». In: *IEEE Xplore* (2015) (cit. on pp. 14, 20, 25).

[27] Bruno Stupfel and Dorcas Poget. «Sufficient uniqueness conditions for the solution of the time harmonic Maxwell's equations associated with surface impedance boundary conditions». In: *Science Direct* (2011). Available at `https://www.sciencedirect.com/science/article/abs/pii/S00219991 11001215` (cit. on p. 21).

[28] Rana Sadaf Anwar Lingfeng Mao and Huansheng Ning. «Frequency Selective Surfaces: A Review». In: *Applied Sciences* (2018). Available at `https://www. mdpi.com/2076-3417/8/9/1689` (cit. on p. 27).